CD45 exclusion and crosslinking-based receptor signaling together broaden FcεRI reactivity

James H. Felce[1,2,3*], Erdinc Sezgin[1*], Madina Wane[1,2], Heather Brouwer[1,2], Michael L. Dustin[3†], Christian Eggeling[1†‡], Simon J. Davis[1,2†]

[1]MRC Human Immunology Unit, MRC Weatherall Institute of Molecular Medicine, University of Oxford. [2]Radcliffe Department of Medicine, University of Oxford. [3]Kennedy Institute of Rheumatology, University of Oxford, Oxford, OX3 7FY, UK.

[*]These authors contributed equally to this work.

[‡]Current address: Institute of Applied Optics Friedrich-Schiller-University Jena and Leibniz Institute of Photonic Technology e.V., Jena, Germany.

[†]Corresponding author. Email: simon.davis@imm.ox.ac.uk (S.J.D.); christian.eggeling@rdm.ox.ac.uk (C.E.); michael.dustin@kennedy.ox.ac.uk (M.L.D.)

ABSTRACT

For many years, the high-affinity receptor for immunoglobulin E (IgE) FcεRI, which is expressed by mast cells and basophils, has been widely held to be the exemplar of cross linking (that is, aggregation-dependent) signaling receptors. We found, however, that FcεRI signaling could occur in the presence or absence of receptor crosslinking. Using both cell and cell-free systems, we showed that FcεRI signaling was stimulated by surface-associated monovalent ligands through the passive, size-dependent exclusion of the receptor-type tyrosine phosphatase CD45 from plasma membrane regions of FcεRI-ligand engagement. Similarly to the T cell receptor, FcεRI signaling could also be initiated in a ligand-independent manner. These data suggest that a simple mechanism of CD45 exclusion–based receptor triggering could function together with crosslinking-based FcεRI signaling, broadening mast cell and basophil reactivity by enabling these cells to respond to both multivalent and surface-presented monovalent antigens. These findings also strengthen the case that a size-dependent, phosphatase exclusion–

based receptor triggering mechanism might serve generally to facilitate signaling by noncatalytic immune receptors.

INTRODUCTION

The high-affinity immunoglobulin E (IgE) receptor, FcεRI, sensitizes mast cells and basophils to IgE-targeted antigens, thus underpinning both anti-parasite and allergic responses (1). FcεRI comprises a tetrameric complex consisting of the IgE-binding chain, FcεRIα, associated with FcεRIβ and a covalent FcεRIγ homodimer (2). Binding of cognate antigen by FcεRI-bound IgE induces rapid phosphorylation of immunoreceptor tyrosine-based activation motifs (ITAMs) in the cytoplasmic domains of FcεRIβ and FcεRIγ by the Src family kinase (SFK) Lyn (3), enabling recruitment and activation of spleen tyrosine kinase (Syk) through interactions of its Src homology 2 (SH2) domains with the phosphorylated ITAMs of FcεRIγ (4). Activated Syk then initiates a signaling cascade through phospholipases and calcium (Ca^{2+}) mobilization that ultimately leads to the exocytosis of pro-inflammatory granules containing, for example, histamine (1).

For many years, IgE-initiated signaling was considered to be the quintessential example of aggregation-driven immunoreceptor triggering (5). Very early studies suggested that for IgE-mediated exocytosis, intermolecular crosslinking of cell-bound antibody was required for signaling (6). Accordingly, it was shown that multivalent antigens were generally capable of eliciting mast-cell responses, whereas univalent, monomeric ligands were not. It was also shown that crosslinking did not necessarily have to be antigen-mediated; bivalent anti-IgE antibody (7) or artificially aggregated IgE, or the Fc fragments of IgE, were all found to be active (8). It was

subsequently proposed that dimers of IgE serve as a minimal signaling "unit" for mast cell degranulation (9), albeit weakly (10, 11). The current view is that for FcεRI to be triggered, the receptor must be crosslinked by multivalent antigens to achieve the necessary density and geometry required for receptor transphosphorylation by FcεRI-associated Lyn (3, 12). Alternatively, cross-linking–based aggregation might induce changes in the distribution of FcεRI within membrane domains that protect it from dephosphorylation (13, 14). Irrespective of the mechanism, constraining FcεRI reactivity to multivalent antigens would have the effect of severely restricting the breadth of mast cell and basophil responses.

Despite the enduring appeal of aggregation-based signaling, it was quickly realized that it created a paradox because antibody receptors were understood to be expressed at sufficiently high amounts, and enough of them are mobile, for dimers to form on a purely stochastic basis; however, spontaneous exocytosis is not observed (5). Further findings have produced new difficulties. The binding of free IgE to mast cells influences numerous cellular responses, including cytokine production, cell survival and differentiation, and FcεRI expression (15-17), implying that FcεRI is capable of sensing IgE in an aggregation-independent manner. These effects are, however, distinct from those of so-called "highly cytokinergic" IgEs, which induce degranulation at very high concentrations, most likely through receptor crosslinking by surface-expressed autoantigens (18). In addition, FcεRI expressed in transfected fibroblasts is spontaneously phosphorylated (19), revealing that aggregation per se is not a strict requirement of receptor triggering. But most importantly, mast cell degranulation is robustly triggered by monovalent antigens attached to supported lipid bilayers (SLBs; 20, 21). Similar to a second immune receptor, that is, the B cell receptor (BCR) (22), which was also widely assumed to be

triggered only by crosslinking, but is now known to be reactive to surface-presented monovalent ligands, it is now accepted that FcεRI can be triggered by both mono- and multivalent antigens.

Alongside these findings, it is becoming recognized that the properties of many common allergens are incompatible with, or at least seem unsuited to, aggregation-based FcεRI triggering in vivo. Firstly, many known allergens are monomeric (e.g. 23, 24-26). These could crosslink FcεRI in the presence of polyclonal IgE against non-overlapping epitopes, but this would only work within a narrow range of binding geometries according to studies of model antigens (11). Secondly, most dimeric allergens that self-associate only do so transiently (27), with reported dissociation constant (K_d)values in the micro- to millimolar range (28, 29). Because exposure to common animal allergens is typically <1 to 300 ng/day (30, 31), which corresponds to ~0.02 to 8 pmol/day for the major cat allergen Fel d 1, and pollen allergens are encountered at 10- to 100-fold lower amounts (31, 32), these types of allergens will most likely be presented to mast cells and basophils as monomers, unless they accumulate in allergen-sensitive tissues.

Intrigued initially by differences in the functionality of surface-exposed and non-exposed mast cells, we explored the surface dependence of FcεRI signaling. We found that FcεRI was triggered by surfaces lacking FcεRI ligands, accounting for the characteristic behavior and morphology of basophilic cells in vitro. We then showed that signaling occurred in both the presence and absence of receptor aggregation and that it was robustly triggered by surface-associated monovalent ligands through the passive, size-dependent exclusion of the large receptor-type protein tyrosine phosphatase CD45 from regions of contact of FcεRI with its ligands. Whereas previous work suggested that CD45 exclusion and FcγR signaling are

dependent on integrins forming an actin-tethered diffusional barrier to the phosphatase (33), we observed strong signaling by FcεRI in the absence of integrin activity, and spontaneous phosphatase exclusion from engaged receptors in both cells and cell-free systems. We propose that a phosphatase exclusion-based mechanism functions alongside aggregation-driven receptor triggering to broaden the reactivity of mast cells. In this way, we propose that the paradoxical features of FcεRI triggering can be reconciled.

RESULTS

Mast cells sense the presence of surfaces

In the course of culturing rat basophilic leukemia (RBL) 2H3 cells, we observed small but statistically significant differences in FcεRI phosphorylation in cells kept in suspension by gentle end-over-end rotation *versus* those allowed to make contact with plastic surfaces (Fig. 1A, *left*, and Fig. 1B). FcεRI phosphorylation was detected on Western blots, using an anti-pY47-FcεRIγ phospho-specific antibody (34), as pairs of bands corresponding to short- and long-lived, mono- and dual-phosphorylated forms of FcεRIγ. We tested whether this was due to surface contact per se by quantifying phosphorylated FcεRIγ as the cells settled onto plastic surfaces in phosphate-buffered saline (PBS). The degree of phosphorylation was expressed as the ratio of dually-phosphorylated FcεRIγ intensity to total receptor intensity, normalized to the ratio of intensities measured in cells activated with anti-trinitrophenol (TNP) IgE and soluble bovine serum albumin-TNP (TNP_{BSA}) as antigen. A small, time-dependent increase in FcεRIγ phosphorylation was observed as the cells settled, peaking at 5 to 10 min (Fig. 1A, *right*, and Fig. 1B). These results indicated that RBL-2H3 cells, as they are usually grown, are not ‘resting’ with respect to FcεRI phosphorylation direct from tissue culture.

Using interference reflection and contrast microscopy to visualize cell contact areas and morphologies after adherence to microscope cover glass, we examined in more detail the effects of cell culture-induced FcεRI signaling in wild-type (WT) RBL-2H3 cells and RBL-2H3 cells lacking FcεRIα ('FcεRI-ve' cells), which were generated using CRISPR-Cas9 mutagenesis (35) (fig. S1A), under conditions that facilitated imaging. WT RBL-2H3 cells that attached to uncoated glass in fetal calf serum (FCS)-supplemented growth medium formed statistically significantly larger contacts after 30 min than did FcεRI-ve cells, whose contacts were similar to those of RBL-2H3 cells treated with the SFK inhibitor PP2 (Fig. 1, C and D). The contact areas formed by WT cells were not affected by the presence of FCS or by preloading with IgE (fig. S1B). Normal contact size was restored for FcεRI-ve cells by re-introduction of FcεRIα ('FcεRI+ve' cells; Fig. 1, C and D, and fig. S1A). Surface-grown WT RBL-2H3 cells exhibited more dendritic morphology (that is, they had protrusions extending away from the main cell body) than did FcεRI-ve cells (Fig. 1, E and F). Under normal culture conditions, RBL-2H3 cells grew predominantly as an adherent monolayer. However, substantially more FcεRI-ve cells grew in suspension compared to WT RBL-2H3 cells (Fig. 1G), and the surface-attached cells were more easily detached (Fig. 1H). FcεRI-ve RBL-2H3 cells were, however, as motile as WT cells (fig. S1C). Poly L-lysine (PLL)-coated surfaces induced RBL-2H3 cells to form large contacts in an FcεRI-independent manner (Fig. 1I), although FcεRI-ve cells formed statistically significantly, albeit slightly smaller, contacts than those of WT cells. Robust Ca^{2+} signaling was observed for WT and FcεRI+ve cells, but not FcεRI-ve cells, upon contact with PLL-coated glass (Fig. 1J), suggesting that this surface led to FcεRI triggering, similar to the case of T cells and the T cell receptor (TCR) (36). PLL also induced substantial FcεRIγ phosphorylation in

RBL-2H3 cells and primary human basophils (fig. S1, D to F). Together, these data suggest that mast cells sense surfaces through FcεRI signaling, a consequence of which might be the characteristic, adherent nature of cultured RBL-2H3 cells. That PLL induced strong signaling was an initial indication that FcεRI signaling was not dependent on integrin mobilization.

FcεRI is triggered by immobilized ligands and sensitive to constitutive kinase and phosphatase activity

The capacity of FcεRI to be triggered without cognate ligands after contact with a surface was reminiscent of the TCR (37), and further undermined the aggregation-only theory of FcεRI signaling. To revisit its actual requirements, we used the classical approach to studying aggregation-based FcεRI signaling (12), that is, BSA-coupled hapten (TNP_{BSA}) and anti-TNP IgE in solution and adsorbed onto glass. We also generated an artificial, monovalent FcεRI ligand mimic (His-Fcε), comprising the C_H2 to C_H4 domains of rat Fcε preceded by an N-terminal His_{12}-tag, which we could present in an FcεRI-accessible orientation (fig. S2A) on Ni-coated glass surfaces (mimicking monovalent immobilized antigens) or SLBs (to mimic mobile, cell-presented monovalent ligands). We used Ca^{2+} signaling as a proxy for receptor triggering.

Previous work showed that soluble monovalent antigen does not trigger FcεRI signaling, whereas when it is attached in a mobile form to a SLB, the same antigen induces RBL-2H3 degranulation (20, 21). As expected, therefore, RBL-2H3 cells did not produce measurable Ca^{2+} responses to soluble His-Fcε or to Ni-coated glass that did not present His-Fcε (Fig. 2A). However, ~80% of cells produced detectable responses within 10 min of making contact with SLBs presenting His-Fcε (Fig. 2A), with an average delay between surface contact and triggering

of 217 s. Equivalent fractions of the cell population produced Ca^{2+} responses within 10 min of contact with surfaces coated with TNP_{BSA}-IgE or with His-Fcε, as did cells exposed to anti-TNP IgE followed by soluble TNP_{BSA} (Fig. 2A). The consistency of the triggering fraction likely reflects the overall number of responsive cells. Nonetheless, phosphorylated FcεRIγ was somewhat more abundant in cells after contact with immobilized, cross-linked IgE than in cells exposed to immobilized monovalent ligand mimics (Fig. 2B). Soluble, cross-linked ligand produced the largest effect (normalized value of 1 in Fig. 2B), likely because it engaged more of the surface FcεRI than did any of the immobilized ligands. These observations indicate that, like the TCR, FcεRI can be triggered by receptor-clustering and surface-associated monovalent ligands.

We sought to establish whether, also like the TCR (38-41), FcεRI is sensitive to the constitutive activities of kinases and phosphatases in situ. FcεRIγ phosphorylation was induced in RBL-2H3 cells and primary human basophils by the tyrosine phosphatase inhibitor, pervanadate (Fig. 2, C and D, and fig. S2B). However, receptor crosslinking resulted in greater amounts of phosphorylated FcεRIγ than were induced by pervanadate, implying that local kinase activity was enhanced by receptor clustering. Near-complete inhibition of FcεRI phosphorylation was observed if the SFK inhibitor PP2 was added 15 min before pervanadate, but not 15 min afterwards. These results indicate that in resting cells, and especially in resting primary basophils in which the spontaneous, PP2-inhibited abundance of phosphorylated FcεRIγ was relatively high (Fig. 2D and fig. S1, E and F), FcεRI is accessible to active SFKs, but its phosphorylation is constrained by constitutive tyrosine phosphatase activity. These observations are inconsistent

with the notion that inactive FcεRIγ is in some way sequestered away from phosphatases (13, 14).

CD45 and FcεRI segregate after engagement by surface-associated IgE

The dependence of FcεRI triggering on the surface attachment of monovalent ligands and the sensitivity of the receptor to constitutively active kinases and phosphatases suggested that FcεRI might be triggered by local, size-dependent phosphatase exclusion. We (37) and others (33, 42) have reported that CD45 is excluded from contacts that leukocytes form with model surfaces. We previously proposed that ligand-induced receptor triggering arises in vivo if receptors, such as the TCR, are held in phosphatase-depleted contacts by ligands, favoring phosphorylation of the receptors [the "kinetic-segregation" (KS) model; (43)].

To test whether phosphatase exclusion accompanies the engagement of FcεRI by ligands, we studied the behavior of CD45, which is expressed by mast cells and regulates FcεRI activity through both inhibitory and activatory effects (44, 45). Basal surfaces of RBL-2H3 cells were imaged by confocal microscopy, detecting FcεRI, CD45R0 (the shortest CD45 isoform), and Syk, which were tagged with SNAP-tag, HaloTag, and Citrine, respectively. For all activating surfaces, that is, His-Fcε on Ni-glass or SLBs, and TNP_{BSA}-IgE on glass, CD45 was excluded from areas containing FcεRI and Syk within 10 to 20 s of cell contact, forming exclusion zones that were 1 to 2 μm in diameter (Fig. 3, A to C; movie S1; additional example images are shown in fig. S3). Recruitment of Citrine-labelled Syk to regions of FcεRI accumulation (fig. S4A), similarly to the recruitment of ZAP70 to the TCR (37), was taken to be evidence of receptor triggering and phosphorylation: photo-bleaching analysis showing loss of the Citrine signal (fig.

S4B), confirmed that Syk was localized at the membrane in FcεRI-, but not CD45-enriched areas. Cells interacting with immobile ligands (His-Fcε on Ni-glass and TNP_{BSA}-IgE on glass) formed stably organized contacts that expanded as the cells spread (Fig. 3, A and C). For TNP_{BSA}-IgE, this led to the formation of a complex network of mutually exclusive CD45- and FcεRI/Syk-enriched zones after 5 min (Fig. 3A, bottom). CD45 exclusion from FcεRI-enriched regions was also observed in cells preloaded with anti-TNP IgE before making contact with TNP_{BSA}-coated glass (fig. S4C). For cells activated on His-Fcε–presenting SLBs (Fig. 3B), the initial contacts led to synapse formation within ~5 min, as reported previously (20), in which CD45 was excluded to the peripheral regions of the contact. CD45 was also excluded from the basal plane of cells cultured on coverslips in the absence of ligand (Fig. 3D), consistent with the greater abundance of phosphorylated FcεRIγ in resting RBL-2H3 cells grown in adherent *versus* suspension culture (Fig. 1, A and B). Similarly, CD45 and FcεRI were excluded from FcεRI-enriched regions when cells made contact with PLL-coated coverslips (Fig. 3E), but more so in the case of CD45, which may account for the signal-potentiating effects of PLL (Fig. 1J). Primary human basophils that made contact with coverslips coated with the common dust mite antigen Der f 1 exhibited exclusion of CD45 from FcεRI-enriched regions if they were first loaded with anti-Der f 1 hIgE (Fig. 3F), but not when either Der f 1 or anti-Der f 1 were absent (fig. S4, D and E).

CD45 exclusion is passive

The observed segregation of CD45 and FcεRI could, in principle, be a result of signaling or effected by surface contact alone. On TNP_{BSA}-IgE–coated glass, we observed the exclusion of CD45 from FcεRI-containing regions of contact in PP2-treated RBL-2H3 cells (Fig. 4, A and B,

and fig. S5A), in which signaling was completely blocked (Fig. 4B). To confirm that CD45 exclusion was entirely passive, we examined the behavior of the tagged proteins in giant plasma membrane vesicles [(GPMVs; 46)] derived from RBL-2H3 cells. GPMVs lack cytoskeletal structures and lose normal cellular energy homeostasis but retain the membrane lipid and protein compositions of the cells from which they are derived. GPMVs produced from RBL-2H3 cells presenting fluorescently tagged FcεRI, CD45, and Syk formed regions of contact upon settling on either TNP_{BSA}-IgE-coated glass or SLBs presenting His-Fcε that were marked by the local exclusion of CD45R0 and accumulation of FcεRI (Fig. 4C and fig. S5B). These observations suggest that the exclusion of CD45 from contacts as they form is an entirely passive process.

Integrins are not required for CD45 exclusion or FcεRI triggering

Previous work on FcγR signaling in macrophages suggested that integrin activation is needed to generate a diffusional barrier that excludes CD45 from the receptor, leading to signaling (33). We tested whether this applied to FcεRI signaling in mast cells using chemical and genetic interventions. We observed very efficient exclusion of CD45 from regions of contact of RBL-2H3 cells with TNP_{BSA}-IgE–coated glass in the absence of free divalent cations, that is, after treatment with 1.5 mM EDTA in the absence of Ca^{2+} or Mg^{2+}, which abrogates the ligand binding activity of integrins [(47); Fig. 4D]. Similar results were obtained for primary basophils (fig. S6A). Similarly, CRISPR-mediated deletion of the expression of CD29 (fig. S6B), which is the most abundant β integrin subunit found in mast cells (48) and pairs with several of the most abundant α integrins present (49), had no effect on the exclusion of CD45 from contacts formed with TNP_{BSA}-IgE–coated glass (Fig. 4E). The degree of exclusion within seconds of contact was

comparable to that in WT cells (Fig. 4F and movie S2), with the cells progressing to also form the characteristic networks of mutually-excluding FcεRI and CD45 accumulation zones.

WT cells tested in divalent cation–free conditions and CD29-ve cells also produced robust Ca^{2+} responses. On TNP_{BSA}-IgE-coated glass (Fig. 4G) and across a range of IgE concentrations (fig. S6C), the triggering fraction was reduced by only ~15% for CD29-ve cells (compared to WT) due to a slight increase in the lag time preceding triggering (fig. S6D). The RBL-2H3 cells tested in the divalent cation–free conditions exhibited a single Ca^{2+} flux of 40- to80-s duration rather than multiple fluxes of 10 to 15 s, and typically showed a reduced Ca^{2+} fluorescence peak (fig. S6E), likely due to the effects of Ca^{2+} chelation by EDTA on intracellular Ca^{2+} store replenishment. Neither EDTA nor CD29 deletion in RBL-2H3 cells impaired FcεRIγ phosphorylation (fig. S6F), and removal of divalent cations had no effect on FcεRIγ phosphorylation in primary basophils in response to Der f 1 (Fig. S6G).

Although integrins did not appear to contribute directly to CD45 exclusion or early signaling detected as Ca^{2+} fluxes, RBL-2H3 cells adhering to immobilized integrin ligands exhibit stronger degranulation and phospholipase activity than those on passivated surfaces (50, 51). FcεRI triggering by surface-bound antigen could conceivably be enhanced by integrin-mediated interactions that stabilize or increase the size of surface contacts, lowering the threshold for signaling. We tested whether RBL-2H3 cells were more sensitive to TNP_{BSA}-IgE in the presence of a peptide derived from rat laminin, which promotes mast cell surface attachment (52) by binding to CD29 in complex with α integrin subunits, such as CD49f (53, 54). Ca^{2+} responses (Fig. 4G and fig. S6C) and the amount of phosphorylated FcεRIγ (fig. S6F) in cells that made

contact with laminin peptide-coated surfaces were comparable to those observed in cells in the absence of laminin, suggesting that, at least for initial receptor signaling, there is little contribution from CD29.

Size-based CD45 exclusion drives FcεRI signaling

A likely cause of CD45 exclusion from regions of FcεRI engagement is the difference in size of IgE/receptor complexes and CD45. This is because the extracellular region of CD45R0 is 215Å (37) and the complex formed by the extracellular region of FcεRI and IgE measures ~100Å along an axis orthogonal to the plane of the plasma membrane (55). We tested this assertion by generating size-variant IgE ligand mimics composed of the short His-Fcε construct and incorporating either one or three copies of the human CD43 extracellular domain (amino acid residues 20 to 254) between the histidine tag and Fcε (generating $CD43_1$Fcε and $CD43_3$Fcε; Fig. 5A). Like His-Fcε, these proteins bound to FcεRI with affinities and specificities comparable to those of rat IgE (fig. S2, C and D). However, the relatively rigid CD43 domain(s) (56) were expected to force FcεRI to engage Fcε further from the SLB surface, reducing the effect of ligand engagement on size-dependent reorganization of kinases and phosphatases.

In contrast to the efficient exclusion observed on His-Fcε–coated surfaces (Fig. 3, B and C), CD45 exclusion was not observed in RBL-2H3 cells that made contact with surfaces presenting either mobile or immobile $CD43_1$Fcε or $CD43_3$Fcε (Fig. 5, B and C). Fewer RBL-2H3 cells produced Ca^{2+} calcium responses after contacting $CD43_1$Fcε- or $CD43_3$Fcε-functionalised surfaces compared to cells that interacted with His-Fcε (Fig. 5D); there was no measurable difference between the behaviors of cells that interacted with $CD43_1$Fcε or $CD43_3$Fcε. CD45 was

excluded from contacts formed by freshly isolated (human IgE–bound) primary human basophils with glass coated with mouse anti-human IgE (Fig. 5E), and much less exclusion when the basophil-surface 'gap' was increased by coating the anti-human IgE indirectly onto the surface using donkey anti-mouse IgG (fig. S6H), despite the densities of anti-human IgE being comparable (fig. S6I). Moreover, primary basophils that interacted with a surface coated with anti-hIgE had an increased abundance of phosphorylated FcεRI than did cells that made contact with anti-hIgE/anti-mouse IgG–coated glass (Fig. 5F).

These observations suggest that FcεRI is triggered by CD45 exclusion, at least for surfaces presenting compact FcεRI ligands, that is, ~100 Å, the size of His-Fcε. Whereas we relied heavily on Ca^{2+} signaling as a reporter of FcεRI triggering *per se*, it seemed possible that the extent of signaling we observed due to CD45 exclusion comprised a background or sub-threshold response that was insufficient to trigger the important effector functions of mast cells. We therefore tested whether mast cell degranulation in response to surface-presented antigen is also dependent on phosphatase exclusion. We observed that mast cell degranulation was no higher than background levels for the $CD43_1Fc\varepsilon$ and $CD43_3Fc\varepsilon$ ligand mimics presented in either mobile or immobile forms (Fig. 5G). Immobile His-Fcε induced approximately three-fold greater degranulation than did mobile His-Fcε, perhaps due to the contact-stabilizing effects of glass-bound Ni^{2+} in the manner of PLL (36).

FcεRI triggering relies on the large extracellular domain of CD45

As a final test of the sensitivity of FcεRI to local, size-based exclusion of CD45, we tested whether signaling was dependent on the size of CD45 itself, as in the case of TCR-driven

signaling (57, 58). We stably transfected RBL-2H3 cells with plasmids expressing chimeric forms of CD45 consisting of the transmembrane and intracellular regions of rat CD45 and the extracellular domains of either CD43 or CD86 (generating CD43CD45 and CD86CD45, respectively). CD43 has a mucin-like extracellular domain comparable in size to those of the longer CD45 isoforms [~400Å; (56)], whereas CD86 is much shorter [~75Å; (59); Fig. 6A]. After expression in RBL-2H3 cells, each form of CD45 was detected through a C-terminal HaloTag, together with FcεRI labeled with a SNAP-tag, and Syk tagged with Citrine. As observed for CD45R0 (Fig. 3D), CD43CD45 exhibited partial exclusion from FcεRI-enriched regions on the basal surface of cells cultured on glass for 24 hours, whereas CD86CD45 did not (Fig. 6, B and C). Measurement of the local concentration of CD45 molecules by fluorescence correlation spectroscopy indicated that there was 3- to 4-fold depletion of CD45R0 and CD43CD45 from the basal surface relative to the apical surface, whereas CD86CD45 was equally distributed at both sites (Fig. 6D).

Truncation of its extracellular domain altered the distribution of CD45 on activating surfaces. CD43CD45, but not CD86CD45, was excluded from FcεRI-enriched regions on TNP_{BSA}-IgE-coated glass, to an extent comparable to that of CD45R0 (Fig. 6, E to G, fig. S7, A and G, and movie S3). The ratio of CD45 fluorescence outside *versus* inside regions of FcεRI fluorescence was ~1 for CD86CD45 and > 1 for CD45R0 and CD43CD45 (Fig. 6F). Indeed, CD43CD45, which is larger than CD45R0, was slightly more excluded (Fig. 6F). Mast cells typically express CD45 isoforms larger than CD45R0 (60), and so native CD45 segregation may be more efficient than that we observed. Transfection of RBL-2H3 cells with vector expressing CD86CD45 reduced the number of cells producing Ca^{2+} responses within 10 min of making contact with

either mobile or immobile His-Fcε by ~two-fold versus CD45R0- or CD43CD45-expressing cells (Fig. 6H). Although the fraction of responding cells was unaffected by CD86CD45 for cells that made contact with TNP_{BSA}-IgE–coated glass (Fig. 6H), the triggering lag time was statistically significantly increased (fig. S7, C to E). CD86CD45-expressing cells also exhibited a reduced abundance of phosphorylated FcεRIγ upon making contact with His-Fcε, but not TNP_{BSA}-IgE (Fig. 6I), and were less efficient at degranulation (fig. S7B). Expression of CD86CD45 but not CD43CD45 also reduced cell adhesion strength, suggestive of reduced basal FcεRI triggering (fig. S7F).

FcεRI triggering by unilamellar vesicles

To confirm that signaling could in principle be driven by passive phosphatase exclusion alone, we tested whether signaling was initiated by unilamellar vesicles presenting FcεRI ligand mimics. Both large and giant unilamellar vesicles (LUVs and GUVs) enable ligand mimics to be presented under conditions more reflective of the membrane curvature and lower resistance to deformational forces of cells versus SLBs (61). GUVs are similar in size or smaller than whole cells but mimic cell-cell associations, whereas LUVs are typically smaller than 2 μm in diameter and so more closely replicate interactions with smaller structures, for example, fragments of opsonized cells or large allergens, such as pollen grains or microvilli. Both exclusion of CD45 and enrichment of FcεRI and Syk were observed at contacts between RBL-2H3 cells and either GUVs or LUVs loaded with His-Fcε (Fig. 7A). Exclusion of CD45 was once again impaired either by truncation of its extracellular domain or by extension of the His-Fcε ligand mimic (fig. S7H). In both cases, Syk recruitment was reduced accordingly, despite the accumulation of comparable amounts of FcεRI.

DISCUSSION

For more than 40 years, FcεRI triggering was considered to be adequately explained by ligand-induced receptor aggregation; however, more recent findings have challenged this view. Principle among these is the observation that some of the best-studied allergens are monovalent (e.g. 23, 24) and that monovalent ligands provoke vigorous mast-cell activation when immobilized on model surfaces (20, 21). Here, we showed that, in the first instance, FcεRI phosphorylation was kept under tonic control by the local balance of kinase and phosphatase activities, which are affected by various factors in addition to receptor aggregation. In this context, the ability of surface-immobilized, monovalent ligands to induce signaling can be explained simply by the exclusion of large phosphatases from regions of FcεRI-ligand engagement. Supporting this view, we went on to show that (i) CD45 was excluded at sites of ligand engagement and Syk recruitment (that is, sites of receptor phosphorylation) after RBL-2H3 cells and primary basophil made contact with ligand-presenting surfaces; (ii) that this effect was size-dependent, that is, that CD45 exclusion and signaling were each abrogated either by increasing the size of the ligand or by reducing the size of the extracellular domain of CD45; (iii) that preventing CD45 exclusion from FcεRI-enriched regions inhibited triggering and degranulation in response to monovalent, surface-associated ligand; and (iv) that the exclusion of CD45 was entirely passive, that is, it occurred both in the absence of signaling in intact cells and spontaneously in GPMVs devoid of any active metabolism or ATP. The strongest argument that signaling does not only depend on ligand-driven FcεRI aggregation is that we observed strong activation of RBL-2H3 cells and primary human basophils on surfaces coated with PLL, which

appears only to be capable of immobilizing receptors and efficiently excluding CD45 from regions of contact (36).

We, and others, have shown that the TCR can be triggered by the passive, size-dependent exclusion of inhibitory phosphatases from sites of ligand engagement (37, 43, 62). Our findings here indicate that FcεRI can be triggered in an analogous manner. Mast cells form a degranulatory synapse upon encountering monovalent, surface-associated ligand (20), resulting in degranulation in the direction of FcεRI signaling (63), which enables a focused, targeted response to pathogens with surface-presented antigens. Given that basophils and mast cells form stable contacts with T cells and dendritic cells (64-66), phosphatase exclusion–dependent receptor triggering likely contributes to optimal basophil and mast cell responses *in vivo*. Our observation of low-level FcεRI triggering in cells that made contact with tissue-culture plastic may explain why increased cell adherence correlates with greater sensitivity to antigen (50, 51, 67), and why RBL-2H3 cells grown in suspension have altered protein expression (68) and pharmacological responses (69) compared to those of adherent cells. Signaling in the absence of FcεRI ligands may occur alongside, or even amplify, the effects of other factors that increase mast cell activity due to adhesion, including activation of focal adhesion kinase (70), integrins (51), or receptor tyrosine kinases (71). Nonetheless, such surface-dependent phosphorylation of FcεRI in the absence of ligands appears to be distinct from surface-driven, adhesion-based amplification of FcεRI-triggering dependent signaling. Our finding that FcεRI triggering is not exclusively dependent on the presence of ligands establishes clear ground between ligand-only theories of signaling and explanations that are not explicitly ligand-dependent, such as segregation-based theories.

In this context, it is noteworthy that FcεRI seems to form the smallest possible complexes with its ligands. FcεRIα comprises a strikingly bent structure, such that the IgE-binding domain is located close to the proximal membrane (72). IgE also forms a curved structure and uses an FcεRIα-binding site located next to the hinge-region of the antibody, helping to minimize the distance between the mast cell membrane and the IgE Fab regions (55). These observations suggest that the small size of the complex formed by FcεRI with its ligands is important for its function, perhaps because it facilitates phosphatase exclusion. For a triggering system that relied on transphosphorylation, the most efficient structure for FcεRI would be one that minimizes its hydrodynamic diameter, enabling the closest approach of neighboring receptors. Simple modeling implies that this would be achieved by FcεRI extending directly from the membrane and binding IgE in such a way as to position the Fc orthogonal to the plane of the membrane. However, such a conformation would increase the membrane-Fab separation distance by 5 to 10 nm, likely preventing phosphatase exclusion. FcγRI adopts a similarly bent conformation and binds to the same region of IgG Fc (73), suggesting that for this receptor, the dimensions of the ligand-bound complex might also be pivotal. Together, the topological arguments appear to strengthen the case that an evolutionarily conserved, size-dependent, phosphatase exclusion–based mechanism might drive signaling by Fc receptors.

Studies indicating that FcγR signaling in macrophages also depends on CD45 exclusion are conflicting with regard to whether redistribution of the phosphatase is passive (74) or dependent on integrins first forming an actin-tethered diffusional barrier (33). We did not observe any integrin-dependence of FcεRI signaling. First, neither disrupting integrin activity with a chelating

agent nor depletion of CD29, the major integrin β subunit expressed by RBL-2H3 cells, substantially affected FcεRI sensitivity to surface-bound ligand. Second, we observed passive CD45 exclusion and receptor triggering in cells interacting with SLBs that presented FcεRI ligand mimics and with both LUVs and GUVs. Finally, we observed CD45 exclusion in GPMVs which, lacking active cytoskeletons, are incapable of mobilizing any form of actin-tethered diffusional barrier. The chemical and genetic interventions we used have their caveats insofar as CD29 deletion does not globally impair integrin function, and removal of free divalent cations does not physically eliminate integrins from the cell. Nevertheless, the sum of our data argues against there being a strict requirement for integrin mobilization to secure phosphatase exclusion. The findings of Freeman *et al*. also raise the issue of what is it that "triggers the trigger", that is, integrin activation, enabling FcγR signaling (33). At the very least, our results suggest that integrin-dependent phosphatase exclusion is not a universal feature of FcR triggering.

Although the case for phosphatase exclusion–based signaling appears to be strong, it needs also to be acknowledged that the role of CD45 in the activation of mast cells is complicated by the fact that it both dephosphorylates ITAMs in activated receptors and activates SFKs by reversing inhibitory phosphorylation at regulatory sites (75). Despite strenuous efforts to understand the role of CD45 in FcεRI signaling, the matter is still incompletely resolved. It has been reported that CD45 is not required for FcεRI phosphorylation or Syk activation in response to receptor aggregation (76), but it is unclear whether this reflects only partial abrogation of SFK activity in the CD45-deficient cells. Crosslinked FcεRI is also proposed to be sequestered into ordered membrane domains with higher kinase activity (14) and reduced phosphatase (including CD45) activity, leading to signaling (13), but other data suggest that rates of dephosphorylation are

comparable for receptors in different membrane domains (77), perhaps because such domains are very short-lived (78). The role of CD45 is therefore very complex, and at present, for example, we cannot rule out the formal possibility that SFKs are activated (through the dephosphorylation of inhibitory tyrosines) in regions abundant in excluded CD45, and that these kinases then diffuse into CD45-depleted areas to promote ligand-dependent and -independent FcεRI signaling.

There is also no denying the very potent effects of soluble, multivalent ligands on FcεRI-mediated signaling. These types of ligands would not be expected to substantially affect phosphatase distribution *per se* (consistent with previous observations; 79), except insofar as crosslinking might lead to the formation of clusters of FcεRI-IgE-antigen that are too dense to allow passive CD45 entry, which could heighten the sensitivity of FcεRI to Lyn. However, even if this is not the case, the two mechanisms need not be mutually exclusive. Aggregation-driven FcεRI triggering likely occurs through local increases in kinase (*i.e.* Lyn) density (12) in a manner analogous to growth-factor induced signaling, which is simply the mirror-image of the local exclusion of inhibitory phosphatases. As we have suggested elsewhere (43), perhaps the common principle is that signaling is achieved no matter how the local balance in kinase and phosphatase activities is perturbed in favor of the kinases.

We propose that an overlap in the triggering mechanisms would enable them to act side-by-side, maximizing the versatility of FcεRI responses to antigens, depending only on their valency and mode of presentation (Fig. 7B). Some antigens are soluble, multimeric proteins that presumably cannot induce phosphatase exclusion but would be capable of FcεRI aggregation. Others may

induce responses principally by excluding phosphatases and may be unable to crosslink FcεRI. Moreover, some antigens may use both mechanisms if they accumulate into aggregates of a sufficient size that they become an effective surface, for example, large aggregates of cytoskeletal proteins, such as the common helminth allergens tropomyosin and paramyosin (80). A capacity for phosphatase exclusion–based receptor triggering may increase the scope for polyclonal IgEs to induce robust responses, because some binding geometries unable to efficiently crosslink the receptor might instead exclude phosphatases in the manner of adhesion proteins, also increasing versatility.

Which triggering mechanism(s) could dominate *in vivo* is difficult to predict. An obvious requirement of the phosphatase exclusion–based mechanism is that IgE-targeted antigens must be surface-associated. Mast cells respond to surface-bound IgE by forming a secretory synapse *in vitro* (63), but it is unclear how commonly surface-associated IgE is presented *in vivo*. Very few protein families (~2%) comprise allergens (80, 81) and they have no shared structural folds (82). However, a shared feature of many common allergens is the ability to bind to cell membranes or components of the extracellular matrix. Lipid-binding activity has been observed for many allergens, including members of the largest allergen family, the prolamins (81), the major birch tree pollen antigen, Bet v 1 (83), and several of the most potent parasite allergens, for example, the fatty acid–binding nematode polyproteins (84, 85). Similarly, the principal cat allergen, Fel d 1, shares close homology with uteroglobin (86), which binds to components of the extracellular matrix (87) and cell membrane (88), whereas many common helminth allergens, for example, the secreted proteins of *Ancylostoma* (89, 90) and other venom and allergen-like proteins in a range of species (91, 92), belong to the cysteine-rich secretory protein family, at least some of which

bind to surface ion channels (93). One sixth of all known allergens are enzymes with hydrolase activity, including lipases and proteases (81) that, together with the potential to increase antigen exposure through weakening of the epithelial barrier, could conceivably form bridging interactions between FcεRI/IgE complexes and physiological surfaces. Examples include dust mite protease allergens that target proteins expressed by human cells (94), and most of the common insect venom antigens, which bind to the extracellular matrix (hyaluronidases) or cell-surface components (phospholipases) (95). The prevalence of surface-binding allergens suggests that phosphatase exclusion–based signaling could be an important factor in many mast cell and basophil responses. Furthermore, although FcεRI is primarily involved in degranulatory responses, it is also a driver of phagocytosis and antibody-dependent cellular cytotoxicity in monocytes (96), for which the IgE-targeted antigens are all surface-associated. The use of IgE in monoclonal antibody therapy has begun to show promise (97) and for this, as in the case of IgG (74), the size of target antigens may need to be a consideration given the likely requirement for phosphatase exclusion.

Our finding that FcεRI is triggered by passive phosphatase exclusion adds to the growing body of evidence that noncatalytic tyrosine-phosphorylated receptors (NTRs) might generally be triggered in this way. In other respects, signaling by this class of immune receptors, members of which are usually relatively compact, shares strikingly consistent features: ligand binding induces phosphorylation of the receptors' immunoreceptor tyrosine-based motif(s) by SFKs, enabling recruitment of SH2 domain–containing tyrosine kinases (for activatory receptors) or tyrosine phosphatases (for inhibitory receptors), which propagate the signal (98). Although best confirmed in the case of the TCR (37, 43), various NTRs are sensitive to the formation and

dimensions of close contacts, including C-type lectins (42), CD28 (99), and natural killer cell receptors (100, 101), consistent with a shared dependence on size-based, phosphatase exclusion–dependent receptor signaling. The capacity of FcεRI to also be triggered by receptor aggregation could be a refinement that enables it to respond to a uniquely broad array of ligands.

MATERIALS AND METHODS

Cell isolation, culture, and handling

RBL-2H3 cells (ATCC CRL-2256) were cultured at 37°C, 5% CO_2 in minimum essential medium eagle (MEM; Sigma-Aldrich) supplemented with 15% FCS, 4mM L-glutamine, and 1% penicillin-streptomycin-neomycin solution (Sigma-Aldrich). Twenty-four hours before imaging (or for experiments requiring suspension culture), cells were seeded at $1x10^6$/ml and incubated in 50-ml culture tubes overnight on an end-over-end rotator (6 rpm) at 37°C. Primary human basophils were isolated from leukocyte cones provided by UK NHS Blood and Transplant. Nucleated cells were separated from erythrocytes with the HetaSep aggregation agent (StemCell Technologies) as per the manufacturer's instructions. Basophils were isolated through negative selection with the EasySep Human Basophil Enrichment Kit (StemCell Technologies) and used immediately after isolation.

Cloning and stable expression of fluorescent constructs

Rat *FceR1a* was amplified from cDNA prepared from total RBL-2H3 cell RNA using the oligonucleotide primers 5'-TAGTAGACGCGTGCCACCATGGATACTGGAGGATCTGCCCGGCTG-3' and 5'-CTACTAGGTACCGCCACTCCCACCTTTTTTTTTGCCTTTTCCAGTC-3' and subcloned

into the lentiviral pHR vector upstream of a SNAP-tag-encoding sequence. The resultant construct contained a flexible Gly-Ser-Gly sequence between *FceR1a* and *SNAP-tag*. Syk-Citrine was also generated in pHR by amplification of rat *Syk* from RBL-2H3 cDNA using the primers 5'-TAGTAGACGCGTGCCACCATGGCGGGCAATGCTGTGGACAATG-3' and 5'-CTACTAGGATCCCCGTTAACCACGTCGTAGTAGTAATTG-3' and subcloned upstream of the *Citrine* sequence. Rat *CD45* was amplified from RBL-2H3 cDNA using the primers 5'-TAGTAGACGCGTGCCACCATGTATTTGTGGCTCAAACTTCTGGCC-3' and 5'-CTACTAGGTACCCCTGAGCTCGGGGTTAGAGCTGGGC-3', which was subcloned into pHR upstream of the *HaloTag* sequence. For the chimeric CD86CD45 and CD43CD45 forms, the transmembrane- and intracellular domain–encoding segments of *rCD45* were amplified using the primers 5'-CCTCCCCCAGACCACGCACTGATTATATTCC-3' or 5'-GAGAACTCACGAGGCGCACTGATTATATTCC-3', respectively, to enable overlap with the extracellular domain–encoding segments of *hCD86* and *hCD43* amplified from cDNA prepared from RNA extracted from human THP-1 cells with the primers 5'-TAGTAGACGCGTGCCACCATGGATCCCCAGTGCACTATG-3' and 5'-GGAATATAATCAGTGCGTGGTCTGGGGGAGG-3' (for *CD86*) or 5'-TAGTAGACGCGTGCCACCATGGCCACGCTTCTCCTTCTCC-3' and 5'-GGAATATAATCAGTGCGCCTCGTGAGTTCTC-3' (for *CD43*). These fragments were used in chimeric PCR reactions to generate the full-length constructs, which were then inserted into pHR upstream of *HaloTag*. For all fluorescent constructs, human embryonic kidney (HEK) 293 cells were cotransfected with pHR vectors and with pMD.G and p8.91 with Genejuice (Novagen) as per the manufacturer's instructions. Harvested lentivirus was incubated with RBL-2H3 cells in culture for 72 hours before expression of the relevant proteins was assessed by flow

cytometry. A pure population of cells expressing all constructs was then derived by fluorescence-activated cell sorting.

Cloning and purification of His-rFcε fragments

The sequence encoding rat IgE heavy chain domains C_H2-C_H4 were amplified from cDNA prepared from total rat spleen RNA using the oligonucleotide primers 5'-TAGTAGGTTTAAACTCGGAGGCGCTCGACCTGTCAACATCACCAAGCC-3' and 5'-CTACTAGAATTCCTACATGGAGGCCTGGGAGGGACGG-3'. For the short His-rFcε form, this was inserted into the pOPINEE12G vector immediately after a sequence encoding the tag N-HHHHHHSRAWRHPQFGGHHHHHH-C. The construct also encoded a heterologous secretory signal peptide (MGILPSPGMPALLSLVSLLSVLLMGCVAE) directly upstream of the His tag. For the $CD43_1$ and $CD43_3$ forms, the sequence encoding the extracellular domain of hCD43 after the native signal peptide (residues 20 to 254) was inserted either once or in three tandem repeats separated by restriction sites for *KpnI*, *XhoI*, and *PmeI*. The pOPINEE12G vectors were used to transfect Chinese hamster ovary K1 cells, which were then enriched through glutamine synthetase selection. Dilution-plated clones were assessed for expression of secreted protein by Western blotting analysis of their culture medium with anti-His_5 and those clones with the best expression were moved to large culture. Cells were cultured in T175 tissue culture flaks in the presence of 2 mM sodium butyrate for 2 weeks before the cell culture medium was harvested and extraction of the His-tagged protein was performed with Ni-NTA agarose beads (Qiagen). Extracted protein was cleaned by fast protein liquid chromatography on a superose 6, 10/300 column (GE Healthcare) and ÄKTA pure system (GE Healthcare). Samples of the proteins were

labeled using the Alexa Fluor 647 antibody labeling kit (ThermoFisher Scientific) as per the manufacturer's instructions for use in flow cytometry experiments.

CRISPR/Cas9 knockout of FcεRIα

Genomic knockout of *FceRIa* from RBL-2H3 cells was performed with the lentiCRISPR v2.0 (Addgene plasmid #52961) system (102), which was a gift from Dr Feng Zhang (Massachusetts Institute of Technology). The guide sequence 5'-ATTACACAATTGAGTATCGT-3' was ligated into the vector using *BsmBI* restriction sites. This sequence targets nucleotides 584 to 603 of rat *FceR1a*, corresponding to residues 196 to 201 of the translated protein, and has a fidelity score of 85 as determined by the CRISPR design tool (crispr.mit.edu). Lentiviral particles containing this vector sequence were generated by cotransfection of HEK 293T cells with lentiCRISPR v2.0 and with pMD.G and p8.91 using Genejuice (Novagen) as per the manufacturer's instructions. Harvested lentivirus was incubated with RBL-2H3 cells in culture for 5 days before the cell surface expression of FcεRIα was assessed by flow cytometry analysis of cells stained with Alexa Fluor 647–conjugated mouse IgE. A pure FcεRI-ve population was then derived by fluorescence-activated cell sorting. To obtain an FcεRI-restored (FcεRI+ve) RBL-2H3 line, a CRISPR-resistant FcεRIα mutant was generated by site-directed mutagenesis of the target sequence to 5'-AcTAtACgATcGAaTAcCGg-3' (mutations in lower case), which translates to the same protein sequence as that encoded by the WT gene. The mutant *FceRIa* gene was inserted into the lentiviral pHR vector and used to transduce FcεRI-ve RBL-2H3 cells as described earlier. As before, FcεRIα cell surface expression was assessed by flow cytometry and a pure FcεRI+ve RBL-2H3 population of cells was obtained by cell sorting.

CRISPR/Cas9 knockout of CD29

CD29-ve RBL-2H3 cells were generated in the same manner as that described for the FcεRI-ve RBL-2H3 cell line but using the guide sequence 5'-TCATCACATCGTGCAGAAGT-3', which targets nucleotides 178 to 197 of rat *Itgb1*. This sequence has a fidelity score of 75 (crispr.mit.edu). A pure population of cells was sorted by staining with FITC-conjugated hamster anti-rat CD29 (Biolegend; 102205).

Flow cytometry

In all cases, cells were labeled with antibody/protein at 1 μg/ml in PBS + 0.05% sodium azide for 1 hour at 4°C. Cells were washed with three times with 4 ml of cold PBS-azide before resuspension in 400 μl of PBS-azide. Fluorescence was measured with a CyAn ADP flow cytometer (Beckman Coulter). To assess cell surface integrin expression, FITC-conjugated hamster anti-rat CD29 (Biolegend; 102205) and FITC-conjugated mouse anti-rat CD49d (Biolegend; 200103) were used. For general rFcεRI staining, mouse anti-TNP IgE conjugated to Alexa Fluor 647 was used. Primary human basophils were stained with anti-CD123 FITC (Biolegend; 306005) and anti-human IgE APC (Biolegend; 325507). To assess Fcε construct binding, RBL-2H3 cells were stained with the relevant Alexa Fluor 647–labeled protein, washed, and then incubated at 37°C in 4 ml of PBS-azide for various times after washing to enable dissociation of Fcε. Cells were then pelleted and resuspended in 400 μl of PBS-azide before analysis.

Preparation of activating surfaces

For all imaging experiments, glass bottom chambers (World Precision Instruments; FD3510) were used for coating, whereas Western blotting experiments were performed in coated plastic 24-well tissue culture plates. For TNP_{BSA}-IgE–coating, surfaces were incubated with 200 μl of trinitrophenol-conjugated bovine serum albumin (TNP_{BSA}; 50 μg/ml, Insight Biotechnology) in coating buffer [50 mM Na_2CO_3, 50mM $NaHCO_3$, (pH 9.6)] overnight at 4°C. The chambers were washed three times with 200 μl of PBS before 200 μl of mouse anti-TNP IgE (5 μg/ml, unless otherwise specified; BD Biosciences; 554118) in PBS was added to the chamber and incubated at 4°C for 2 hours. Chambers were then washed three times with 200 μl of PBS and covered with 200 μl for PBS for experiments. For PLL coating, surfaces were incubated with 200 μl of 0.01% PLL for 30 min at room temperature and then washed three times with 200 μl of PBS before use. For laminin peptide coating, surfaces were coated with 200 μl of rat laminin peptide (150 μg/ml; Merck Millipore; SCR127) and TNP_{BSA} in coating buffer (50 μg/ml) overnight at 4°C. Chambers were washed and coated with IgE as described earlier. For Der f 1 coating, surfaces were coated with 200 μl of purified Der f 1 (50 μg/ml; Indoor Biotechnologies; NA-DF1-2) in coating buffer overnight at 4°C, and washed three times with 200 μl PBS before use. Before they were stimulated on these surfaces, primary basophils were loaded with human anti-Der f 1 IgE (Absolute Antibody; 1 μg/ml; Ab00132-14.0) for 10 min then washed three times with PBS. For anti-IgE coating, surfaces were coated either with 200 μl of mouse anti-human IgE (50 μg/ml; Biolegend; 325507) or donkey anti-mouse IgG (50 μg/ml; Stratech; 715-001-003 JIR) in coating buffer overnight at 4°C. Surfaces were washed three times with 200 μl of PBS and then the donkey anti-mouse–coated surfaces were incubated with mouse anti-human IgE (5 μg/ml) for 2 hours at room temperature before washing three times with 200 μl of PBS. Coating efficiency was determined with anti-human IgE labeled with the Alexa Fluor 647

antibody-labeling kit (ThermoFisher Scientific) as per the manufacturer's instructions, with fluorescence intensity at the coverslip surface measured with a Zeiss 780 LSM. SLBs were prepared as described previously (37). Briefly, glass slides were cleaned with piranha solution. Lipid mix (POPC:nickelated lipid, 96:4; 1 mg/ml) was deposited on the glass slides on a spin coater at 3000 rpm for 30 s and hydrated in HBS. His-Fcε (1 μg/ml) or equimolar equivalents of other Fcε chimeras were coated and washed as described previously (37). Ni-coated glass coverslips (Nanocs; CS-NTA-5) were coated with His-Fcε (1 μg/ml) or equimolar equivalents of other Fcε chimeras for 30 min before being washed three times with 500 μl of PBS. Coverslips were then blocked with 5% BSA for 30 min and washed three times with 500 μl of PBS.

Preparation of GPMVs

GPMVs were prepared as described previously (46). Briefly, RBL-2H3 cells were grown in 35-mm plastic cell culture petri dishes. Before GPMV preparation, cells were labeled with HaloTag and SNAP-tag probes and then washed twice with GPMV buffer [10 mM HEPES, 150 NaCl, 2 mM $CaCl_2$, (pH 7.4)] and incubated for 1 hour in GPMV buffer containing 2 mM DTT and 25 mM PFA at 37 °C. GPMVs were then imaged on activating surfaces as described earlier.

Preparation of GUVs and LUVs

GUVs were prepared through an electro-formation method. Lipid mixture (POPC:nickelated lipid, 96:4 molar ratio; 1 mg/ml) was deposited on a platinum wire and dried. the wire was then dipped into a Teflon-coated chamber filled with 300 mM sucrose. GUV formation was triggered by applying a 10-Hz AC field for 1 hour, which was followed by the application of a 2-Hz AC field for 30 min. After GUV formation, 100 μl of the GUV suspension was incubated with His-

tagged protein (1 µg/ml) for 30 min. To wash out any unbound protein, the GUV mixture was gently mixed with 1 ml of PBS and allowed to sediment for 30 min. The bottom 100-µl fraction was transferred to a new tube containing 1 ml of PBS. This process was repeated twice. GUVs were imaged in PBS as described earlier. To prepare LUVs, 50 µl of a lipid mix (POPC:nickelated lipid, 96:4 with 0.001 mol% Laurdan; 1 mg/ml) was dried in a glass vial under N_2 flow. Next, 200 µl of HBS was added to the dried lipid film, which was then vortexed for 20 s. The suspension was then sonicated for 20 min and the LUVs were loaded in the same manner as described for GUVs.

Cell labeling

Cells were incubated with TMR-HaloTag ligand and SiR-SNAPtag ligand (each at a final concentration of 0.5 µM) at 37ºC for 30 min. Cells were then washed twice with fresh prewarmed medium supplemented with FCS by centrifugation (500g for 2 min) and were incubated in fresh full medium at 37ºC for 30 min to remove unbound fluorescent ligands. Finally, the cells were washed twice by centrifugation (500g for 2 min) and resuspended in imaging medium.

Confocal and IRM imaging

Confocal images were acquired using a Zeiss 780 LSM. Labeled cells were excited at 488 nm, 561 nm, and 633 nm for Citrine, the TMR-HaloTag ligand, and the SiR-SNAP-tag ligand, respectively. All channels were acquired with different tracks to eliminate crosstalk. A 40x W (NA 1.2) objective was used to acquire images. IRM images were obtained using the same instrument with a 488-nm laser line for excitation and 470 to 505 nm for detection in the

transmission channel. Values for individual cell surface areas were determined from IRM images by measuring the number of pixels corresponding to thresholded images of each cell using the tracing tool in the ImageJ software. This was converted to μm^2 by reference to pixel size.

Fluorescence correlation spectroscopy

FCS was measured using a 40x objective (NA 1.2) on a Zeiss 780 LSM. A diffraction-limited spot was focused on the basal or apical plane of the cells and three measurements for 10 s each were taken on each point. We measured a minimum of 10 cells for each condition. The autocorrelation functions were fitted with a 2D + Triplet model to obtain the transit diffusion time and the number of particles.

Ca^{2+} imaging

RBL-2H3 cells were labeled with 4 μM Fluo-4 for 30 min at room temperature in RPMI with no supplement. Cells were then washed in PBS and resuspended at ~$1x10^6$ cells/ml in PBS. A cell suspension (50 μl) was gently added to the 200 μl of solution on imaging coverslips and image collection was begun immediately. Cells were imaged with a 10x objective (NA=0.45) on a Zeiss spinning disk confocal microscope with 488 nm laser excitation for 600 frames at 1 frame/s and an exposure time of 800 ms. All imaging was performed inside a heated cabinet at 37°C and coverslips, cells, and solutions were allowed to equilibrate to 37°C before imaging. Ca^{2+} images were analyzed with CalQuo software (103), generating a triggering fraction value for each video and a triggering frame value for each triggered cell. For experiments with PP2-treated or divalent cation–free samples, cells were labeled with Fluo-4 as described earlier and resuspended in either PBS containing 10 μM PP2 or Mg^{2+}/Ca^{2}+-free PBS containing 1.5 mM EDTA. The solution

used on the coverslip was the same as that used for cell treatment (that is, +PP2/EDTA). For experiments using soluble ligand, RBL-2H3 cells were plated onto glass coverslips at ~1x10^5/ml and cultured for 24 hours to obtain adherent cells. Cells were washed with PBS, labeled with Fluo-4, and washed as described earlier before being covered with 200 µl of PBS containing anti-TNP IgE (0.1 µg/ml) at 37°C for 10 min. Cells were washed three times with 200 µl of PBS and image acquisition was begun. At 20 frames (20 s), 20 µl of TNP_{BSA} in PBS (1 µg/ml) was added to give a final concentration of 100 ng/ml.

Cell stimulation and Western blotting analysis

Cells were treated with either 10 µM PP2 or 10 µM pervanadate for 15 min at room temperature, or with PP2 for 15 min and then pervanadate for 15 min, or *vice versa*. Pervanadate was freshly prepared using 1 mM sodium orthovanadate and 0.3% hydrogen peroxide in 20 mM HEPES for 5 min before neutralization with bovine catalase. Stimulation of RBL-2H3 cells by soluble ligand was performed by incubation with anti-TNP IgE (1 µg/ml) for 15 min at room temperature, before washing and incubating with TNP_{BSA} (100 ng/ml) for 15 min at room temperature. Primary basophils were stimulated in solution using mouse anti-human IgE (0.5 µg/ml). Cells stimulated on surfaces were allowed to settle at room temperature for various times before solublization. After stimulation, 0.5x10^6 cells in 100 µl of PBS were solublized for 20 min on ice by the addition of 10 µl of 10x RIPA buffer (Cell Signaling Technology) supplemented with 20 mM sodium orthovanadate, 30 mM EDTA-free protease inhibitors (Sigma-Aldrich; 4693132001), and 1% protease inhibitor cocktail (Sigma-Aldrich; P5726). Solublized samples were centrifuged at 14000g for 5 min to remove protein aggregates, diluted in 4x SDS protein loading buffer with 10% β-mercaptoethanol, and separated on mini-PROTEAN TGX

polyacrylamide gels (BioRad). Proteins were transferred to nitrocellulose membrane, blocked with Odyssesy blocking buffer (Li-Cor) for 3 hours, and then incubated with rabbit anti-FcεRIγ (Merck-Millipore; 06727) and mouse phopho-specific anti-FcεRIγ antibodies (34), kindly provided by Dr Ryo Suzuki, Nagoya City University, Japan. Donkey anti-rabbit IRDye 680RD (Li-Cor) and donkey anti-mouse IRDye 800CW (Li-Cor) secondary antibodies were used to enable simultaneous imaging and quantification in both channels using a Li-Cor Odyessey CLx infrared imaging system. In all experiments, a soluble triggered sample was included for normalization. All data were normalized to this value using the following equation:

$$Normalized\,\frac{pY47}{FcR}\,signal\;=$$

$$\left(\frac{pY47\ fluorescence^{sample}}{Total\ Fc\varepsilon R1\gamma\ fluorescence^{sample}}\right)/\left(\frac{pY47\ fluorescence^{soluble\ trigger}}{Total\ Fc\varepsilon R1\gamma\ fluorescence^{soluble\ trigger}}\right)$$

β-hexosaminidase release assay

RBL-2H3 cells (5 x 10^4) were allowed to settle onto activating or non-activating surfaces in a total volume of 100 µl of HEPES buffer (10 mM HEPES, 137 mM NaCl, 2.7 mM KCl, 0.4 mM $Na_2HPO_4.7H_2O$, 5.6 mM glucose 1.3 mM $MgSO_4$.7H2O, 0.04% BSA) for 30 min at 37°C without CO_2. A sample of supernatant (75 µl) was removed and centrifuged at 11,000*g* for 1 min in a 1.5-ml tube to remove any cells. Of this, 50 µl was then transferred to a well of a transparent, flat-bottomed 96-well plate. Negative control wells containing only HEPES buffer were also plated. We then added 100 µl of p-nitrophenyl N-acetyl-β-D-glucosamide (3.5 mg/ml in 40 mM citric acid), 20 mM $Na_2HPO_4.7H_2O$ (pH 4.5) to each well and incubated the samples for 90 min at 37°C without CO_2. The reaction was stopped after 90 min by the addition of 50 µl of 400 mM glycine (pH 10.7). Absorbance at 405 nm was measured using a SPECTROstar Nano

platereader. Background was established relative to the wells containing HEPES buffer alone. The percentage degranulation was calculated by reference to the absorbance at 405 nm of RBL-2H3 cells solublized with 0.1% Triton X-100, which was defined as 100%.

Measurement of cell adhesion and dendricity

Cell adhesion was measured as a function of the mechanical force required to detach cells from a cultured plastic surface. RBL-2H3 cells were plated at $3x10^5$ cells/well in a plastic 6-well plate in supplemented MEM and incubated for 24 hours. Medium containing any non-adherent cells was removed and the adherent cells were washed with 1 ml of PBS. Cells were then covered with 2 ml of PBS and placed onto a bench-top orbital shaker at varying speeds for 30 min at room temperature. After shaking, the number of detached cells in solution was counted using a hemocytometer. The remaining adherent cells were detached by incubation with trypsin and EDTA for 10 min and counted in the same manner. Spontaneous growth in suspension was determined by plating the RBL-2H3 cells at $3x10^5$ cells/well in a plastic 6-well plate in supplemented MEM and incubating them for 24 to 72 hours before assessing the suspension and adherent fractions as described earlier. Cell dendricity was determined by collecting DiC images of RBL-2H3 cell populations cultured on glass coverslips for 24 hours after plating at $3x10^5$ cells/ml. Cells were qualitatively classed as dendritic if they exhibited protruding dendrites from the main cell body, whereas those cells with roughly spherical morphologies were classed as non-dendritic.

Statistical analysis

All statistical analysis was performed using the GraphPad Prism 7.0a software. Datasets were assessed for significant differences using an unpaired two-tailed t test. For comparisons of values from individual cells (cell contact area; time to triggering; FCS data), data from all cells were pooled before analysis. For all others, an individual value was determined for each independent experiment (for example, percentage cells triggered) and these were pooled for analysis.

Supplementary Materials

Fig. S1. FcεRI-negative RBL-2H3 cells move like WT cells, and PLL leads to FcεRIγ phosphorylation in RBL-2H3 cells and primary basophils.
Fig. S2. Equivalent FcεRI-dependent binding is exhibited by all Fcε-containing ligands used for RBL-2H3 cell activation, and FcεRIγ phosphorylation in primary basophils is regulated by the global kinase-phosphatase balance.
Fig. S3. Additional examples of CD45 exclusion from the basal planes of RBL-2H3 cells on ligand-presenting surfaces.
Fig. S4. Syk is recruited to FcεRI bound to surface-associated ligand, and robust CD45 exclusion in primary basophils requires specific IgE-ligand interactions.
Fig. S5. CD45 exclusion is a passive process.
Fig. S6. Integrin activity is not required for CD45 exclusion or FcεRI-triggering in either RBL-2H3 cells or primary basophils.
Fig. S7. Reducing the size of CD45 or increasing the size of ligand impairs both CD45 exclusion and FcεRI triggering.
Movie S1. CD45 is excluded from regions of FcεR1-ligand interactions on glass.
Movie S2. CD45 exclusion is not affected by depletion of the β integrin CD29.
Movie S3. Decreasing the extracellular domain size of CD45 impairs its exclusion from regions of FcεR1-ligand interactions.

REFERENCES AND NOTES

1. Rivera, J., and A. Olivera. 2008. A current understanding of Fc epsilon RI-dependent mast cell activation. *Current allergy and asthma reports* 8: 14-20.
2. Blank, U., C. Ra, L. Miller, K. White, H. Metzger, and J. P. Kinet. 1989. Complete structure and expression in transfected cells of high affinity IgE receptor. *Nature* 337: 187-189.
3. Suzuki, R., J. Scheffel, and J. Rivera. 2015. New insights on the signaling and function of the high-affinity receptor for IgE. *Current topics in microbiology and immunology* 388: 63-90.
4. Yamashita, T., R. Suzuki, P. S. Backlund, Y. Yamashita, A. L. Yergey, and J. Rivera. 2008. Differential dephosphorylation of the FcR gamma immunoreceptor tyrosine-based activation motif tyrosines with dissimilar potential for activating Syk. *Journal of Biological Chemistry* 283: 28584-28594.
5. Metzger, H. 1978. The IgE-mast cell system as a paradigm for the study of antibody mechanisms. *Immunol Rev* 41: 186-199.
6. Metzger, H. 1977. The cellular receptor for IgE. *In Receptors and Recognition (Cuatrecasas, P., and Greaves, M. F., eds.)* 4: 75. London , Chapman & Hall.

7. Ishizaka, K., and T. Ishizaka. 1969. Immune mechanisms of reversed type reaginic hypersensitivity. *J. Immunol.* 103: 588-&.
8. Ishizaka, K., T. Ishizaka, and E. H. Lee. 1970. Biologic function of the Fc fragments of E myeloma protein. *Immunochemistry* 7: 687-702.
9. Segal, D. M., J. D. Taurog, and H. Metzger. 1977. Dimeric immunoglobulin E serves as a unit signal for mast cell degranulation. *Proc. Natl. Acad. Sci. U. S. A.* 74: 2993-2997.
10. Paar, J. M., N. T. Harris, D. Holowka, and B. Baird. 2002. Bivalent Ligands with rigid double-stranded DNA spacers reveal structural constraints on signaling by Fc epsilon RI. *Journal of Immunology* 169: 856-864.
11. Sil, D., J. B. Lee, D. Luo, D. Holowka, and B. Baird. 2007. Trivalent ligands with rigid DNA spacers reveal structural requirements for IgE receptor signaling in RBL mast cells. *Acs Chemical Biology* 2: 674-684.
12. Vonakis, B. M., H. X. Chen, H. HaleemSmith, and H. Metzger. 1997. The unique domain as the site on Lyn kinase for its constitutive association with the high affinity receptor for IgE. *Journal of Biological Chemistry* 272: 24072-24080.
13. Young, R. M., X. M. Zheng, D. Holowka, and B. Baird. 2005. Reconstitution of regulated phosphorylation of Fc epsilon RI by a lipid raft-excluded protein-tyrosine phosphatase. *Journal of Biological Chemistry* 280: 1230-1235.
14. Young, R. M., D. Holowka, and B. Baird. 2003. A lipid raft environment enhances Lyn kinase activity by protecting the active site tyrosine from dephosphorylation. *Journal of Biological Chemistry* 278: 20746-20752.
15. Kalesnikoff, J., M. Huber, V. Lam, J. E. Damen, J. Zhang, R. P. Siraganian, and G. Krystal. 2001. Monomeric IgE stimulates signaling pathways in mast cells that lead to cytokine production and cell survival. *Immunity* 14: 801-811.
16. Kashiwakura, J. I., I. M. Otani, and T. Kawakami. 2011. Monomeric IgE and mast cell development, survival, and function. *Mast Cell Biology: Contemporary and Emerging Topics* 716: 29-46.
17. Yamaguchi, M., C. S. Lantz, H. C. Oettgen, I. M. Katona, T. Fleming, I. Miyajima, J. P. Kinet, and S. J. Galli. 1997. IgE enhances mouse mast cell Fc epsilon RI expression in vitro and in vivo: Evidence for a novel amplification mechanism in IgE-dependent reactions. *Journal of Experimental Medicine* 185: 663-672.
18. Kashiwakura, J. I., Y. Okayama, M. Furue, K. Kabashima, S. Shimada, C. Ra, R. P. Siraganian, Y. Kawakami, and T. Kawakami. 2012. Most Highly Cytokinergic IgEs Have Polyreactivity to Autoantigens. *Allergy Asthma & Immunology Research* 4: 332-340.
19. Torigoe, C., and H. Metzger. 2001. Spontaneous phosphorylation of the receptor with high affinity for IgE in transfected fibroblasts. *Biochemistry* 40: 4016-4025.
20. Carroll-Portillo, A., K. Spendier, J. Pfeiffer, G. Griffiths, H. T. Li, K. A. Lidke, J. M. Oliver, D. S. Lidke, J. L. Thomas, B. S. Wilson, and J. A. Timlin. 2010. Formation of a Mast Cell Synapse: Fc epsilon RI Membrane Dynamics upon Binding Mobile or Immobilized Ligands on Surfaces. *Journal of Immunology* 184: 1328-1338.
21. Balakrishnan, K., F. J. Hsu, A. D. Cooper, and H. M. McConnell. 1982. Lipid Hapten Containing Membrane Targets Can Trigger Specific Immunoglobulin E-dependent Degranulation of Rat Basophil Leukemia Cells. *Journal of Biological Chemistry* 257: 6427-6433.
22. Volkmann, C., N. Brings, M. Becker, E. Hobeika, J. Yang, and M. Reth. 2016. Molecular requirements of the B-cell antigen receptor for sensing monovalent antigens. *Embo J.* 35: 2371-2381.
23. Chruszcz, M., M. D. Chapman, L. D. Vailes, E. A. Stura, J. M. Saint-Remy, W. Minor, and A. Pomes. 2009. Crystal Structures of Mite Allergens Der f 1 and Der p 1 Reveal Differences in Surface-Exposed Residues that May Influence Antibody Binding. *Journal of Molecular Biology* 386: 520-530.

24. Rouvinen, J., J. Rautiainen, T. Virtanen, T. Zeiler, J. Kauppinen, A. Taivainen, and R. Mantyjarvi. 1999. Probing the molecular basis of allergy - Three-dimensional structure of the bovine lipocalin allergen Bos d 2. *Journal of Biological Chemistry* 274: 2337-2343.
25. Shin, D. H., J. Y. Lee, K. Y. Hwang, K. K. Kim, and S. W. Suh. 1995. High-resolution crystal structure of the non-specific lipid-transfer protein from maize seedlings. *Structure* 3: 189-199.
26. Yang, X. J., and K. Moffat. 1996. Insights into specificity of cleavage and mechanism of cell entry from the crystal structure of the highly specific Aspergillus ribotoxin, restrictocin. *Structure* 4: 837-852.
27. Rouvinen, J., J. Janis, M.-L. Laukkanen, S. Jylha, M. Niemi, T. Paivinen, S. Makinen-Kiljunen, T. Haahtela, H. Soderlund, and K. Takkinen. 2010. Transient Dimers of Allergens. *Plos One* 5.
28. Niemi, M. H., M. Rytkonen-Nissinen, I. Miettinen, J. Janis, T. Virtanen, and J. Rouvinen. 2015. Dimerization of lipocalin allergens. *Scientific Reports* 5.
29. Sakurai, K., and Y. Goto. 2002. Manipulating monomer-dimer equilibrium of bovine beta-lactoglobulin by amino acid substitution. *Journal of Biological Chemistry* 277: 25735-25740.
30. Antens, C. J. M., M. Oldenwening, A. Wolse, U. Gehring, H. A. Smit, R. C. Aalberse, M. Kerkhof, J. Gerritsen, J. C. de Jongste, and B. Brunekreef. 2006. Repeated measurements of mite and pet allergen levels in house dust over a time period of 8 years. *Clinical and Experimental Allergy* 36: 1525-1531.
31. Custis, N. J., J. A. Woodfolk, J. W. Vaughan, and T. A. E. Platts-Mills. 2003. Quantitative measurement of airborne allergens from dust mites, dogs, and cats using an ion-charging device. *Clinical and Experimental Allergy* 33: 986-991.
32. Traidl-Hoffmann, C., T. Jakob, and H. Behrendt. 2009. Determinants of allergenicity. *Journal of Allergy and Clinical Immunology* 123: 558-566.
33. Freeman, S. A., J. Goyette, W. Furuya, E. C. Woods, C. R. Bertozzi, W. Bergmeier, B. Hinz, P. A. van der Merwe, R. Das, and S. Grinstein. 2016. Integrins Form an Expanding Diffusional Barrier that Coordinates Phagocytosis. *Cell* 164: 128-140.
34. Suzuki, R., S. Leach, B. Dema, and J. Rivera. 2013. Characterization of a Phospho-Specific Antibody to the Fc epsilon Receptor γ Chain, Reveals Differences in the Regulation of Syk and Akt Phosphorylation. *Antibodies* 2: 321-337.
35. Wang, H. F., M. La Russa, and L. S. Qi. 2016. CRISPR/Cas9 in Genome Editing and Beyond. In *Annual Review of Biochemistry, Vol 85*. R. D. Kornberg, ed. Annual Reviews, Palo Alto. 227-264.
36. Santos, A. M., A. Ponjavic, M. Fritzsche, R. A. Fernandes, J. Bernardino de la Serna, M. J. Wilcock, F. Schneider, I. Urbančič, J. McColl, C. Anzilotti, K. A. Ganzinger, M. Assmann, D. Depoil, R. J. Cornall, M. L. Dustin, D. Klenerman, S. J. Davis, C. Eggeling, and S. F. Lee. 2018. Capturing resting T-cells: perils of PLL. *Naure Immunology* 19: 203-105.
37. Chang, V. T., R. A. Fernandes, K. A. Ganzinger, S. F. Lee, C. Siebold, J. McColl, P. Jonsson, M. Palayret, K. Harlos, C. H. Coles, E. Y. Jones, Y. Lui, E. Huang, R. J. C. Gilbert, D. Klenerman, A. R. Aricescu, and S. J. Davis. 2016. Initiation of T cell signaling by CD45 segregation at 'close contacts'. *Nature Immunology* 17: 574-+.
38. Fernandes, R. A., C. Yu, A. M. Carmo, E. J. Evans, P. A. van der Merwe, and S. J. Davis. 2010. What Controls T Cell Receptor Phosphorylation? *Cell* 142: 668-669.
39. Manz, B. N., Y. X. Tan, A. H. Courtney, F. Rutaganira, E. Palmer, K. M. Shokat, and A. Weiss. 2015. Small molecule inhibition of Csk alters affinity recognition by T cells. *Elife* 4.
40. Mustelin, T., K. M. Coggeshall, N. Isakov, and A. Altman. 1990. T cell antigen receptor-mediated activation of phospholipase C requires tyrosine phosphorylation. *Science* 247: 1584-1587.
41. Secrist, J. P., L. A. Burns, L. Karnitz, G. A. Koretzky, and R. T. Abraham. 1993. Stimulatory effects of the protein tyrosine phosphatase inhibitor, pervanadate, on T-cell activation events. *J. Biol. Chem.* 268: 5886-5893.

42. Goodridge, H. S., C. N. Reyes, C. A. Becker, T. R. Katsumoto, J. Ma, A. J. Wolf, N. Bose, A. S. H. Chan, A. S. Magee, M. E. Danielson, A. Weiss, J. P. Vasilakos, and D. M. Underhill. 2011. Activation of the innate immune receptor Dectin-1 upon formation of a 'phagocytic synapse'. *Nature* 472: 471-U541.
43. Davis, S. J., and P. A. van der Merwe. 2006. The kinetic-segregation model: TCR triggering and beyond. *Nature Immunology* 7: 803-809.
44. Grochowy, G., M. L. Hermiston, M. Kuhny, A. Weiss, and M. Huber. 2009. Requirement for CD45 in fine-tuning mast cell responses mediated by different ligand-receptor systems. *Cellular Signalling* 21: 1277-1286.
45. Murakami, K., S. Sato, S. Nagasawa, and T. Yamashita. 2000. Regulation of mast cell signaling through high-affinity IgE receptor by CD45 protein tyrosine phosphatase. *International Immunology* 12: 169-176.
46. Sezgin, E., H. J. Kaiser, T. Baumgart, P. Schwille, K. Simons, and I. Levental. 2012. Elucidating membrane structure and protein behavior using giant plasma membrane vesicles. *Nature protocols* 7: 1042-1051.
47. Zhang, K., and J. F. Chen. 2012. The regulation of integrin function by divalent cations. *Celll Adhes. Migr.* 6: 20-29.
48. Motakis, E., S. Guhl, Y. Ishizu, M. Itoh, H. Kawaji, M. de Hoon, T. Lassmann, P. Carninci, Y. Hayashizaki, T. Zuberbier, A. R. R. Forrest, M. Babina, and F. Consortium. 2014. Redefinition of the human mast cell transcriptome by deep-CAGE sequencing. *Blood* 123: E58-E67.
49. Sperr, W. R., H. Agis, K. Czerwenka, W. Klepetko, E. Kubista, G. Boltznitulescu, K. Lechner, and P. Valent. 1992. Differential expression of cell surface integrins on human mast cells and human basophils. *Annals of Hematology* 65: 10-16.
50. Apgar, J. R. 1997. Increased degranulation and phospholipase A(2), C, and D activity in RBL cells stimulated through Fc epsilon R1 is due to spreading and not simply adhesion. *Journal of Cell Science* 110: 771-780.
51. Ra, C. S., M. Yasuda, H. Yagita, and K. Okumura. 1994. Fibronectin receptor integrins are involved in mast cell activation. *Journal of Allergy and Clinical Immunology* 94: 625-628.
52. Thompson, H. L., P. D. Burbelo, B. Seguireal, Y. Yamada, and D. D. Metcalfe. 1989. Laminin promotes mast cell attachment. *Journal of Immunology* 143: 2323-2327.
53. Belkin, A. M., and M. A. Stepp. 2000. Integrins as receptors for laminins. *Microscopy Research and Technique* 51: 280-301.
54. Vliagoftis, H., and D. D. Metcalfe. 1997. Characterization of adhesive interactions between mast cells and laminin isoforms: evidence of a principal role for alpha 6 integrin. *Immunology* 92: 553-560.
55. Holdom, M. D., A. M. Davies, J. E. Nettleship, S. C. Bagby, B. Dhaliwal, E. Girardi, J. Hunt, H. J. Gould, A. J. Beavil, J. M. McDonnell, R. J. Owens, and B. J. Sutton. 2011. Conformational changes in IgE contribute to its uniquely slow dissociation rate from receptor Fc epsilon RI. *Nature Structural & Molecular Biology* 18: 571-U187.
56. Cyster, J. G., D. M. Shotton, and A. F. Williams. 1991. The dimensions of the T lymphocyte glycoprotein leukosialin and identification of linear protein epitopes that can be modified by glycosylation. *Embo Journal* 10: 893-902.
57. Cordoba, S.-P., K. Choudhuri, H. Zhang, M. Bridge, A. B. Basat, M. L. Dustin, and P. A. van der Merwe. 2013. The large ectodomains of CD45 and CD148 regulate their segregation from and inhibition of ligated T-cell receptor. *Blood* 121: 4295-4302.
58. Irles, C., A. Symons, F. Michel, T. R. Bakker, P. A. van der Merwe, and O. Acuto. 2003. CD45 ectodomain controls interaction with GEMs and Lck activity for optimal TCR signaling. *Nature Immunology* 4: 189-197.
59. Schwartz, J. C. D., X. W. Zhang, A. A. Fedorov, S. G. Nathenson, and S. C. Almo. 2001. Structural basis for co-stimulation by the human CTLA-4/B7-2 complex. *Nature* 410: 604-608.

60. Virts, E., D. Barritt, E. Siden, and W. C. Raschke. 1997. Murine mast cells and monocytes express distinctive sets of CD45 isoforms. *Molecular Immunology* 34: 1191-1197.
61. Jenkins, E., A. M. Santos, C. O'Brien-Ball, J. H. Felce, M. J. Wilcock, D. Hatherley, M. L. Dustin, S. J. Davis, C. Eggeling, and E. Sezgin. 2018. Reconstitution of immune cell interactions in free-standing membranes. *J Cell Sci* 132.
62. James, J. R., and R. D. Vale. 2012. Biophysical mechanism of T-cell receptor triggering in a reconstituted system. *Nature* 487: 64-69.
63. Joulia, R., N. Gaudenzio, M. Rodrigues, J. Lopez, N. Blanchard, S. Valitutti, and E. Espinosa. 2015. Mast cells form antibody-dependent degranulatory synapse for dedicated secretion and defence. *Nature Communications* 6.
64. Perrigoue, J. G., S. A. Saenz, M. C. Siracusa, E. J. Allenspach, B. C. Taylor, P. R. Giacomin, M. G. Nair, Y. R. Du, C. Zaph, N. van Rooijen, M. R. Comeau, E. J. Pearce, T. M. Laufer, and D. Artis. 2009. MHC class II-dependent basophil-CD4(+) T cell interactions promote T(H)2 cytokine-dependent immunity. *Nature Immunology* 10: 697-U645.
65. Sokol, C. L., N. Q. Chu, S. Yu, S. A. Nish, T. M. Laufer, and R. Medzhitov. 2009. Basophils function as antigen-presenting cells for an allergen-induced T helper type 2 response. *Nature Immunology* 10: 713-U763.
66. Yoshimoto, T., K. Yasuda, H. Tanaka, M. Nakahira, Y. Imai, Y. Fujimori, and K. Nakanishi. 2009. Basophils contribute to T(H)2-IgE responses in vivo via IL-4 production and presentation of peptide-MHC class II complexes to CD4(+) T cells. *Nature Immunology* 10: 706-U754.
67. Hamawy, M. M., S. E. Mergenhagen, and R. P. Siraganian. 1993. Cell adherence to fibronectin and the aggregation of the high affinity immunoglobulin E receptor synergistically regulate tyrosine phosphorylation of 105-115-kDa proteins. *Journal of Biological Chemistry* 268: 5227-5233.
68. Grodzki, A. C. G., M. V. D. Pastor, J. F. Sousa, C. Oliver, and M. C. Jamur. 2003. Differential expression of integrin subunits on adherent and nonadherent mast cells. *Brazilian Journal of Medical and Biological Research* 36: 1101-1109.
69. Wolfe, P. C., E. Y. Chang, J. Rivera, and C. Fewtrell. 1996. Differential effects of the protein kinase C activator phorbol 12-myristate 13-acetate on calcium responses and secretion in adherent and suspended RBL-2H3 mucosal mast cells. *Journal of Biological Chemistry* 271: 6658-6665.
70. Vial, D., C. Oliver, M. C. Jamur, M. V. D. Pastor, E. D. Trindade, E. Berenstein, J. Zhang, and R. P. Siraganian. 2003. Alterations in granule matrix and cell surface of focal adhesion kinase-deficient mast cells. *J. Immunol.* 171: 6178-6186.
71. Tan, B. L., M. N. Yazicioglu, D. Ingram, J. McCarthy, J. Borneo, D. A. Williams, and R. Kapur. 2003. Genetic evidence for convergence of c-Kit- and alpha(4) integrin-mediated signals on class IAPI-3kinase and the Rac pathway in regulating integrin-directed migration in mast cells. *Blood* 101: 4725-4732.
72. Garman, S. C., B. A. Wurzburg, S. S. Tarchevskaya, J. P. Kinet, and T. S. Jardetzky. 2000. Structure of the Fc fragment of human IgE bound to its high-affinity receptor Fc epsilon RI alpha. *Nature* 406: 259-266.
73. Kiyoshi, M., J. M. M. Caaveiro, T. Kawai, S. Tashiro, T. Ide, Y. Asaoka, K. Hatayama, and K. Tsumoto. 2015. Structural basis for binding of human IgG1 to its high-affinity human receptor Fc gamma RI. *Nature Communications* 6.
74. Bakalar, M. H., A. M. Joffe, E. M. Schmid, S. Son, M. Podolski, and D. A. Fletcher. 2018. Size-Dependent Segregation Controls Macrophage Phagocytosis of Antibody-Opsonized Targets. *Cell* 174: 131-142 e113.
75. Justement, L. B. 1997. The role of CD45 in signal transduction. *Advances in Immunology, Vol 66* 66: 1-65.
76. Zhang, J., and R. P. Siraganian. 1999. CD45 is essential for Fc epsilon RI signaling by ZAP70, but not Syk, in Syk-negative mast cells. *J. Immunol.* 163: 2508-2516.

77. Peirce, M., and H. Metzger. 2000. Detergent-resistant microdomains offer no refuge for proteins phosphorylated by the IgE receptor. *J. Biol. Chem.* 275: 34976-34982.
78. Barua, D., and B. Goldstein. 2012. A Mechanistic Model of Early Fc epsilon RI Signaling: Lipid Rafts and the Question of Protection from Dephosphorylation. *Plos One* 7.
79. Mao, S. Y., and H. Metzger. 1997. Characterization of protein-tyrosine phosphatases that dephosphorylate the high affinity IgE receptor. *J. Biol. Chem.* 272: 14067-14073.
80. Fitzsimmons, C. M., F. H. Fakone, and D. W. Dunne. 2014. Helminth allergens, parasite-specific IgE, and its protective role in human immunity. *Frontiers in Immunology* 5.
81. Radauer, C., M. Bublin, S. Wagner, A. Mari, and H. Breiteneder. 2008. Allergens are distributed into few protein families and possess a restricted number of biochemical functions. *Journal of Allergy and Clinical Immunology* 121: 847-852.
82. Aalberse, R. C. 2000. Structural biology of allergens. *Journal of Allergy and Clinical Immunology* 106: 228-238.
83. Mogensen, J. E., M. Ferreras, R. Wimmer, S. V. Petersen, J. J. Enghild, and D. E. Otzen. 2007. The major allergen from birch tree pollen, Bet v 1, binds and permeabilizes membranes. *Biochemistry* 46: 3356-3365.
84. Kennedy, M. W. 2000. The nematode polyprotein allergens/antigens. *Parasitology Today* 16: 373-380.
85. Tweedie, S., W. A. Paxton, L. Ingram, R. M. Maizels, L. A. McReynolds, and M. E. Selkirk. 1993. Brugia-pahangi and Brugia-malayi - a surface-associated glycoprotein (gp15-400) is composed of multiple tandemly repeated units and processed from a 400-kDa precursor. *Experimental Parasitology* 76: 156-164.
86. Morgenstern, J. P., I. J. Griffith, A. W. Brauer, B. L. Rogers, J. F. Bond, M. D. Chapman, and M. C. Kuo. 1991. Amino acid sequence of Fel dI, the major allergen of the domestic cat: protein sequence analysis and cDNA cloning. *Proceedings of the National Academy of Sciences of the United States of America* 88: 9690-9694.
87. Chowdhury, B., Z. J. Zhang, and A. B. Mukherjee. 2008. Uteroglobin interacts with the heparin-binding site of fibronectin and prevents fibronectin-IgA complex formation found in IgA-nephropathy. *Febs Letters* 582: 611-615.
88. Gonzalez, K. D., and A. Nieto. 1995. Binding of uteroglobin to microsomes and plasmatic membranes. *Febs Letters* 361: 255-258.
89. Bethony, J., A. Loukas, M. Smout, S. Brooker, S. Mendez, J. Plieskatt, G. Goud, M. E. Bottazzi, B. Zhan, Y. Wang, A. Williamson, S. Lustigman, R. Correa-Oliveira, S. H. Xiao, and P. J. Hotez. 2005. Antibodies against a secreted protein from hookworm larvae reduce the intensity of hookworm infection in humans and vaccinated laboratory animals. *Faseb Journal* 19: 1743-+.
90. Zhan, B., Y. Y. Liu, M. Badamchian, A. Williamson, J. J. Feng, A. Loukas, J. M. Hawdon, and P. J. Hotez. 2003. Molecular characterisation of the Ancylostoma-secreted protein family from the adult stage of Ancylostoma caninum. *International Journal for Parasitology* 33: 897-907.
91. Tawe, W., E. Pearlman, T. R. Unnasch, and S. Lustigman. 2000. Angiogenic activity of Onchocerca volvulus recombinant proteins similar to vespid venom antigen 5. *Molecular and Biochemical Parasitology* 109: 91-99.
92. Tsai, I. J., M. Zarowiecki, N. Holroyd, A. Garciarrubio, A. Sanchez-Flores, K. L. Brooks, A. Tracey, R. J. Bobes, G. Fragoso, E. Sciutto, M. Aslett, H. Beasley, H. M. Bennett, J. P. Cai, F. Camicia, R. Clark, M. Cucher, N. De Silva, T. A. Day, P. Deplazes, K. Estrada, C. Fernandez, P. W. H. Holland, J. L. Hou, S. N. Hu, T. Huckvale, S. S. Hung, L. Kamenetzky, J. A. Keane, F. Kiss, U. Koziol, O. Lambert, K. Liu, X. N. Luo, Y. F. Luo, N. Macchiaroli, S. Nichol, J. Paps, J. Parkinson, N. Pouchkina-Stantcheva, N. Riddiford, M. Rosenzvit, G. Salinas, J. D. Wasmuth, M. Zamanian, Y. D. Zheng, X. P. Cai, X. Soberon, P. D. Olson, J. P. Laclette, K. Brehm, M. Berriman, and C. Taenia Solium Genome. 2013. The genomes of four tapeworm species reveal adaptations to parasitism. *Nature* 496: 57-63.

93. Yamazaki, Y., H. Koike, Y. Sugiyama, K. Motoyoshi, T. Wada, S. Hishinuma, M. Mita, and T. Morita. 2002. Cloning and characterization of novel snake venom proteins that block smooth muscle contraction. *European Journal of Biochemistry* 269: 2708-2715.
94. Schulz, O., P. Laing, H. E. Sewell, and F. Shakib. 1995. Der p I, a major allergen of the house dust mite, proteolytically cleaves the low-affinity receptor for human IgE (CD23). *European Journal of Immunology* 25: 3191-3194.
95. Ludman, S. W., and R. J. Boyle. 2015. Stinging insect allergy: current perspectives on venom immunotherapy. *J Asthma Allergy* 8: 75-86.
96. Josephs, D. H., H. J. Bax, T. Dodev, M. Georgouli, M. Nakamura, G. Pellizzari, L. Saul, P. Karagiannis, A. Cheung, C. Herraiz, K. M. Ilieva, I. Correa, M. Fittall, S. Crescioli, P. Gazinska, N. Woodman, S. Mele, G. Chiaruttini, A. E. Gilbert, A. Koers, M. Bracher, C. Selkirk, H. Lentfer, C. Barton, E. Lever, G. Muirhead, S. Tsoka, S. Canevari, M. Figini, A. Montes, N. Downes, D. Dombrowicz, C. J. Corrigan, A. J. Beavil, F. O. Nestle, P. S. Jones, H. J. Gould, V. Sanz-Moreno, P. J. Blower, J. F. Spicer, and S. N. Karagiannis. 2017. Anti-Folate Receptor-alpha IgE but not IgG Recruits Macrophages to Attack Tumors via TNFalpha/MCP-1 Signaling. *Cancer Res* 77: 1127-1141.
97. Karagiannis, S. N., M. G. Bracher, J. Hunt, N. McCloskey, R. L. Beavil, A. J. Beavil, D. J. Fear, R. G. Thompson, N. East, F. Burke, R. J. Moore, D. D. Dombrowicz, F. R. Balkwill, and H. J. Gould. 2007. IgE-antibody-dependent immunotherapy of solid tumors: cytotoxic and phagocytic mechanisms of eradication of ovarian cancer cells. *J Immunol* 179: 2832-2843.
98. Dushek, O., J. Goyette, and P. A. van der Merwe. 2012. Non-catalytic tyrosine-phosphorylated receptors. *Immunological Reviews* 250: 258-276.
99. Evans, E. J., R. M. Esnouf, R. Manso-Sancho, R. J. C. Gilbert, J. R. James, C. Yu, J. A. Fennelly, C. Vowles, T. Hanke, B. Walse, T. Hunig, P. Sorensen, D. I. Stuart, and S. J. Davis. 2005. Crystal structure of a soluble CD28-Fab complex. *Nature Immunology* 6: 271-279.
100. Brzostek, J., J. G. Chai, F. Gebhardt, D. H. Busch, R. Zhao, P. A. van der Merwe, and K. G. Gould. 2010. Ligand dimensions are important in controlling NK-cell responses. *European Journal of Immunology* 40: 2050-2059.
101. Kohler, K., S. Q. Xiong, J. Brzostek, M. Mehrabi, P. Eissmann, A. Harrison, S. P. Cordoba, S. Oddos, V. Miloserdov, K. Gould, N. J. Burroughs, P. A. van der Merwe, and D. M. Davis. 2010. Matched Sizes of Activating and Inhibitory Receptor/Ligand Pairs Are Required for Optimal Signal Integration by Human Natural Killer Cells. *Plos One* 5.
102. Sanjana, N. E., O. Shalem, and F. Zhang. 2014. Improved vectors and genome-wide libraries for CRISPR screening. *Nature Methods* 11: 783-784.
103. Fritzsche, M., R. A. Fernandes, H. Colin-York, A. M. Santos, S. F. Lee, B. C. Lagerholm, S. J. Davis, and C. Eggeling. 2015. CalQuo: automated, simultaneous single-cell and population-level quantification of global intracellular Ca2+ responses. *Sci Rep* 5: 16487.

Acknowledgments: We thank Dr Ryo Suzuki (Nagoya City University, Japan) for kindly providing the phospho-specific FcεRIγ antibody, and Dr Feng Zhang (Massachusetts Institute of Technology) for supplying Addgene plasmid #52961. **Funding:** This work was supported by the Wellcome Trust (098274/Z/12/Z to S.J.D., 100262/Z/12/Z to M.L.D., 104924/14/Z/14 to C.E., and 107375/Z/15/Z to J.H.F.) and the Kennedy Trust for Rheumatology. We further acknowledge financial support from the Wolfson Foundation, the Medical Research Council (MRC; grant MC_UU_12010/Unit Programmes G0902418 and MC_UU_12025), UK Research Councils (grant MR/K01577X/1), and Oxford internal funds (EPA Cephalosporin Fund and John Fell Fund). We especially thank the Wolfson Imaging Centre as well as the Micron Advanced Imaging Unit (Welcome Trust Strategic Award 091911) for microscopy support. E.S. was supported by EMBO Long Term (ALTF 636-2013) and Marie Skłodowska-Curie Intra-

European Fellowships (MEMBRANE DYNAMICS-627088). The Li-Cor Odyssey CLX imaging system was purchased with funding from the European Research Council (AdG 670930). **Author contributions:** S.J.D., C.E., J.H.F., and E.S. conceptualized the project; S.J.D., C.E., and M.L.D. provided management and supervision; S.J.D., C.E., J.H.F., E.S., and M.L.D. devised the experimental approach; J.H.F., E.S., M.W., and H.B. performed the experiments; J.H.F. and E.S. analyzed the data; J.H.F., S.J.D., E.S., C.E., and M.L.D. wrote the manuscript. **Competing interests:** The authors declare that they have no competing interests.

Fig. 1. Mast cells sense the presence of surfaces. (**A**) FcεRIγ phosphorylation detected on Western blots of whole-cell lysates of RBL-2H3 cells grown for 24 hours in suspension (Susp) or adherent (Adh) culture (*left*) or after contacting uncoated plastic for 0 to 15 min (*right*). The blots were incubated with anti-pY47 FcεRIγ (top) or anti-FcεRIγ (bottom) antibodies. (**B**) Anti-pY47 FcεRIγ signal relative to anti-FcεRIγ signal normalized against that for cell stimulate with anti-TNP IgE and TNP_{BSA}. Statistical significance was calculated versus non-contacting cells (0 min). (**C** and **D**) Interference reflection microscopy (IRM) images of WT, PP2-treated WT, FcεRI-ve, and FcεRI+ve RBL-2H3 cells 30 min after contacting uncoated glass in growth medium (C). The size of the contact areas of cells under the indicated conditions were quantified (D). Each spot represents a single cell. (**E** and **F**) Differential interference contrast images of WT, FcεRI-ve, and FcεRI+ve RBL-2H3 cells cultured for 24 hours on uncoated glass revealing dendritic morphology (E). The percentage of the indicated cells with a dendritic morphology was quantified (F). (**G**) Percentage of RBL-2H3 cells that grew spontaneously in suspension under normal culturing conditions. (**H**) Percentage of cells that detach at different levels of mechanical agitation. For (G) and (H), WT cells are in red; FcεRI-ve cells are in green; FcεRI+ve cells are in blue. (**I**) The contact area of RBL-2H3 cells 30 min after making contact with PLL-coated glass. Each spot represents a single cell. (**J**) The percentages of WT, FcεRI-ve, and FcεRI+ve RBL-2H3 cells that exhibited Ca^{2+} flux responses within 10 min of making contact with uncoated glass (‘glass’) or PLL-coated glass. For all bar graphs, data are means ± SD of three independent

experiments. Blots and images are representative of three independent experiments. Scale bars, 5 μm. *$P < 0.05$, **$P < 0.01$, ***$P < 0.001$; ns, not significant.

Fig. 2. FcεRI responds to immobilized ligands and is sensitive to constitutive kinase and phosphatase activities. (**A**) Percentages of RBL-2H3 cells that exhibited Ca^{2+} flux responses within 10 min of making contact with glass or SLBs functionalized with His-Fcε or TNP_{BSA}-IgE versus uncoated surfaces or in response to soluble His-Fcε. Statistically significant differences refer to differences from zero. (**B**) Normalized anti-pY47 FcεRIγ signals relative to anti-FcεRIγ signals in whole-cell lysates from RBL-2H3 cells that made contact with the indicated surfaces. Statistically significant differences are in comparison to cells at time zero. Data are from four independent experiments. (**C**) Western blotting analysis of FcεRIγ phosphorylation in RBL-2H3 cells after acute inhibition of kinase or phosphatase activity with PP2 or pervanadate (Na_3VO_4), respectively. (**D**) Quantitation of the effects measured in (C) in RBL-2H3 cells (*left*) and primary human basophils (*right*). Significances represent differences from unstimulated cells. Replicate primary basophil measurements were performed with blood from different donors. For all bar graphs, data are means ± SD of three independent experiments, unless stated otherwise. *$P < 0.05$, **$P < 0.01$, ***$P < 0.001$; ns, not significant.

Fig. 3. CD45 and FcεRI segregate following engagement of surface-associated IgE. (**A** to **E**) Left: Confocal fluorescence images of Syk, FcεRI, and CD45 at the basal surfaces of RBL-2H3 cells that had made contact with (A) TNP_{BSA}-IgE-coated glass, (B) a His-Fcε-functionalized SLB, (C) Ni-glass, (D) uncoated glass, or (E) PLL-coated glass. Timings indicate the period of contact with the surface. Right: intensity line profiles correspond to the arrows in the merged

views. (**F**) Exclusion of CD45 relative to FcεRI was observed for primary human basophils that were loaded with anti-Der f 1 IgE and then interacted with Der f 1–coated glass. Images are representative of observations made in at least three independent experiments. Replicates with primary basophils were performed with blood from different donors. Scale bars, 5 μm.

Fig. 4. CD45 exclusion is passive and independent of integrin activity. (**A**) Confocal fluorescence images of Syk, FcεRI, and CD45 at the basal surface of an RBL-2H3 cell treated with PP2 after making contact with TNP_{BSA}-IgE-coated glass (a line profile is shown in fig. S5). (**B**) Effect of PP2, as used in (A), on FcεRI triggering as measured by Ca^{2+} flux intensity. Images are 10-min maximum intensity projections for Ca^{2+} intensity scaled as a heat map; blue, low intensity; red, high intensity. (**C**) Confocal fluorescence images of Syk, FcεRI, and CD45 at the basal surface of RBL-2H3–derived GPMVs after making contact with TNP_{BSA}-IgE-coated glass (*upper*) or a His-Fcε–functionalized SLB (*lower*). (**D**) Confocal fluorescence images of Syk, FcεRI, and CD45 at the basal surface of RBL-2H3 cells after making contact for the indicated times with TNP_{BSA}-IgE-coated glass in the presence of EDTA to chelate divalent cations. (**E**) Confocal fluorescence images of Syk, FcεRI, and CD45 at the basal surface of CD29-ve RBL-2H3 cells after making contact for the indicated times with TNP_{BSA}-IgE-coated glass. (**F**) Ratio of CD45 fluorescence intensity outside (O) *versus* inside (I) areas of enriched FcεRI intensity, for WT, CD29-ve, and EDTA-treated RBL-2H3 cells. Data are means ± SD of three independent experiments, with > 5 cells assessed per experiment. (**G**) Percentages of WT, CD29-ve, and EDTA-treated RBL-2H3 cells that produced Ca^{2+} flux responses within 10 min of making contact with glass coated with TNP_{BSA}-IgE or TNP_{BSA}-IgE and rat laminin peptide. Data are

means ± SD of four independent experiments. Images are representative of observations made in at least three independent experiments. Scale bars, 5 μm. $^{**}P < 0.01$; ns, not significant.

Fig. 5. CD45 exclusion is sensitive to the size of the surface-associated ligand. (**A**) Schematic representation of CD43Fcε chimeras. (**B** and **C**) Confocal fluorescence images of Syk, FcεRI, and CD45 at the basal surface of an RBL-2H3 cell after making contact with an SLB (B) or Ni-glass (C) presenting extended $CD43_1$Fcε and $CD43_3$Fcε chimeras. (**D**) Percentages of RBL-2H3 cells producing Ca^{2+} fluxes within 10 min of making contact with an SLB or Ni-coated glass functionalized with extended $CD43_1$Fcε and $CD43_3$Fcε chimeras versus the same surfaces presenting His-Fcε. Data are means ± SD of four independent experiments. (**E**) Confocal fluorescence image of CD45 (that is, anti-CD45 Fab) at the basal surface of primary human basophils after making contact with anti-IgE–coated glass. (**F**) Normalized anti-pY47 FcεRIγ signals relative to anti-FcεRIγ signals obtained from Western blots of whole-cell lysates from primary human basophils after making contact anti-IgE conjugated directly or indirectly (through donkey anti-mouse; DaM) to glass. Data are means ± SD of three independent experiments. Resting denotes cells kept in suspension. (**G**) Percentage maximal degranulation of RBL-2H3 cells 30 min after making contact with an SLB or Ni-coated glass functionalized with extended $CD43_1$Fcε and $CD43_3$Fcε chimeras versus the same surfaces presenting His-Fcε. Data are means ± SD of four independent experiments. Images are representative of observations made in at least three independent experiments. Replicates with primary basophils were performed with blood from different donors. Scale bars, 5 μm. $^{*}P < 0.05$, $^{**}P < 0.01$, $^{***}P < 0.001$; ns, not significant.

Fig. 6. FcεRI triggering relies on the large extracellular domain of CD45. (**A**) Schematic of WT and chimeric CD45 constructs, which are colored purple to reflect their color in the fluorescence images. (**B** and **C**) Left: FcεRI and CD43CD45 (B) or CD86CD45 (C) fluorescence at the basal surface of RBL-2H3 cells cultured for 24 hours on glass. Right: line profiles of fluorescence intensity corresponding to the arrows in the images. (**D**) Local concentration, that is, the average number of molecules in the observation volume (measured by fluorescence correlation spectroscopy), for CD45 and CD43CD45 at the basal *versus* apical surfaces of RBL-2H3 cells compared to those for CD86CD45. Data are means ± SD of three independent experiments, with >3 cells analyzed per experiment. (**E**) Confocal fluorescence images of Syk, FcεRI, and CD43CD45 at the basal surface of an RBL-2H3 cell after making contact for the indicated times with TNP_{BSA}-IgE-coated glass. (**F**) Fluorescence intensity for CD45, CD86CD45, and CD43CD45 outside (O) *versus* inside (I) areas of enriched FcεRI intensity. Data are means ± SD of three independent experiments, with >5 cells assessed per experiment. (**G**) Confocal fluorescence images of Syk, FcεRI, and CD86CD45 at the basal surface of an RBL-2H3 cell after making contact for the indicated times with TNP_{BSA}-IgE-coated glass. (**H**) Percentages of RBL-2H3 cells expressing CD45, CD86CD45, or CD43CD45, that produced Ca^{2+} fluxes within 10 min of making contact with an SLB or Ni-coated glass functionalized with His-Fcε, TNP_{BSA}-IgE-coated glass, or after being incubated with soluble anti-TNP and TNP_{BSA}. Data are means ± SD of four independent experiments. (**I**) Normalized anti-pY47 FcεRIγ signals relative to anti-FcεRIγ signals for whole-cell lysates prepared from RBL-2H3 cells expressing CD45, CD86CD45, and CD43CD45 after making contact for the indicated times with Ni-coated glass functionalized with His-Fcε (*top*) or with TNP_{BSA}-IgE-coated glass (*bottom*). Data are means ± SD of three independent experiments. All images are representative of observations

made in at least three independent experiments. Scale bars, 5 μm. *$P < 0.05$, **$P < 0.01$, ***$P < 0.001$; ns, not significant.

Fig. 7. FcεRI signaling can be triggered by unilamellar vesicles. (**A**) Confocal fluorescence images of Syk, FcεRI, and CD45 at the equatorial plane of RBL-2H3 cells that interacted with GUVs (*top*) or laudan-stained LUVs (*bottom*) loaded with His-Fcε. G, GUV; L, LUV. Scale bars, are 5 μm. Images are representative of observations made in three independent experiments. (**B**) Schematic representation of the non-triggered state of the resting basophil surface (*top*) and after the triggering of FcεRI by polyvalent antigen (pAg; *middle*) or surface-associated monovalent antigen (mAg; *bottom*).

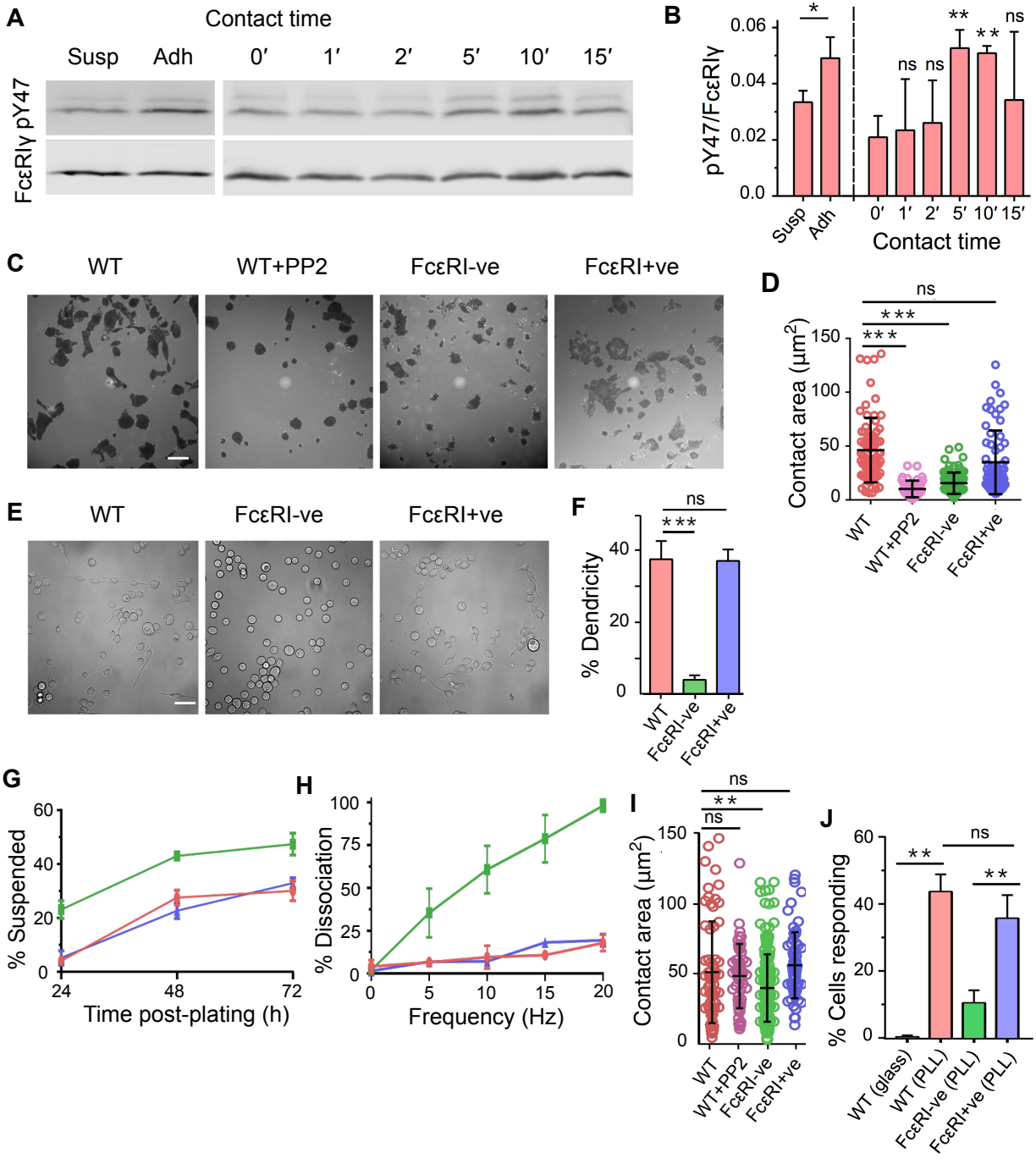
A
Contact time
Susp
Adh
0′
1′
2′
5′
10′
15′
FcεRIγ pY47
B
pY47/FcεRIγ
0.06
0.04
0.02
0.0
*
ns
ns
**
**
ns
Susp
Adh
0′
1′
2′
5′
10′
15′
Contact time
C
WT
WT+PP2
FcεRI-ve
FcεRI+ve
D
Contact area (μm2)
150
100
50
0
ns
***
***
WT
WT+PP2
FcεRI-ve
FcεRI+ve
E
WT
FcεRI-ve
FcεRI+ve
F
% Dendricity
40
20
0
ns
***
WT
FcεRI-ve
FcεRI+ve
G
% Suspended
60
40
20
0
24
48
72
Time post-plating (h)
H
% Dissociation
100
75
50
25
0
0
5
10
15
20
Frequency (Hz)
I
Contact area (μm2)
150
100
50
0
ns
**
ns
WT
WT+PP2
FcεRI-ve
FcεRI+ve
J
% Cells responding
60
40
20
0
**
ns
**
WT (glass)
WT (PLL)
FcεRI-ve (PLL)
FcεRI+ve (PLL)

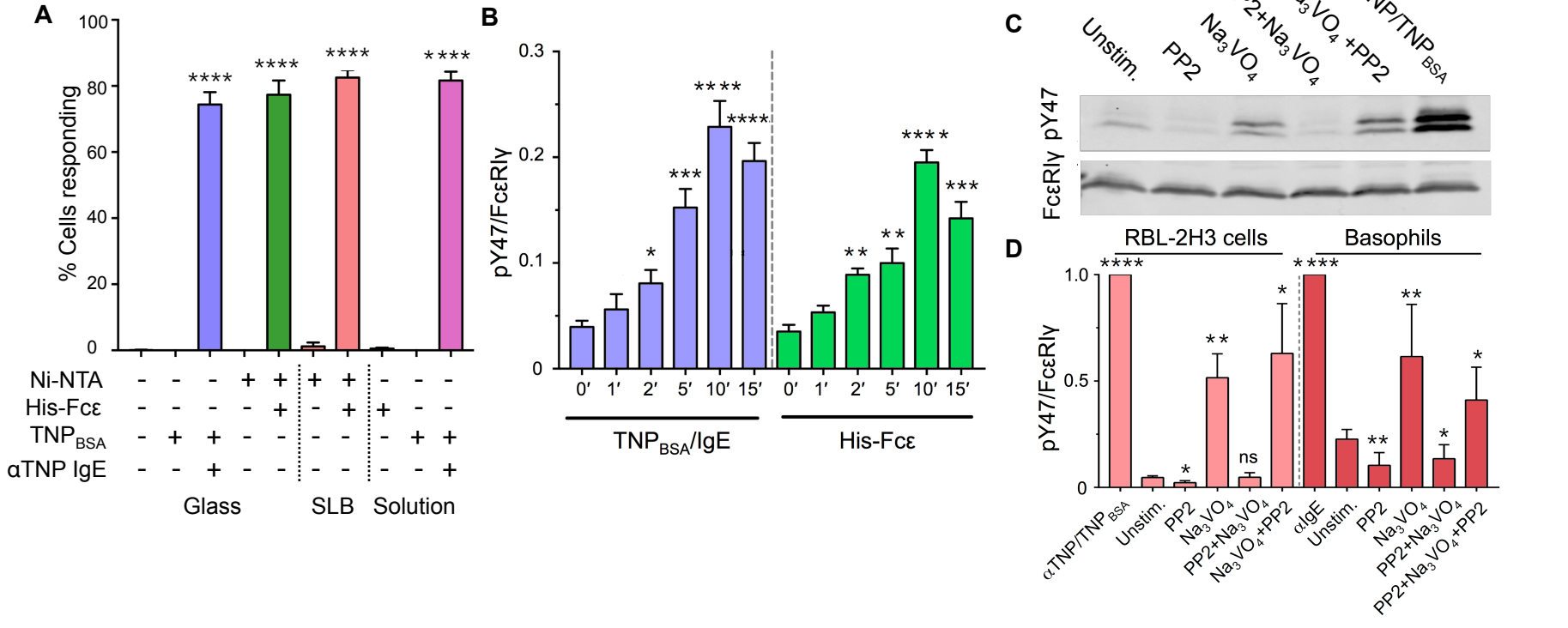
A
% Cells responding
100
80
60
40
20
0
****
****
****
****
Ni-NTA
His-Fcε
TNP$_{BSA}$
αTNP IgE
Glass
SLB
Solution
B
pY47/FcεRIγ
0.3
0.2
0.1
0
0′ 1′ 2′ 5′ 10′ 15′ 0′ 1′ 2′ 5′ 10′ 15′
TNP$_{BSA}$/IgE
His-Fcε
C
Unstim.
PP2
Na$_3$VO$_4$
PP2+Na$_3$VO$_4$
Na$_3$VO$_4$ +PP2
αTNP/TNP$_{BSA}$
FcεRIγ pY47
D
RBL-2H3 cells
Basophils
pY47/FcεRIγ
1.0
0.5
0
ns
αTNP/TNP$_{BSA}$
Unstim.
PP2
Na$_3$VO$_4$
PP2+Na$_3$VO$_4$
Na$_3$VO$_4$+PP2
αIgE
Unstim.
PP2
Na$_3$VO$_4$
PP2+Na$_3$VO$_4$
PP2+Na$_3$VO$_4$+PP2

A Glass/TNP_{BSA}-αTNP IgE

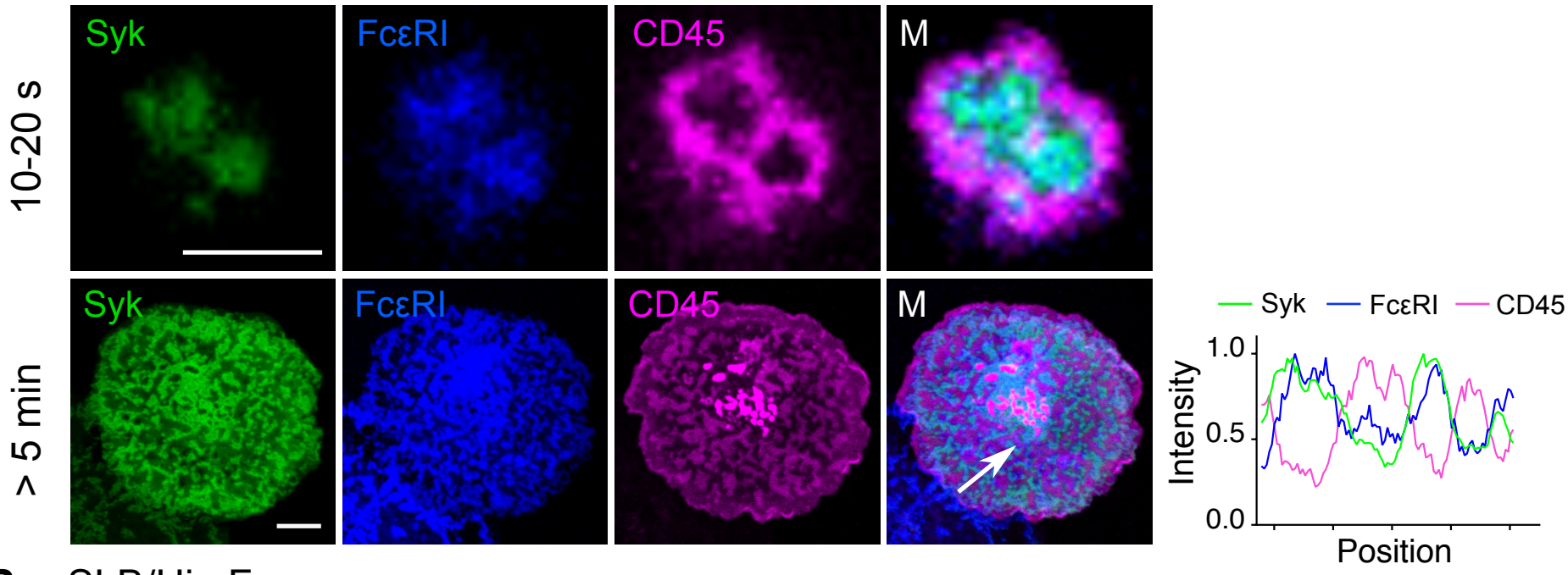

B SLB/His-Fcε

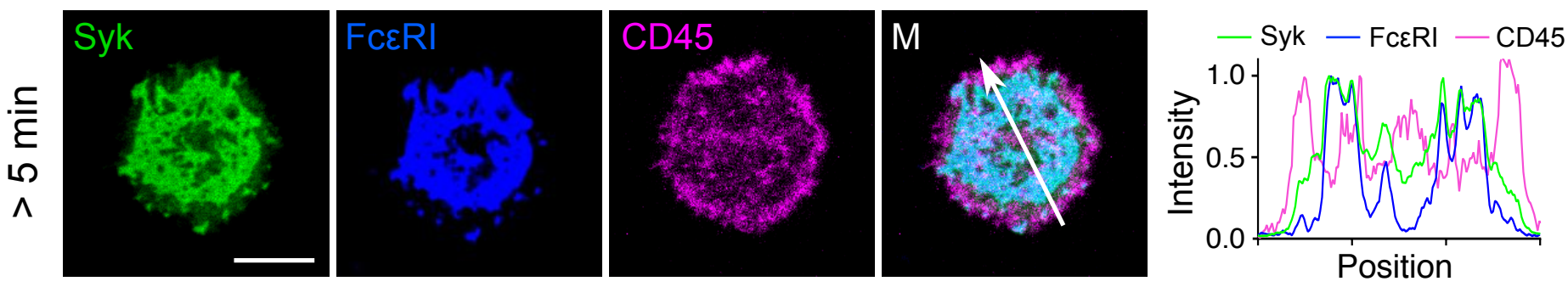

C Ni-glass/His-Fcε

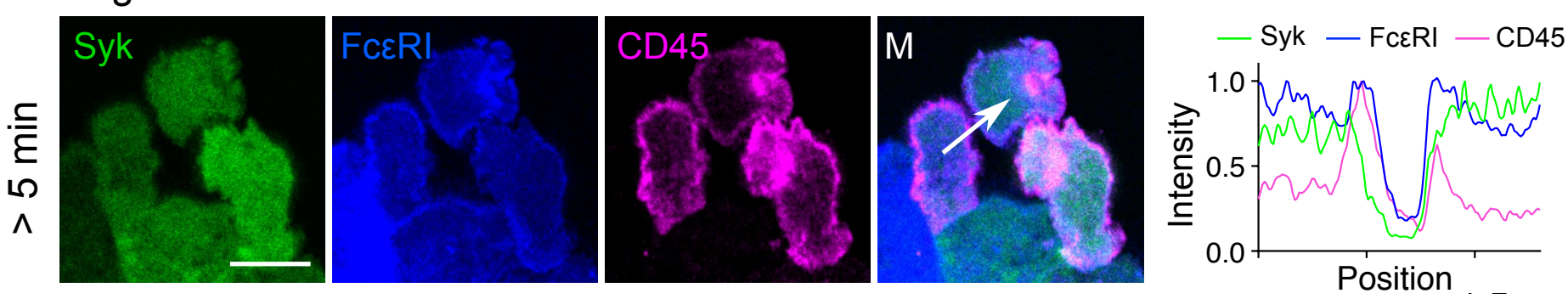

D Glass/RBL-2H3 culture

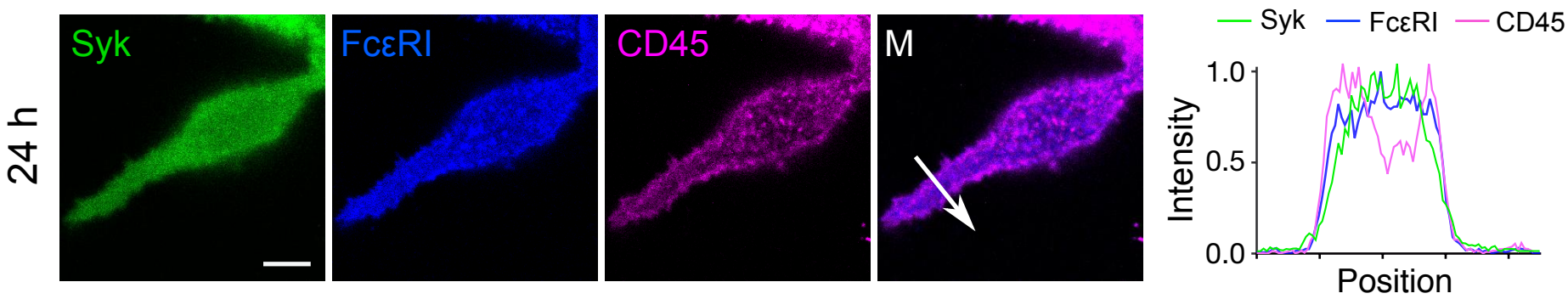

E Glass/PLL

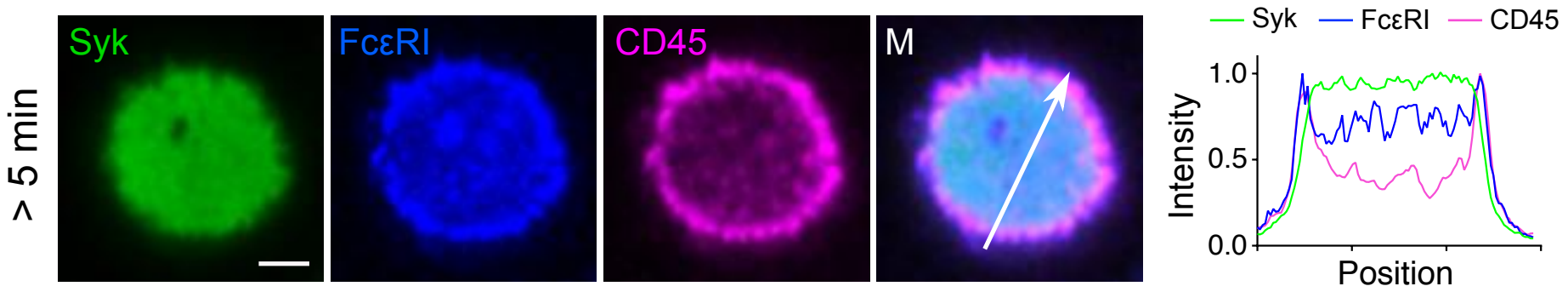

F Glass/Der f 1

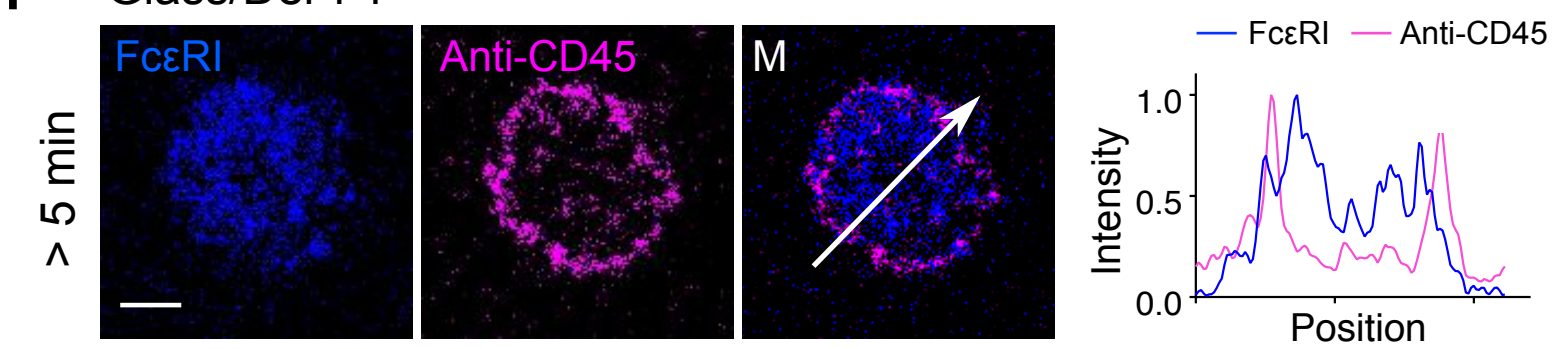

A Glass/TNP_{BSA}-αTNP IgE

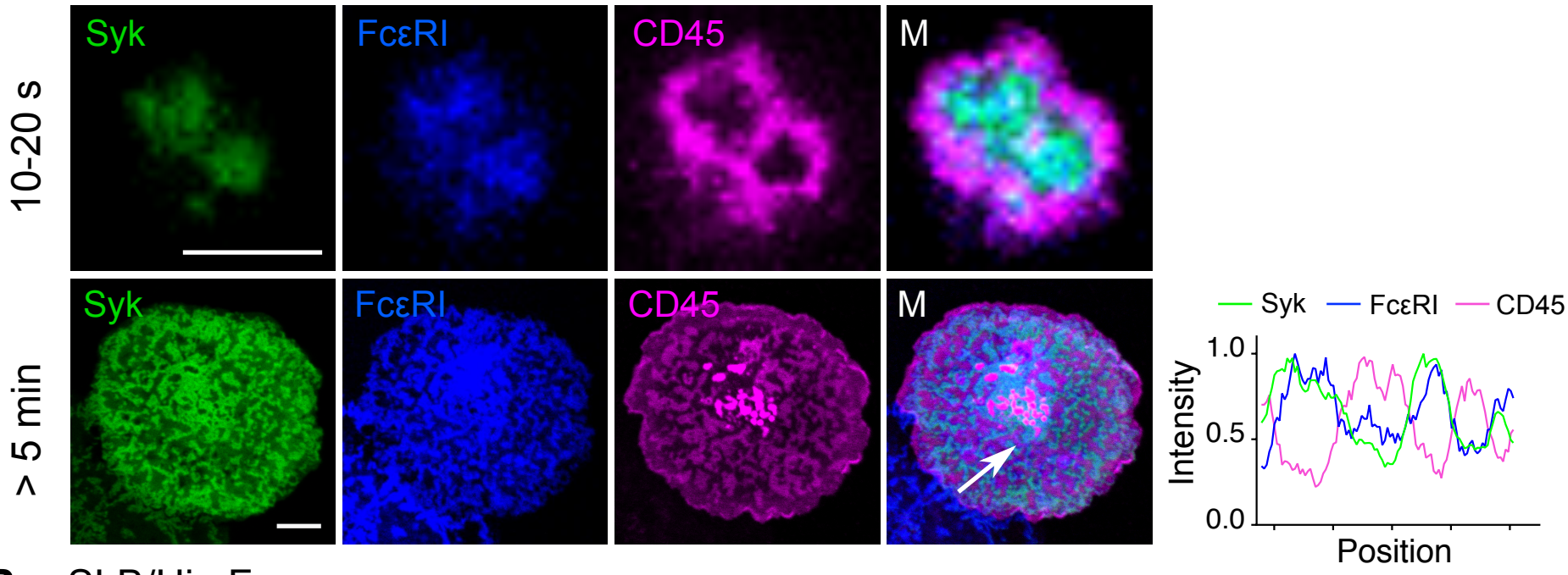

B SLB/His-Fcε

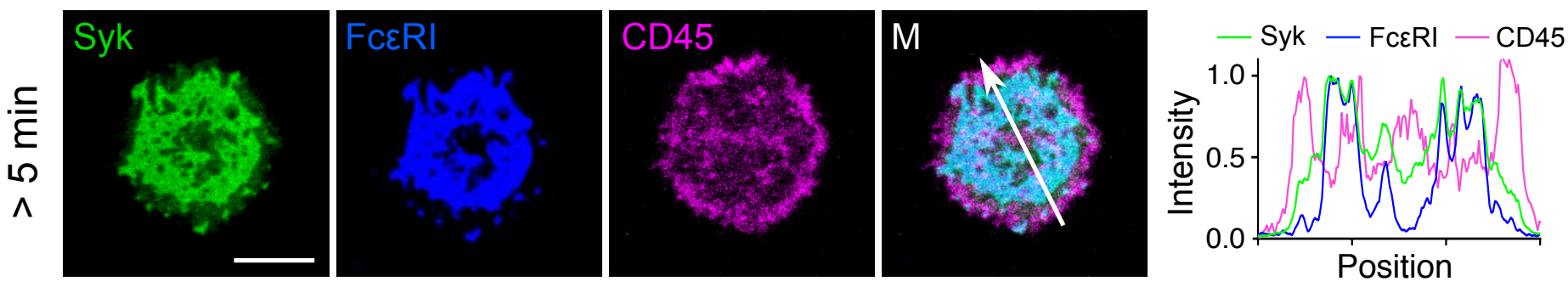

C Ni-glass/His-Fcε

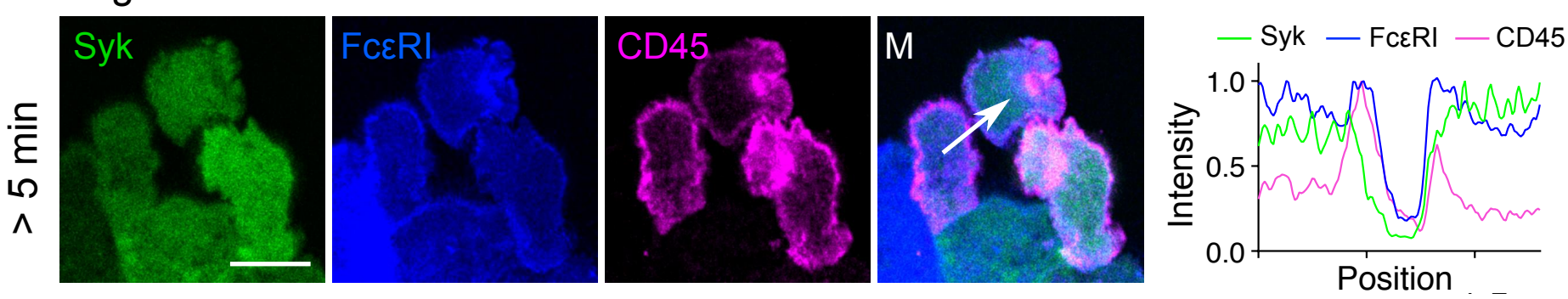

D Glass/RBL-2H3 culture

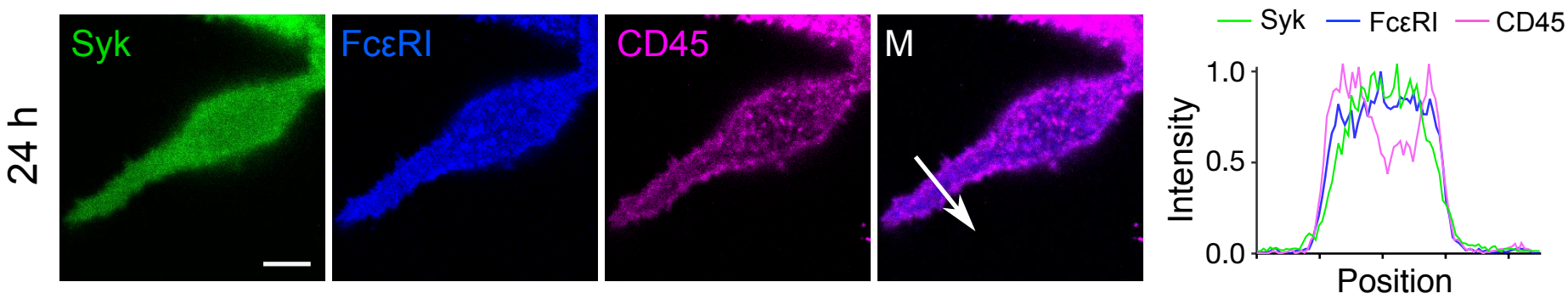

E Glass/PLL

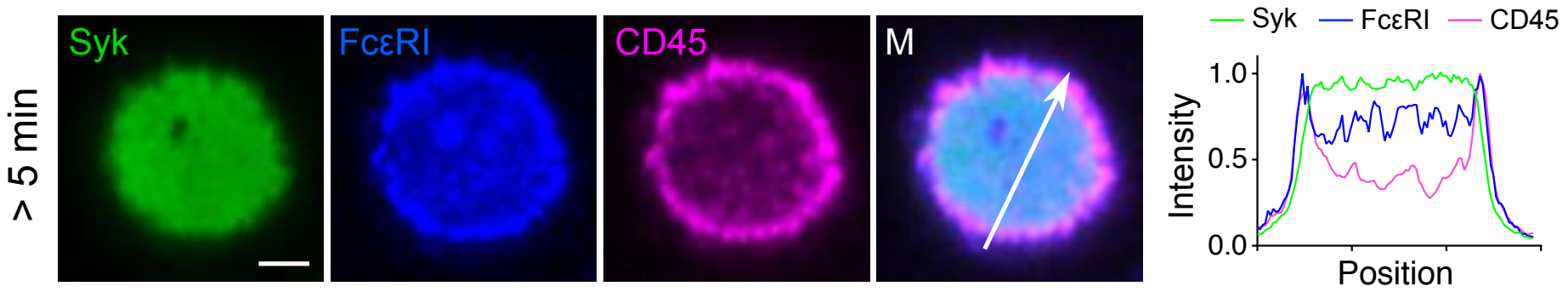

F Glass/Der f 1

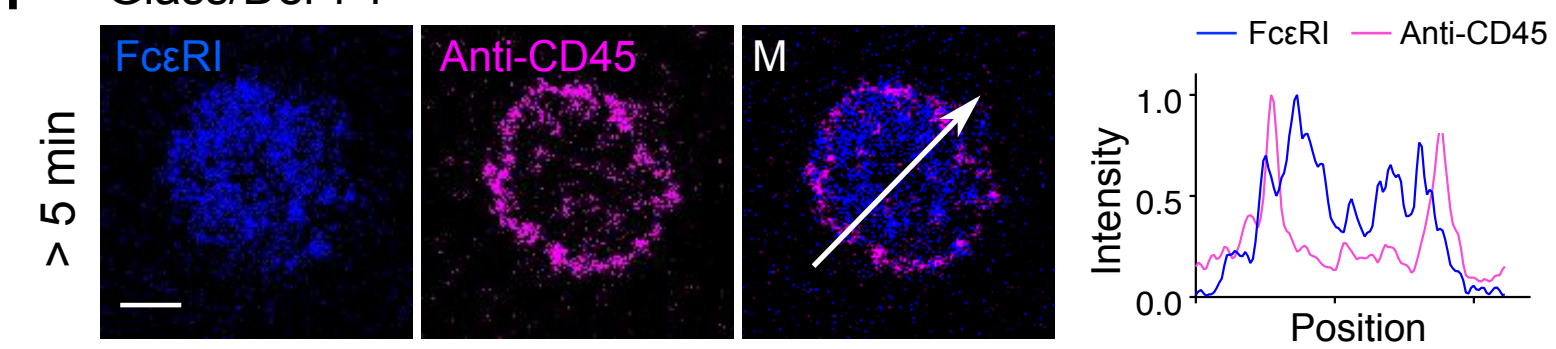

A RBL-2H3 + PP2

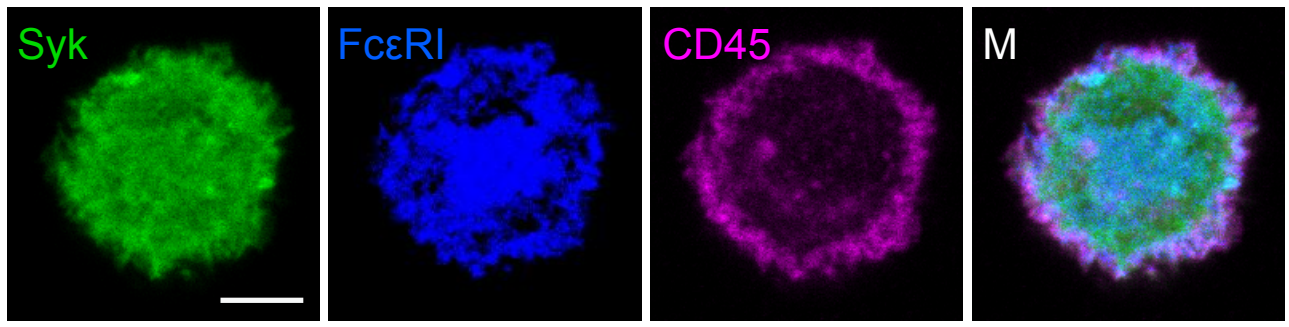

B RBL-2H3

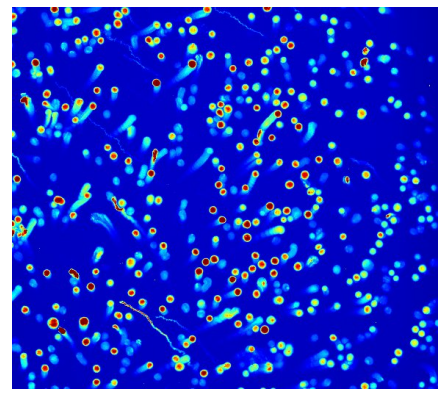

RBL-2H3 + PP2

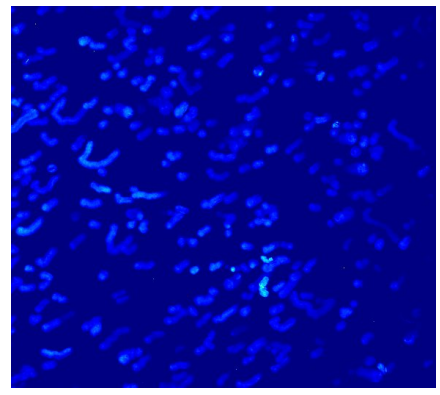

C GPMVs

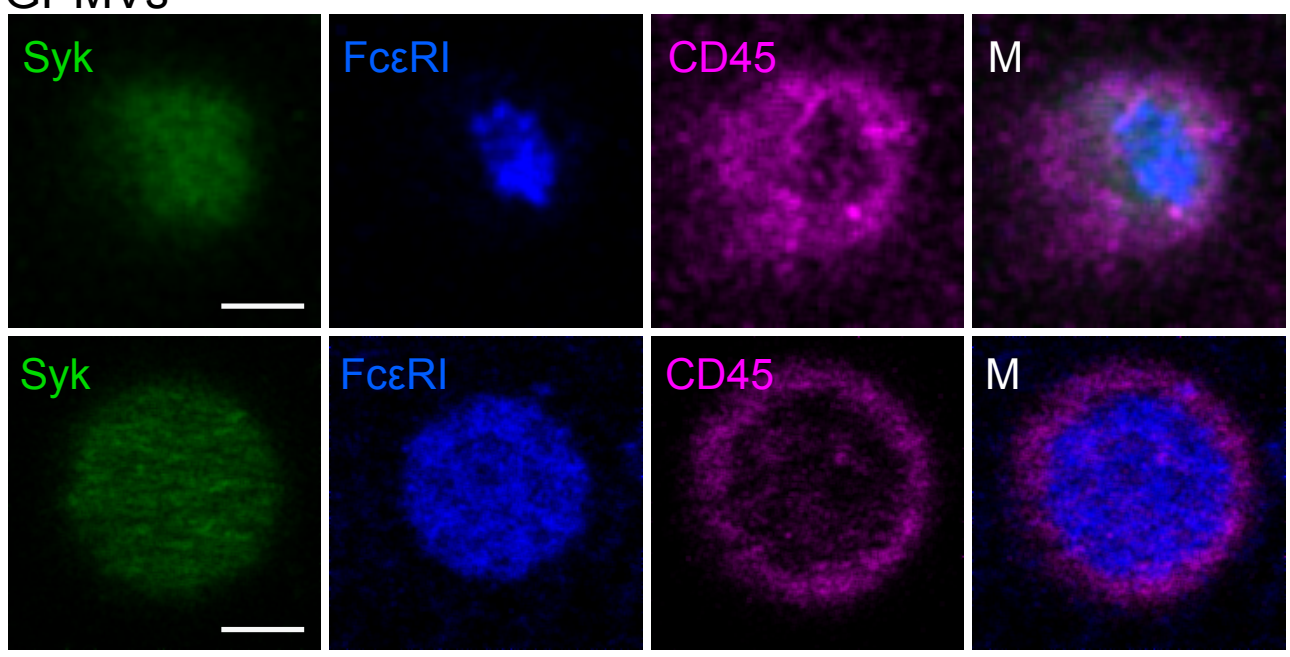

D RBL-2H3 + EDTA

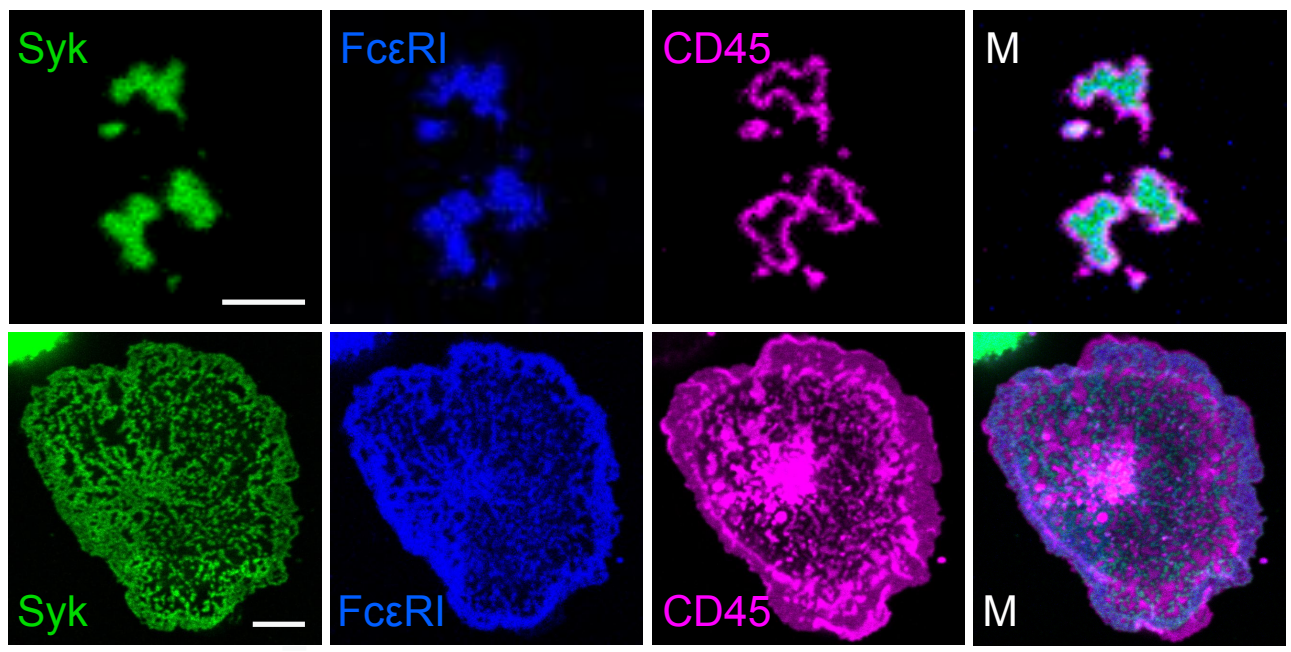

E CD29-ve RBL-2H3

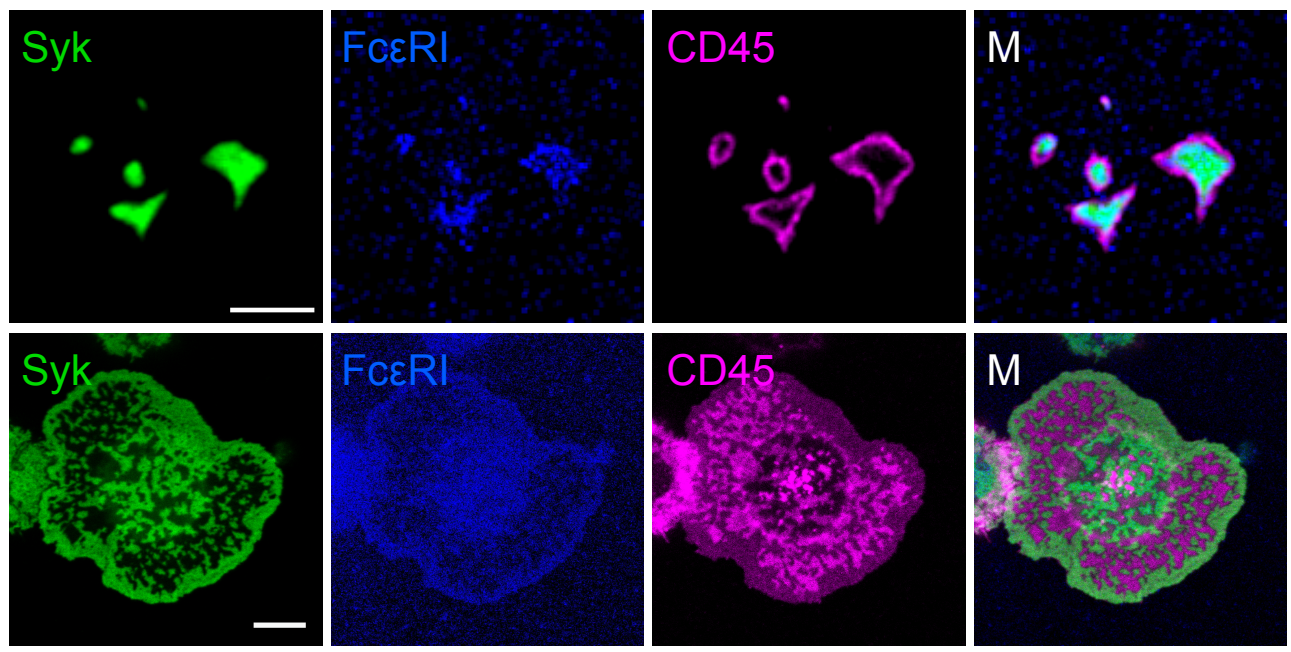

F

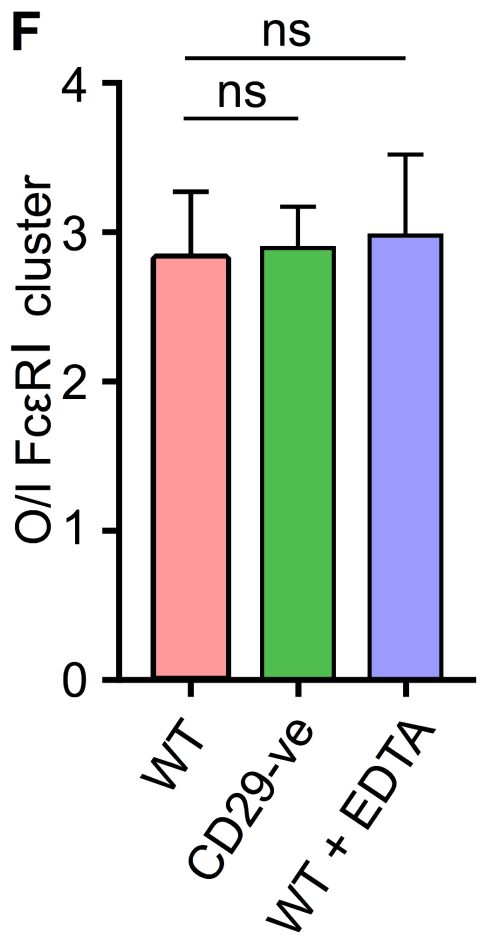

G

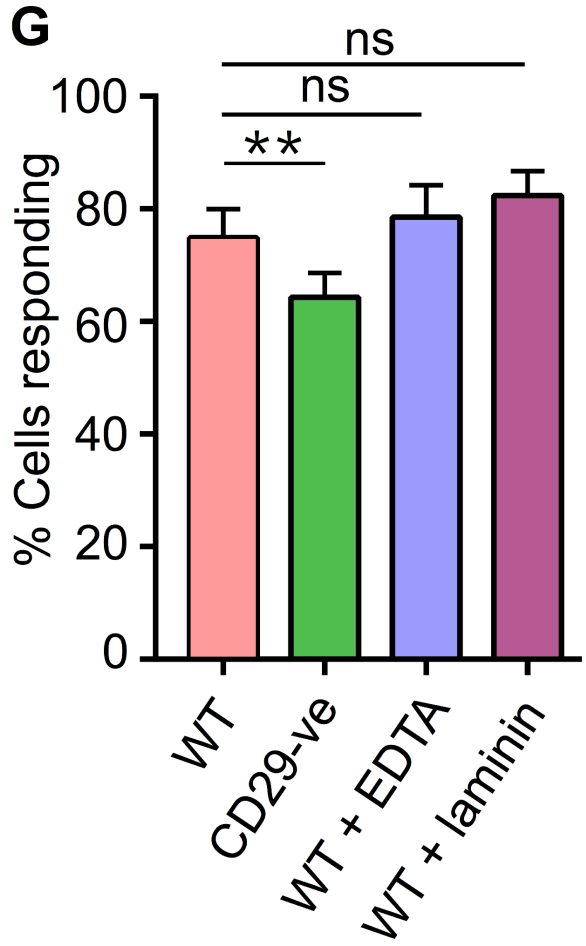

A

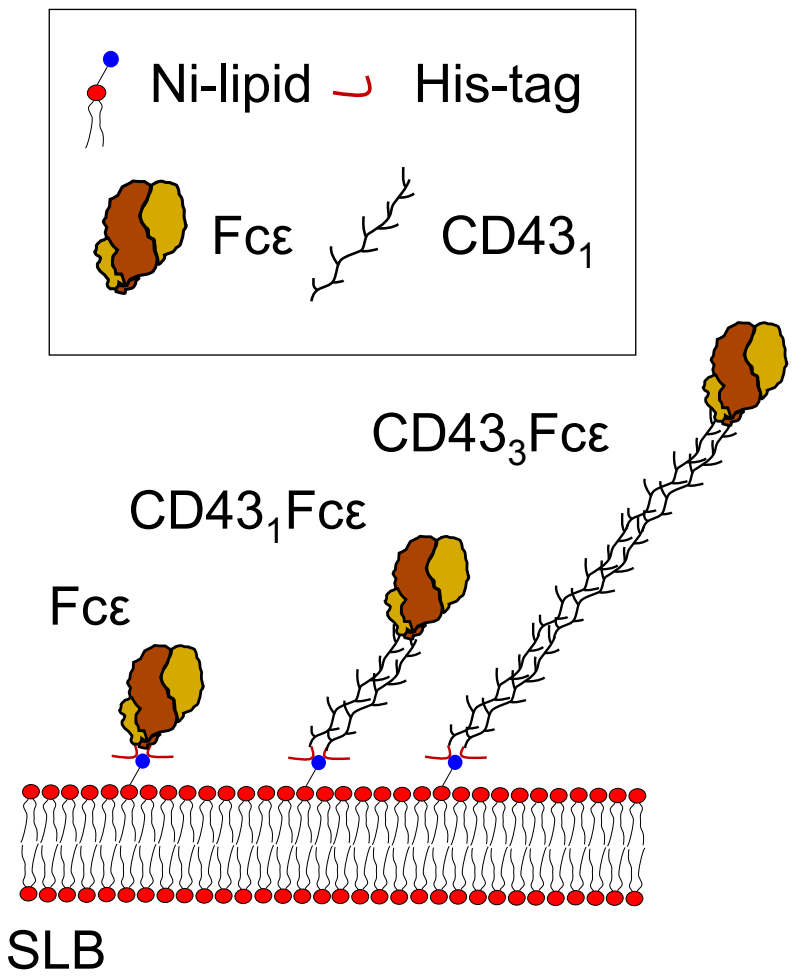
Ni-lipid
His-tag
Fcε
CD43$_1$
CD43$_3$Fcε
CD43$_1$Fcε
Fcε
SLB

B

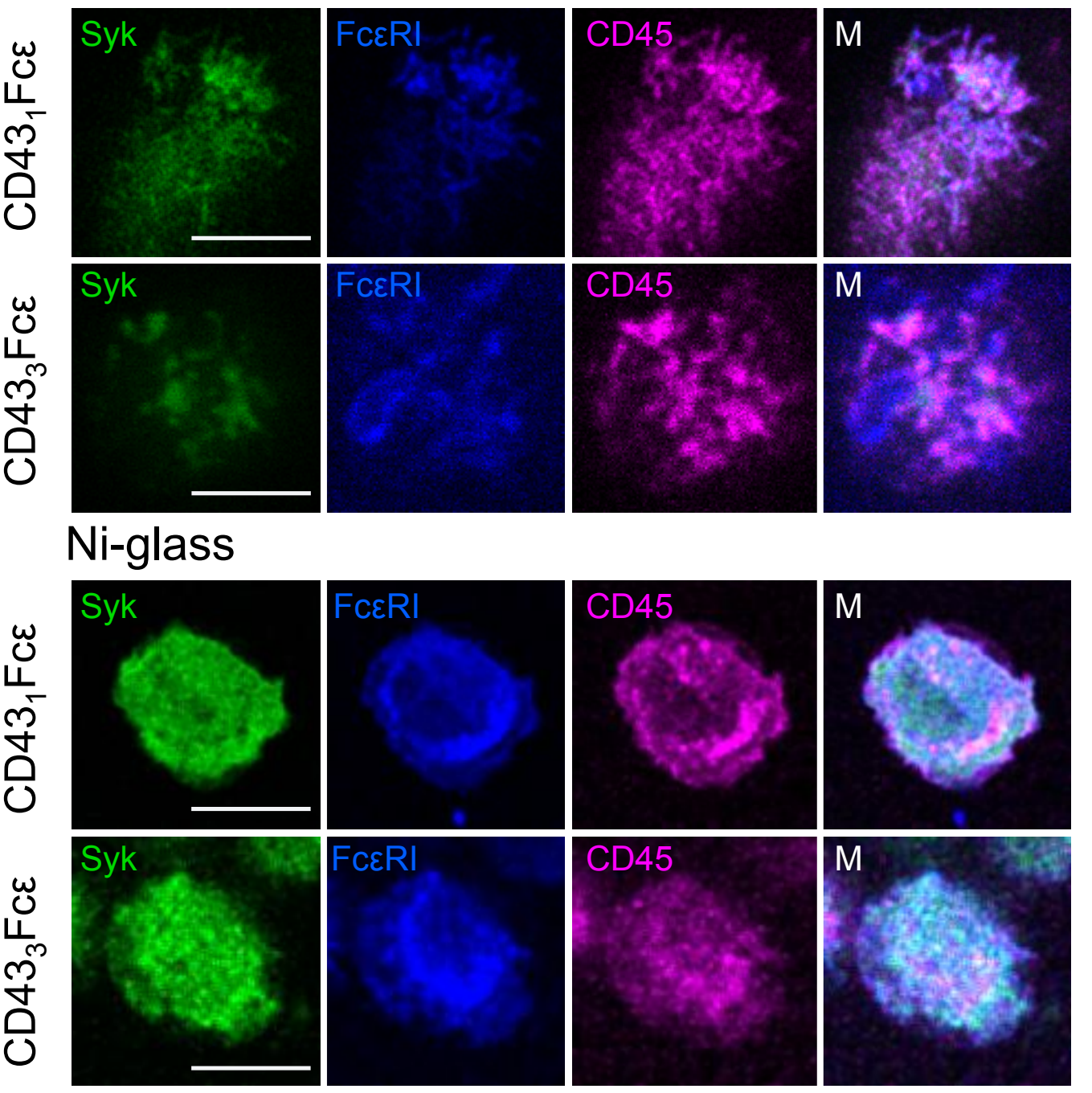
SLB
CD43$_1$Fcε
CD43$_3$Fcε
Syk
FcεRI
CD45
M

C

Ni-glass
CD43$_1$Fcε
CD43$_3$Fcε
Syk
FcεRI
CD45
M

D

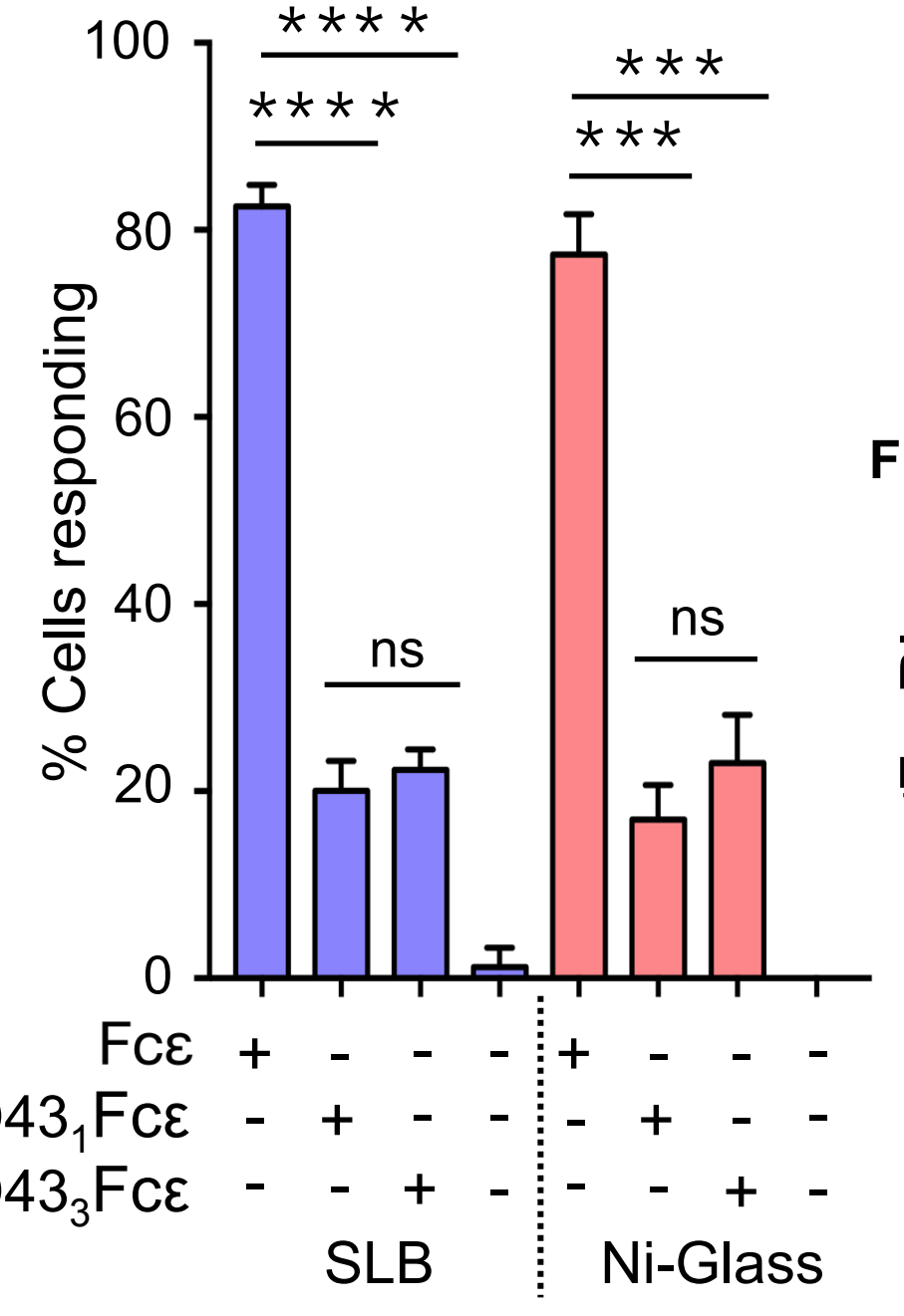
% Cells responding
100
80
60
40
20
0
****
****
***
***
ns
ns
Fcε + - - - + - - -
CD43$_1$Fcε - + - - - + - -
CD43$_3$Fcε - - + - - - + -
SLB
Ni-Glass

E

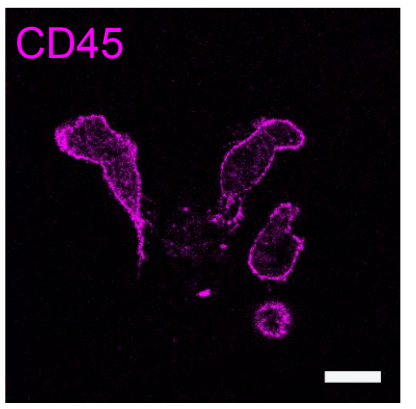
CD45

F

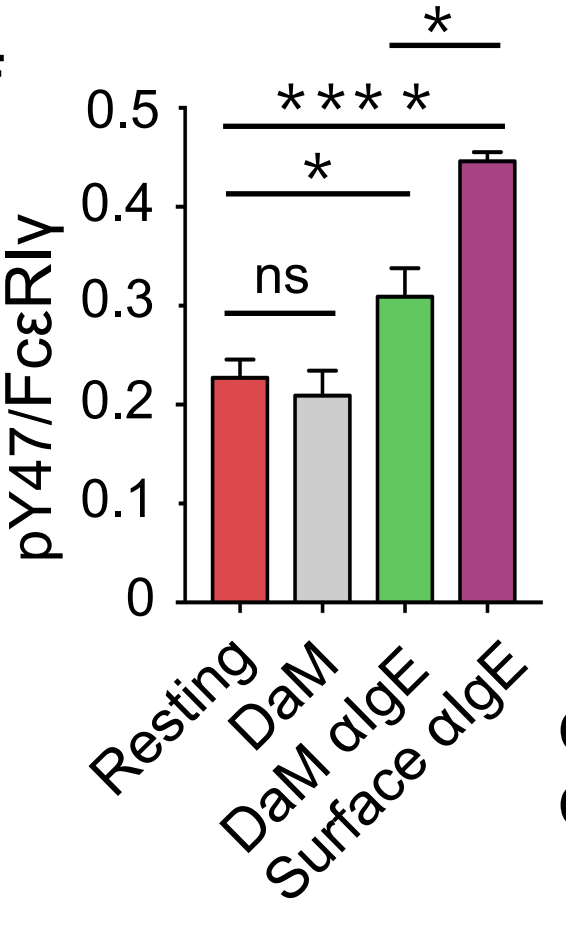
pY47/FcεRIγ
0.5
0.4
0.3
0.2
0.1
0
****
*
*
ns
Resting
DaM
DaM αIgE
Surface αIgE

G

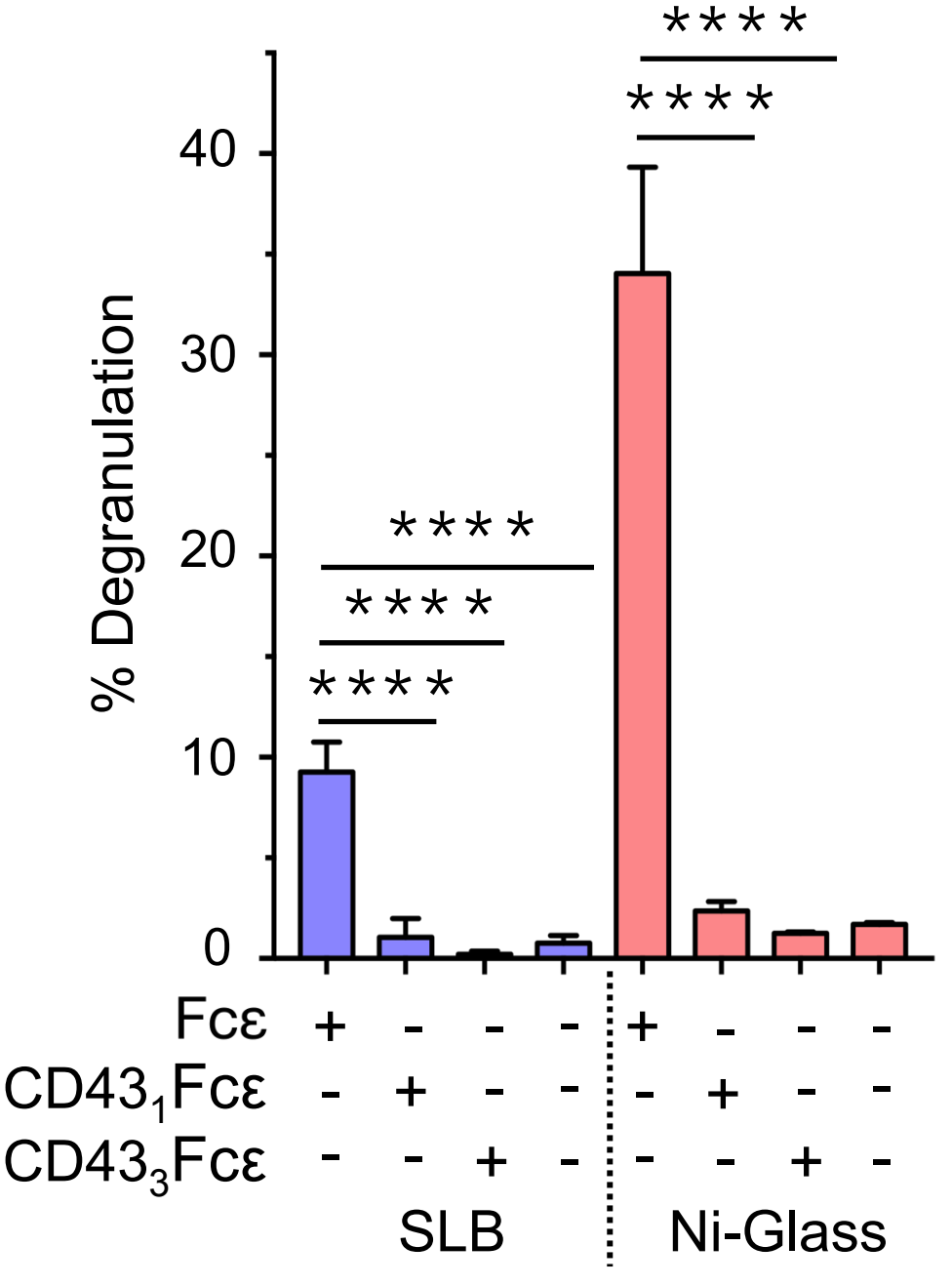
% Degranulation
40
30
20
10
0
****
****
****
****
****
Fcε + - - - + - - -
CD43$_1$Fcε - + - - - + - -
CD43$_3$Fcε - - + - - - + -
SLB
Ni-Glass

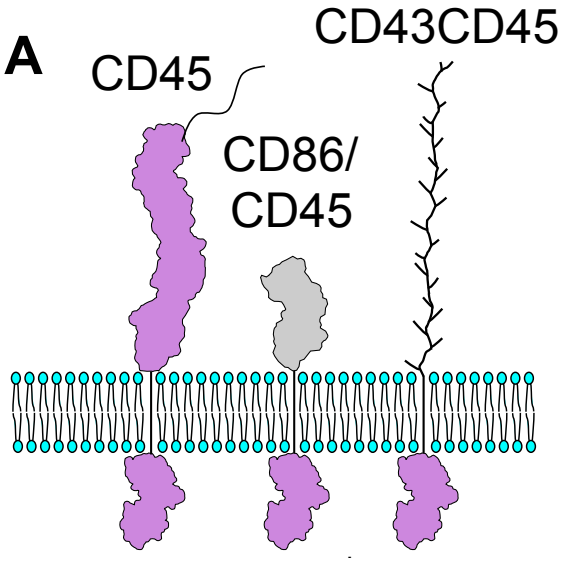
A
CD43CD45
CD45
CD86/
CD45

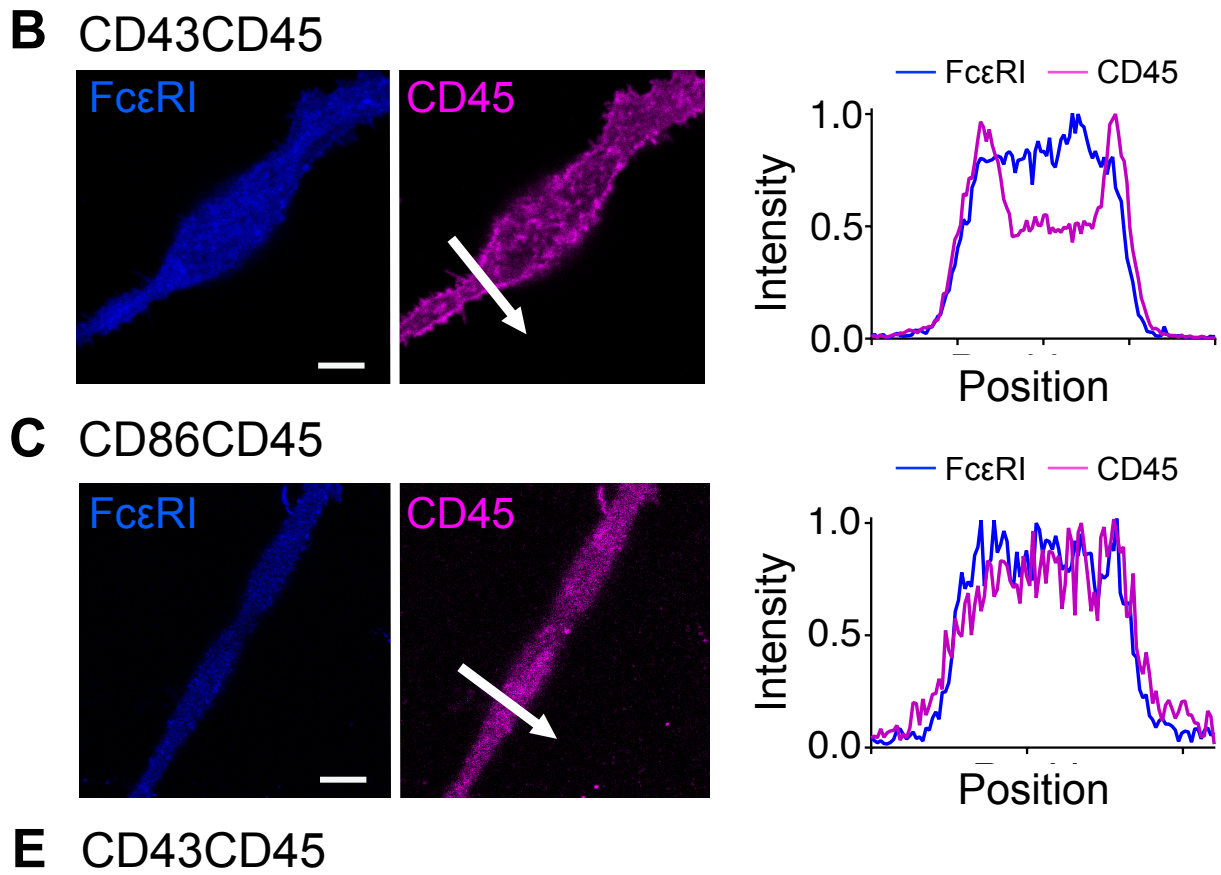
B
CD43CD45
FcεRI
CD45
FcεRI
CD45
1.0
0.5
0.0
Intensity
Position
C
CD86CD45
FcεRI
CD45
FcεRI
CD45
1.0
0.5
0.0
Intensity
Position

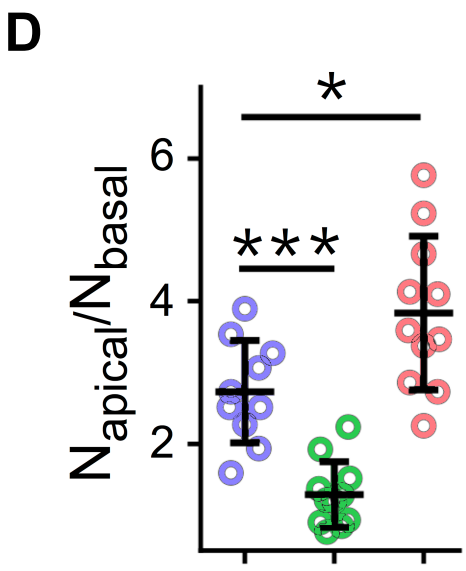
D
*
***
6
4
2
Napical/Nbasal
CD45
CD86CD45
CD43CD45

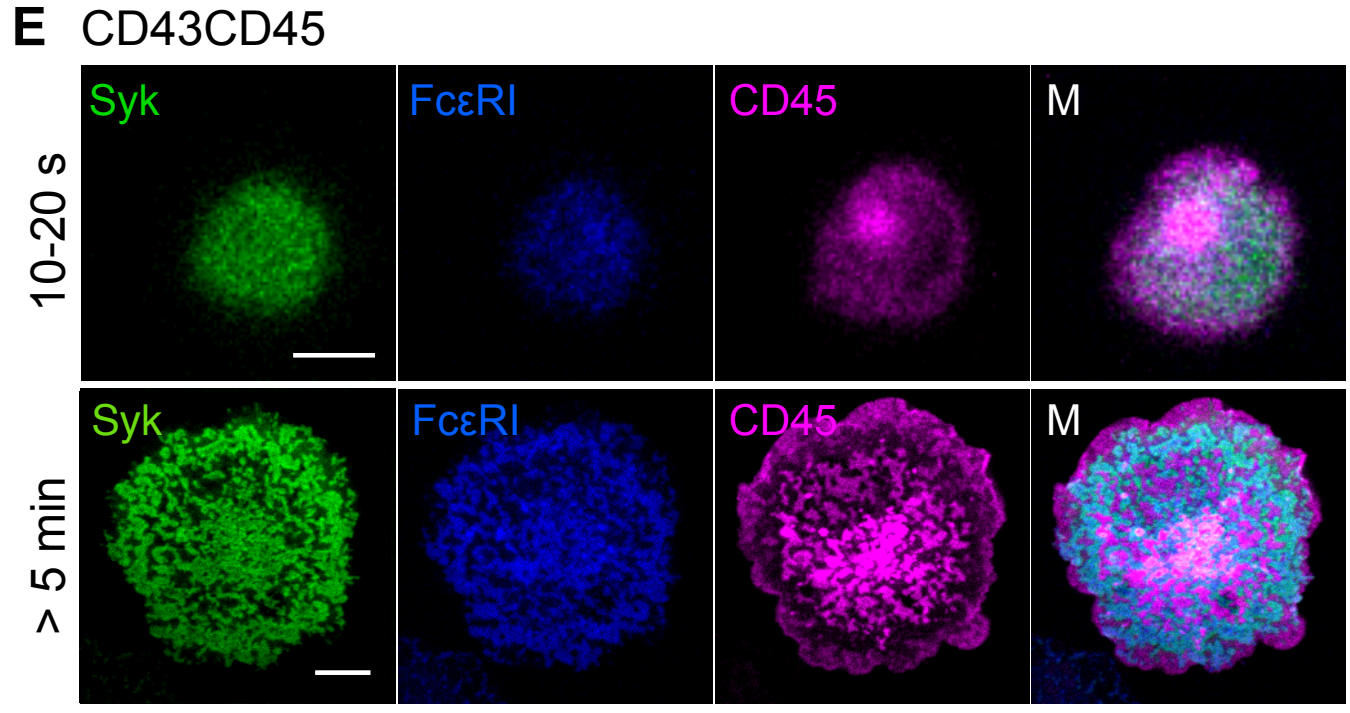
E
CD43CD45
10-20 s
> 5 min
Syk
FcεRI
CD45
M

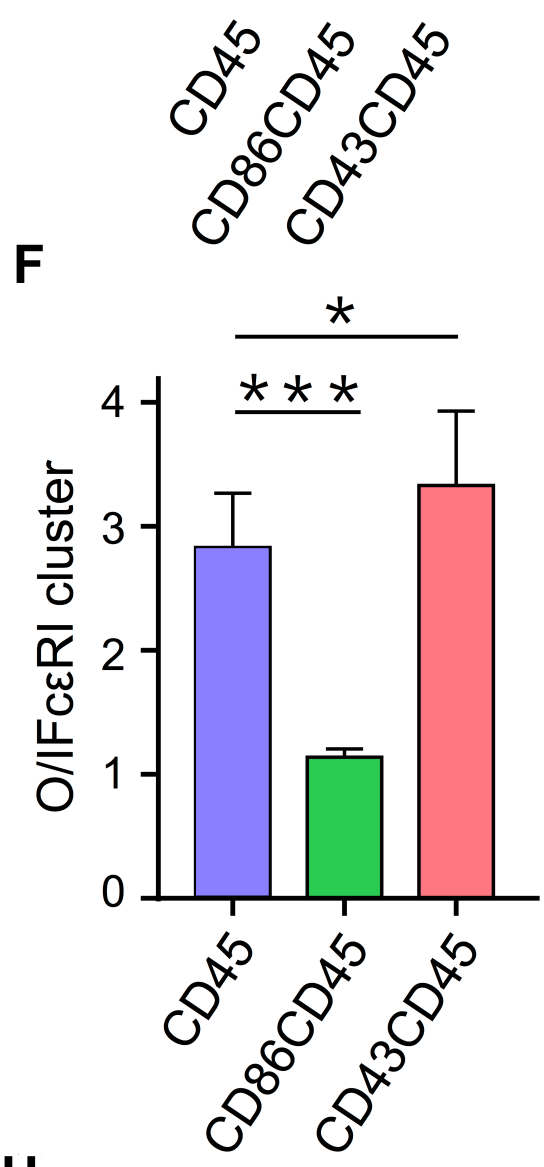
F
*
***
4
3
2
1
0
O/IFcεRI cluster
CD45
CD86CD45
CD43CD45

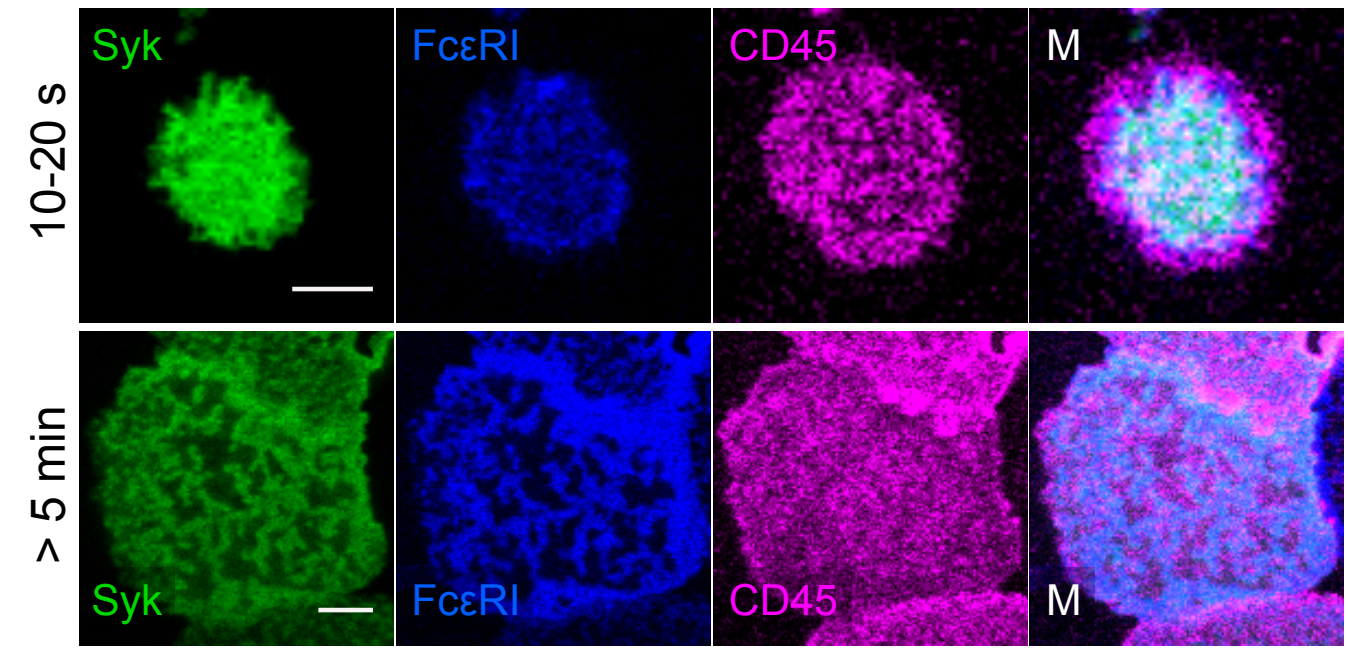
G
CD86CD45
10-20 s
> 5 min
Syk
FcεRI
CD45
M

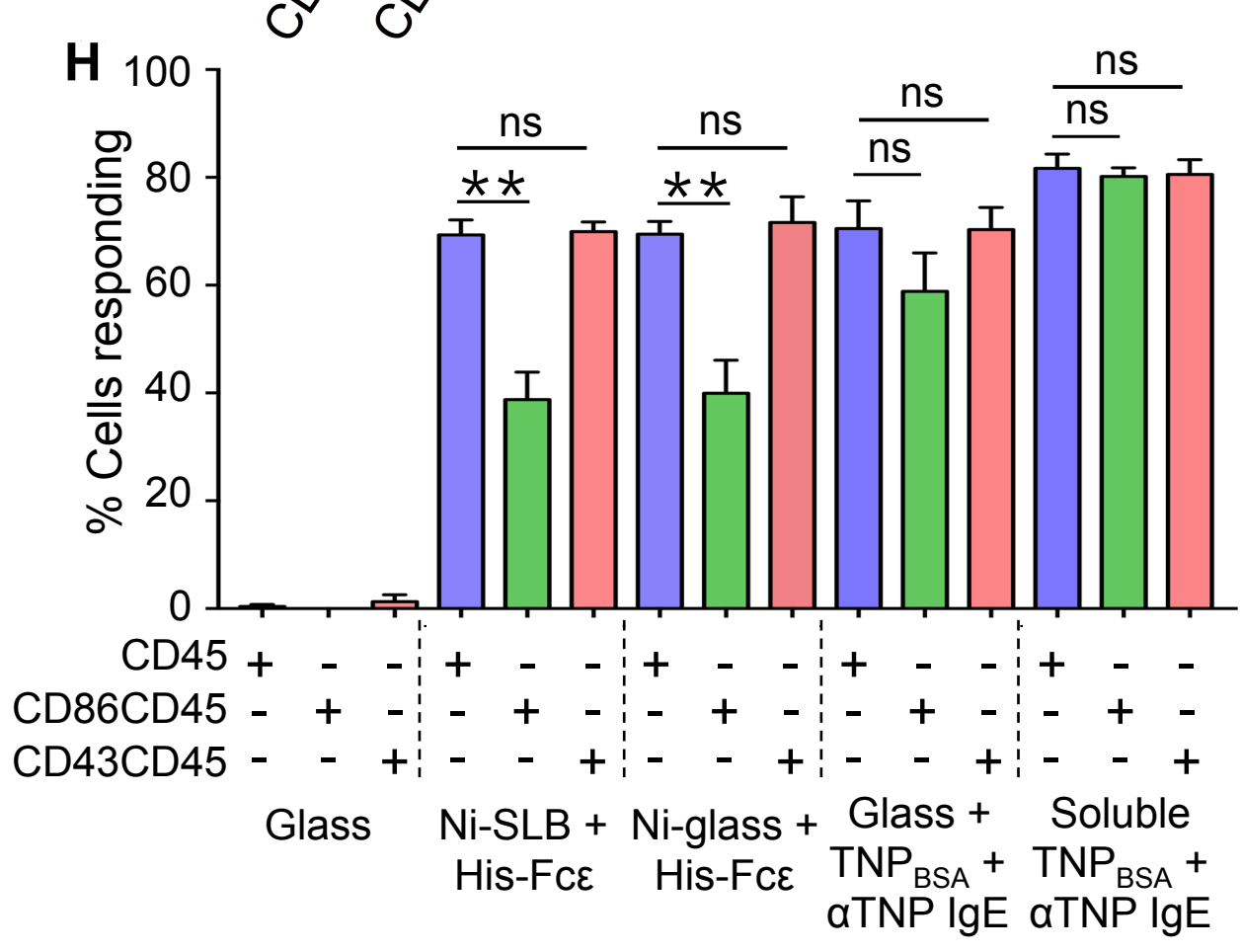
H
100
80
60
40
20
0
% Cells responding
ns
**
CD45
CD86CD45
CD43CD45
Glass
Ni-SLB + His-Fcε
Ni-glass + His-Fcε
Glass + TNPBSA + αTNP IgE
Soluble TNPBSA + αTNP IgE

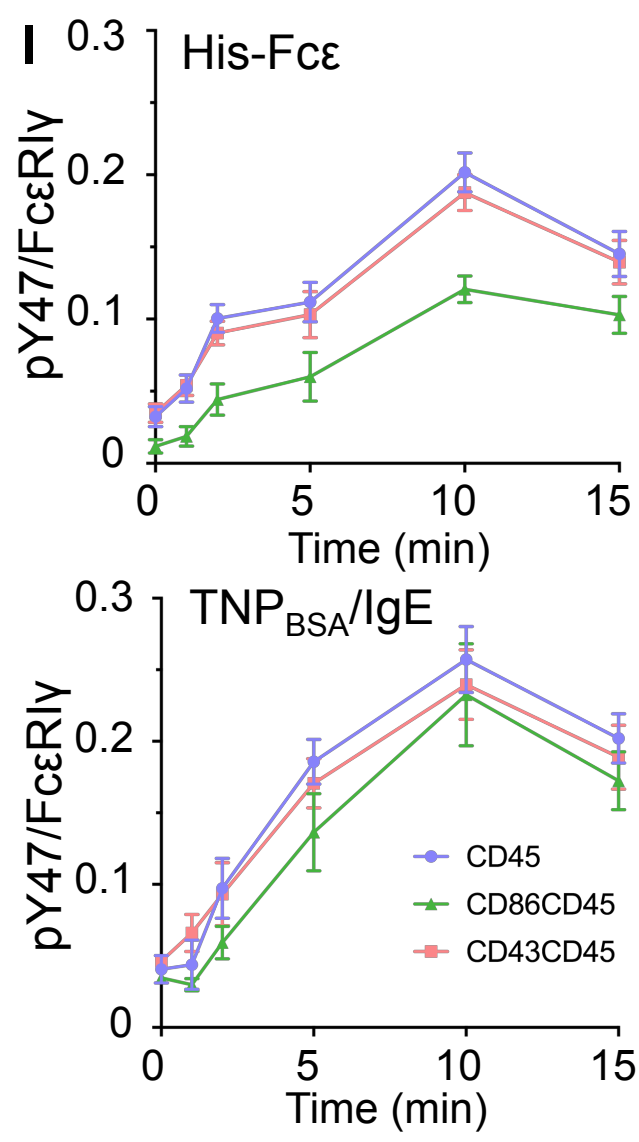
I
His-Fcε
0.3
0.2
0.1
0
pY47/FcεRIγ
0
5
10
15
Time (min)
TNPBSA/IgE
CD45
CD86CD45
CD43CD45

A GUV

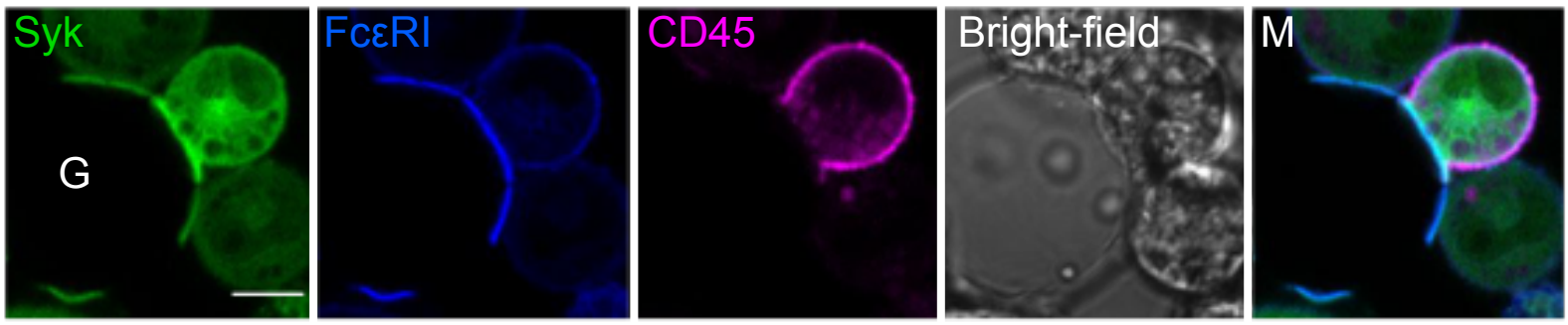

LUV

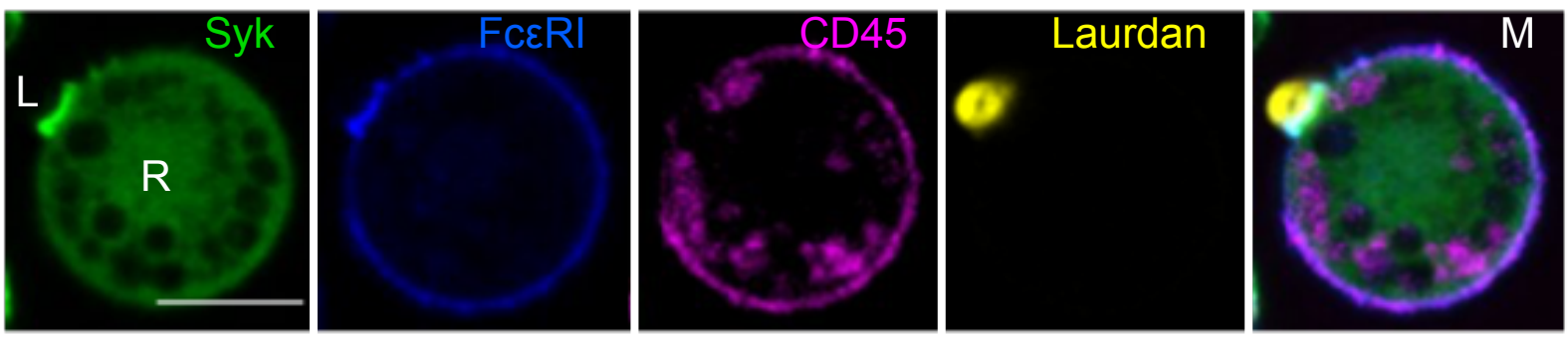

B FcεRI signaling

1. Resting mast-cell

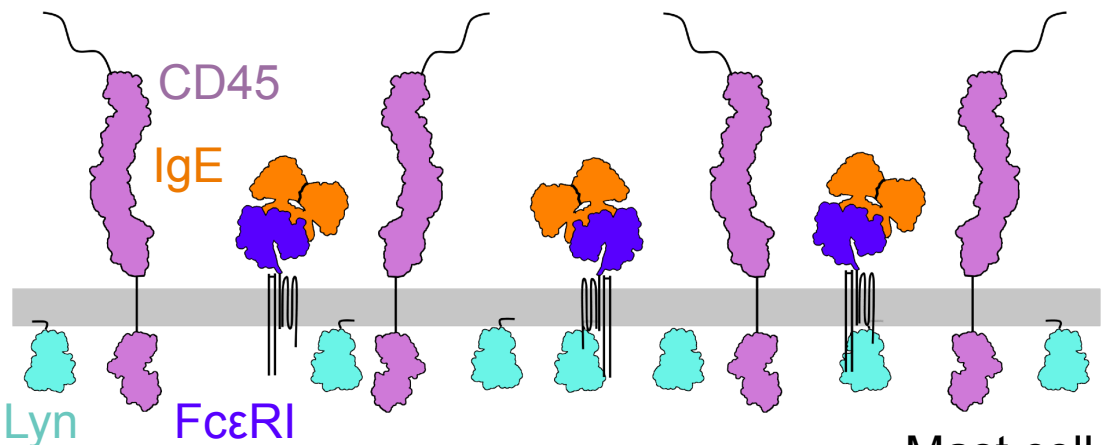

2. Aggregation-based signaling
   - kinase density increases
   - phosphatase density unchanged

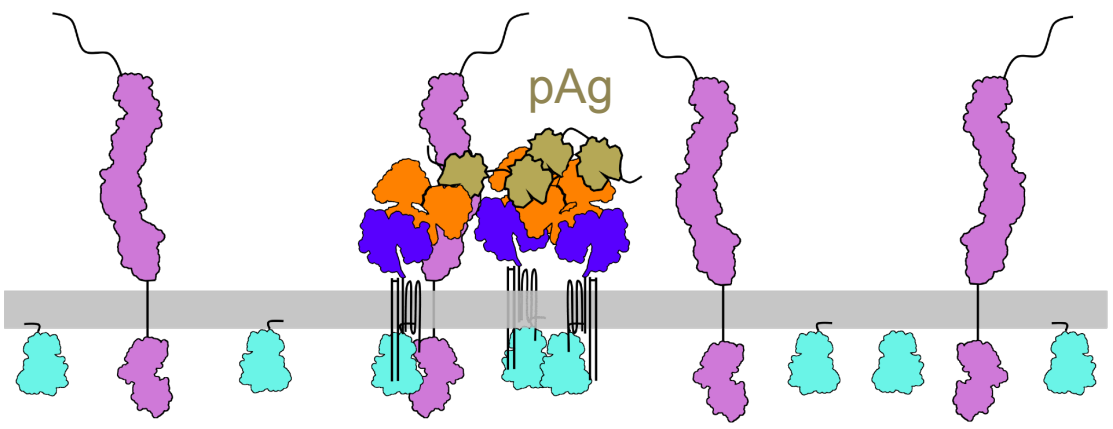

3. Phosphatase exclusion-based signaling
   - kinase density unchanged
   - phosphatase density decreases

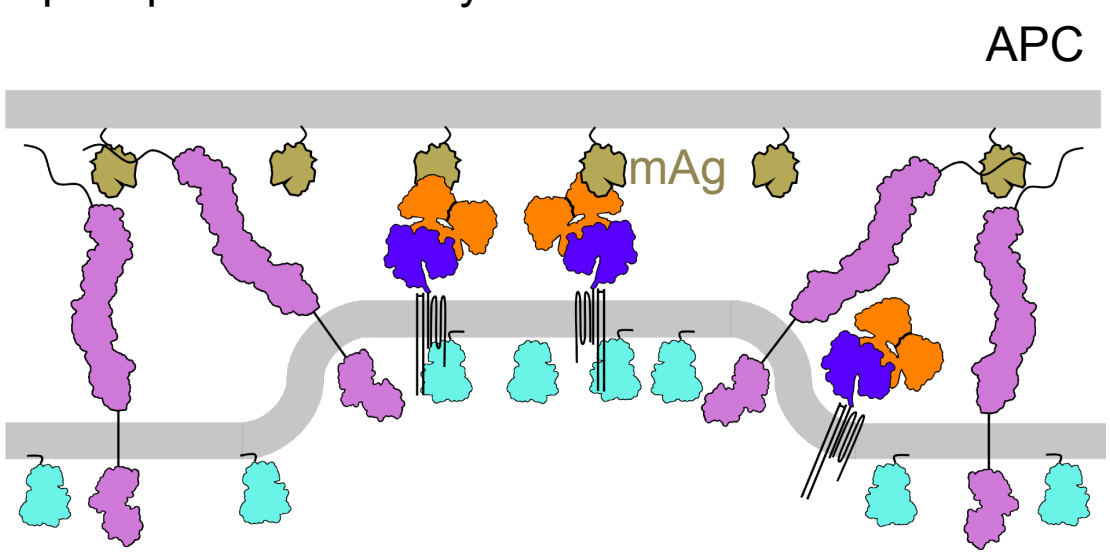

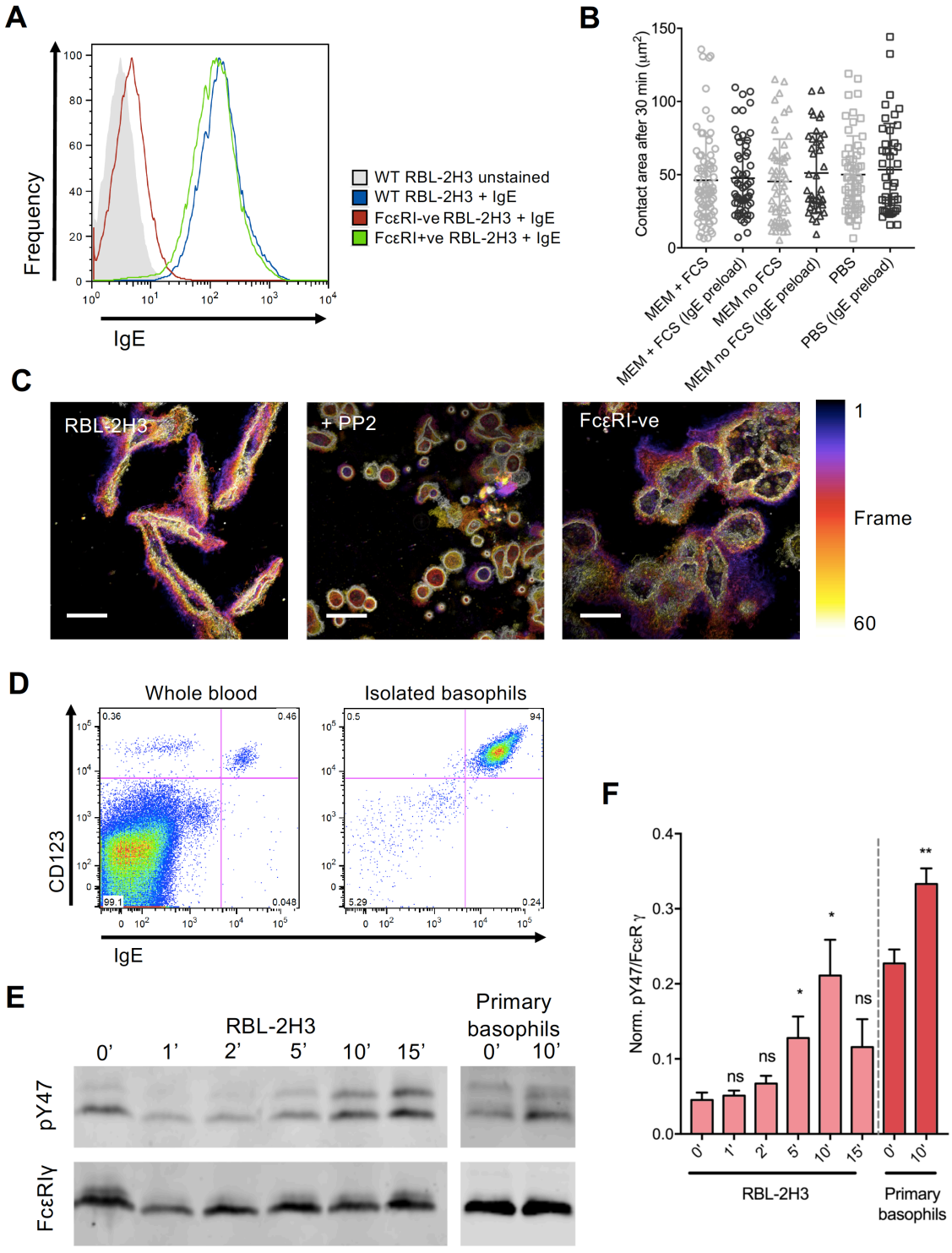

Fig. S1. FcεRI-negative RBL-2H3 cells move like WT cells, and PLL leads to FcεRIγ phosphorylation in RBL-2H3 cells and primary basophils. (**A**) Flow cytometry measurement of IgE binding to WT, FcεRI-negative (FcεRI-ve), and FcεRI-positive (FcεRI+ve) RBL-2H3 cells. (**B**) Contact areas of RBL-2H3 cells 30 min after landing on uncoated glass in MEM with or without 15% FCS or in PBS with or without preloading with anti-TNP IgE, as indicated. Each data point represents a single cell and data are from three

independent experiments. (**C**) Temporal projection of IRM cell outlines for untreated WT RBL-2H3 cells, WT cells exposed to 10μM PP2 5 min before imaging, and FcεRI-ve RBL-2H3 cells, all 24 hours after plating on uncoated glass. Outlines of areas of cell contact with the glass as determined by IRM are color-coded from frame 1 (0 s, black) to frame 60 (600 s, white). Data are representative of three independent experiments. Scale bars, 5 μm. (**D**) Staining intensity for CD123 and IgE on the surface of cells from whole blood and on isolated basophils. The representative data are an example of basophil purities typically achieved in multiple independent experiments. (**E**) Whole-cell lysates from RBL-2H3 cells and primary basophils that were in contact with PLL-coated glass for the indicated times were analyzed by Western blotting with anti-FcεRIγ and anti–FcεRIγ-pY47. Blots are representative of three independent experiments. (**F**) Normalized FcεRIγ-pY47 signals relative to total FcεRIγ signals for lysates from RBL-2H3 cells and primary basophils landing on PLL-coated glass for the indicated times. Data are means ± SD of three independent experiments. **P* < 0.05, ***P* < 0.01 relative to resting (0') cells; ns, not significant.

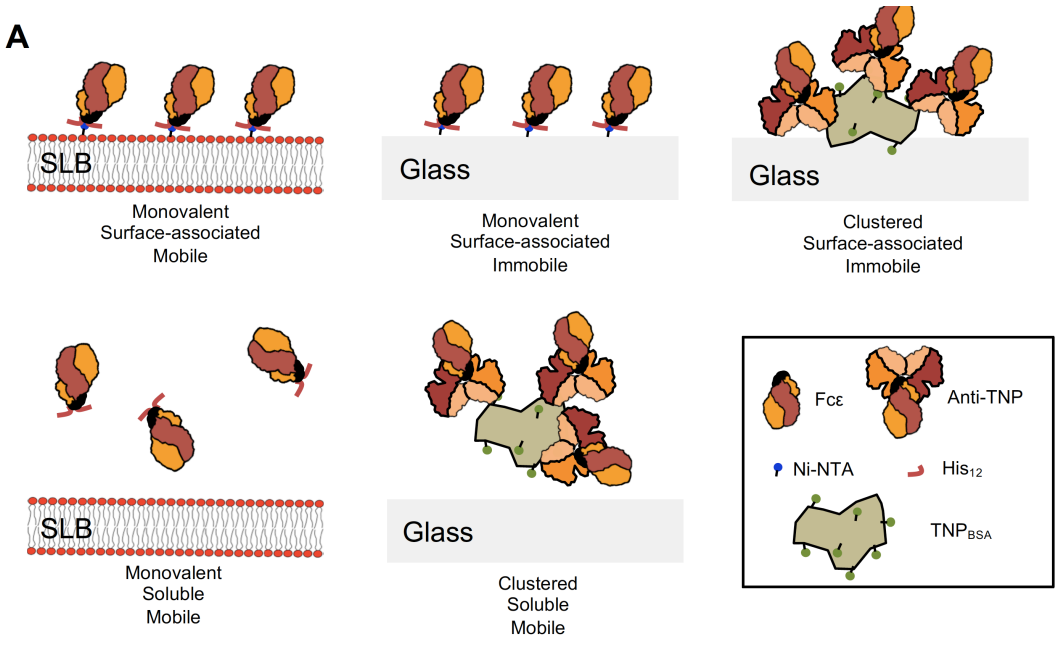
A
SLB
Monovalent
Surface-associated
Mobile
Glass
Monovalent
Surface-associated
Immobile
Glass
Clustered
Surface-associated
Immobile
SLB
Monovalent
Soluble
Mobile
Glass
Clustered
Soluble
Mobile
Fcε
Anti-TNP
Ni-NTA
His12
TNPBSA

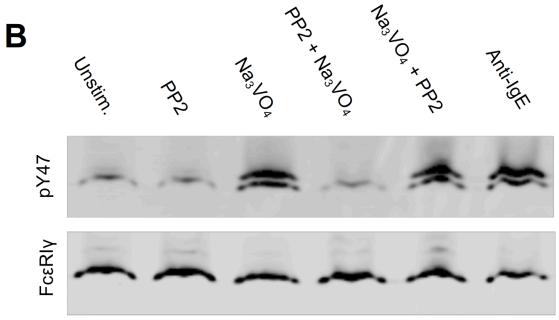
B
Unstim.
PP2
Na3VO4
PP2 + Na3VO4
Na3VO4 + PP2
Anti-IgE
pY47
FcεRIγ

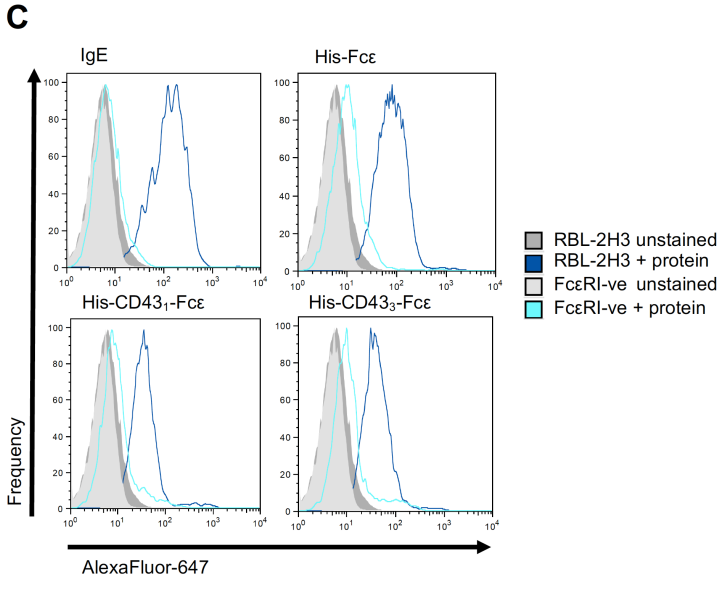
C
IgE
His-Fcε
His-CD431-Fcε
His-CD433-Fcε
Frequency
AlexaFluor-647
RBL-2H3 unstained
RBL-2H3 + protein
FcεRI-ve unstained
FcεRI-ve + protein

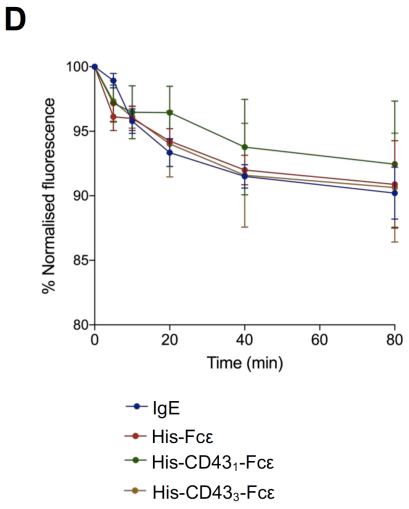
D
% Normalised fluorescence
Time (min)
IgE
His-Fcε
His-CD431-Fcε
His-CD433-Fcε

Fig. S2. Equivalent FcεRI-dependent binding is exhibited by all Fcε-containing ligands used for RBL-2H3 cell activation, and FcεRIγ phosphorylation in primary basophils is regulated by the global kinase-phosphatase balance. (**A**) Schematic representation of the activating surfaces and solutions used in the experiments measuring Ca^{2+} intensity. (**B**) Primary basophils were left unstimulated or were treated for 15 min with PP2 or pervanadate singly or sequentially, as indicated, or were treated with mouse anti-hIgE. Whole-cell lysates were then analyzed by Western blotting with anti-FcεRIγ and anti–FcεRIγ-pY47. Blots are representative of three independent experiments. Quantified data are shown in Fig. 2D. (**C**) Flow cytometry analysis of the binding of Alexa Fluor 647–conjugated, Fcε-containing proteins or recombinant IgE (rIgE) to WT and FcεRI-ve RBL-2H3 cells. Data are representative of three independent experiments. (**D**) Normalized residual fluorescence for Fcε-containing proteins and rIgE bound to RBL-2H3 cells after washing and incubation at 37°C for the indicated times. Data are means ± SD of three independent experiments.

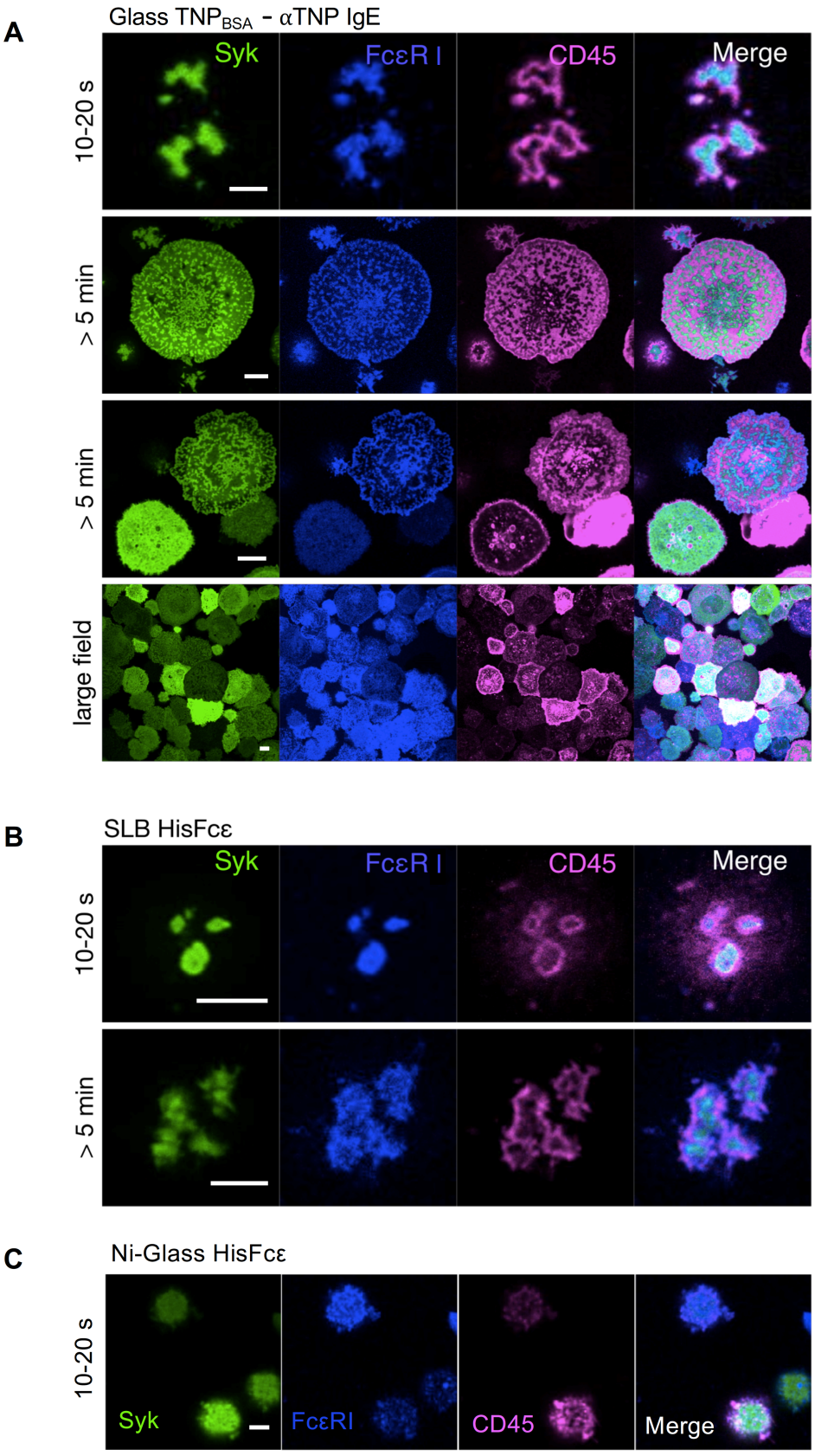
A
Glass TNP$_{BSA}$ - αTNP IgE
Syk
FcεR I
CD45
Merge
10-20 s
> 5 min
> 5 min
large field
B
SLB HisFcε
Syk
FcεR I
CD45
Merge
10-20 s
> 5 min
C
Ni-Glass HisFcε
10-20 s
Syk
FcεRI
CD45
Merge

Fig. S3. Additional examples of CD45 exclusion from the basal planes of RBL-2H3 cells on ligand-presenting surfaces. (**A**) Confocal microscopy analysis of Syk, FcεRI, and CD45 fluorescence at the basal plane of RBL-2H3 cells 10 to 20 s (top) or > 5 min (middle and bottom) after contacting glass coated with TNP_{BSA}-IgE. (**B**) Confocal microscopy analysis of Syk, FcεRI, and CD45 fluorescence at the basal plane of RBL-2H3 cells 10 to 20 s (top) or > 5 min (bottom) after contacting His-Fcε–functionalized SLB. (**C**) Confocal microscopy analysis of Syk, FcεRI, and CD45 fluorescence at the basal plane of RBL-2H3 cells 10 to 20 s after contacting His-Fcε–functionalized Ni-Glass. Scale bars, 5 μm. All images are representative of at least three independent experiments.

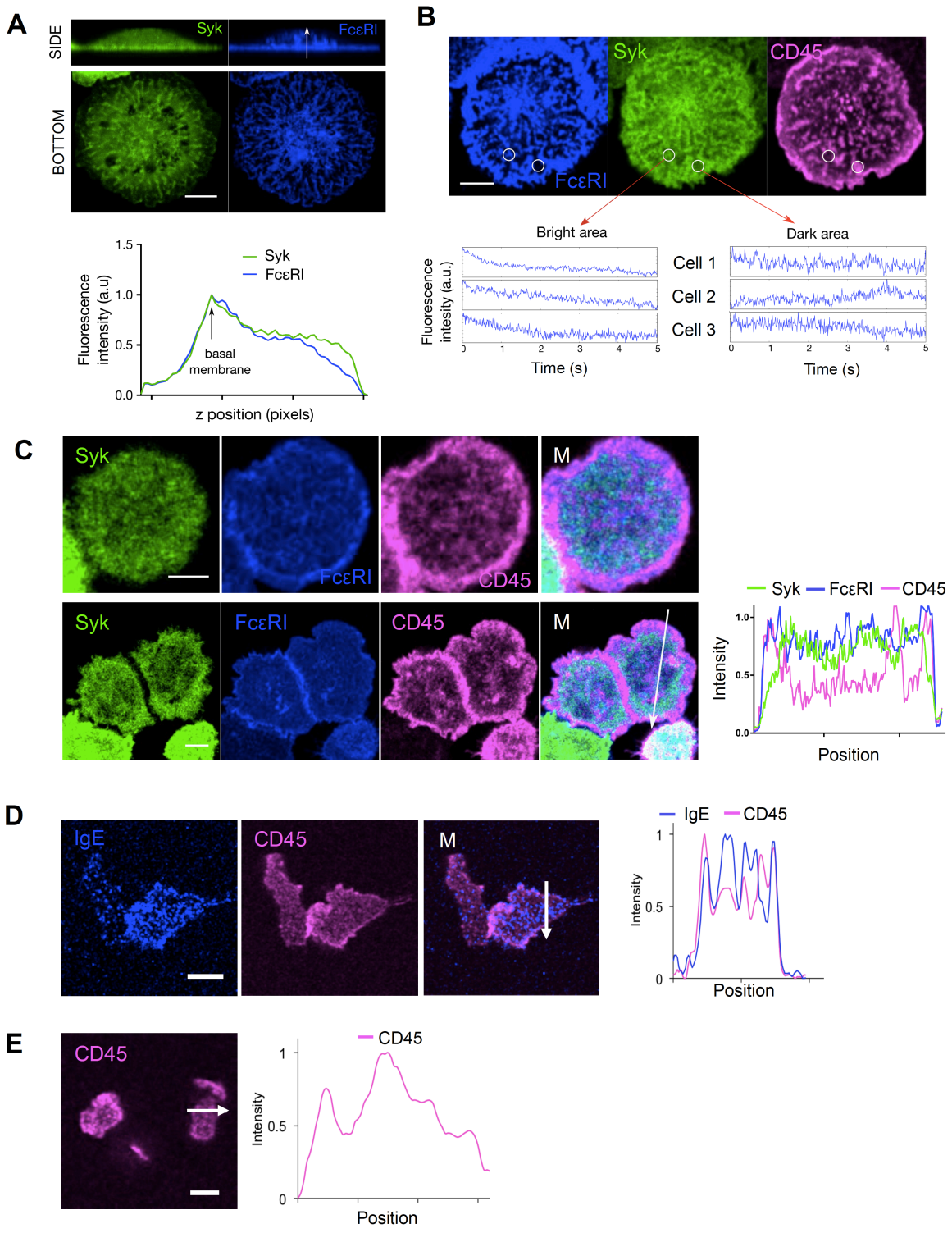

Fig. S4. Syk is recruited to FcεRI bound to surface-associated ligand, and robust CD45 exclusion in primary basophils requires specific IgE-ligand interactions. (**A**) Left: Confocal microscopy analysis of Syk, FcεRI, and CD45 fluorescence at the basal surface of RBL-2H3 cells loaded with anti-TNP IgE >5 min after contacting TNP_{BSA}-coated glass. M, merged images. Right: Line profile of fluorescence intensity corresponding to the arrow in the merged image. (**B**) Top: Confocal microscopy analysis of Syk and FcεRI fluorescence in RBL-2H3 cells >5 min after contacting glass coated with TNP_{BSA}-IgE shown as *z*-stack

cross-section ("Side") and the *x*-*y* plane of the basal cell membrane ("Bottom"). Bottom: Line profile of fluorescence intensity across the region corresponding to the arrow in the FcεRI fluorescence image. (**C**) Top: Examples of FcεRI-enriched ("Bright area") and CD45-enriched ("Dark area") zones assessed for Syk dynamics using fluorescence correlation spectroscopy. Bottom: Representative FCS data for both types of area in RBL-2H3 cells >5 min after contacting glass coated with TNP_{BSA}-IgE. Photobleaching over time is consistent with a membrane-bound fraction. (**D**) Top: CD45 and IgE fluorescence at the basal surface of anti-Der f 1 hIgE–loaded primary human basophils >5 min after contacting FCS-coated glass. Bottom: Line profile of fluorescence intensity across the region of the cell corresponding to the arrow in the merged image. (**E**) Left: CD45 fluorescence at the basal surface of primary human basophils >5 min after contacting Der f 1–coated glass in the absence of anti–Der f 1 hIgE. Scale bar, 5 μm. Right: Line profile of the fluorescence intensity across the section corresponding to the arrows. Images in all panels are representative of three independent experiments.

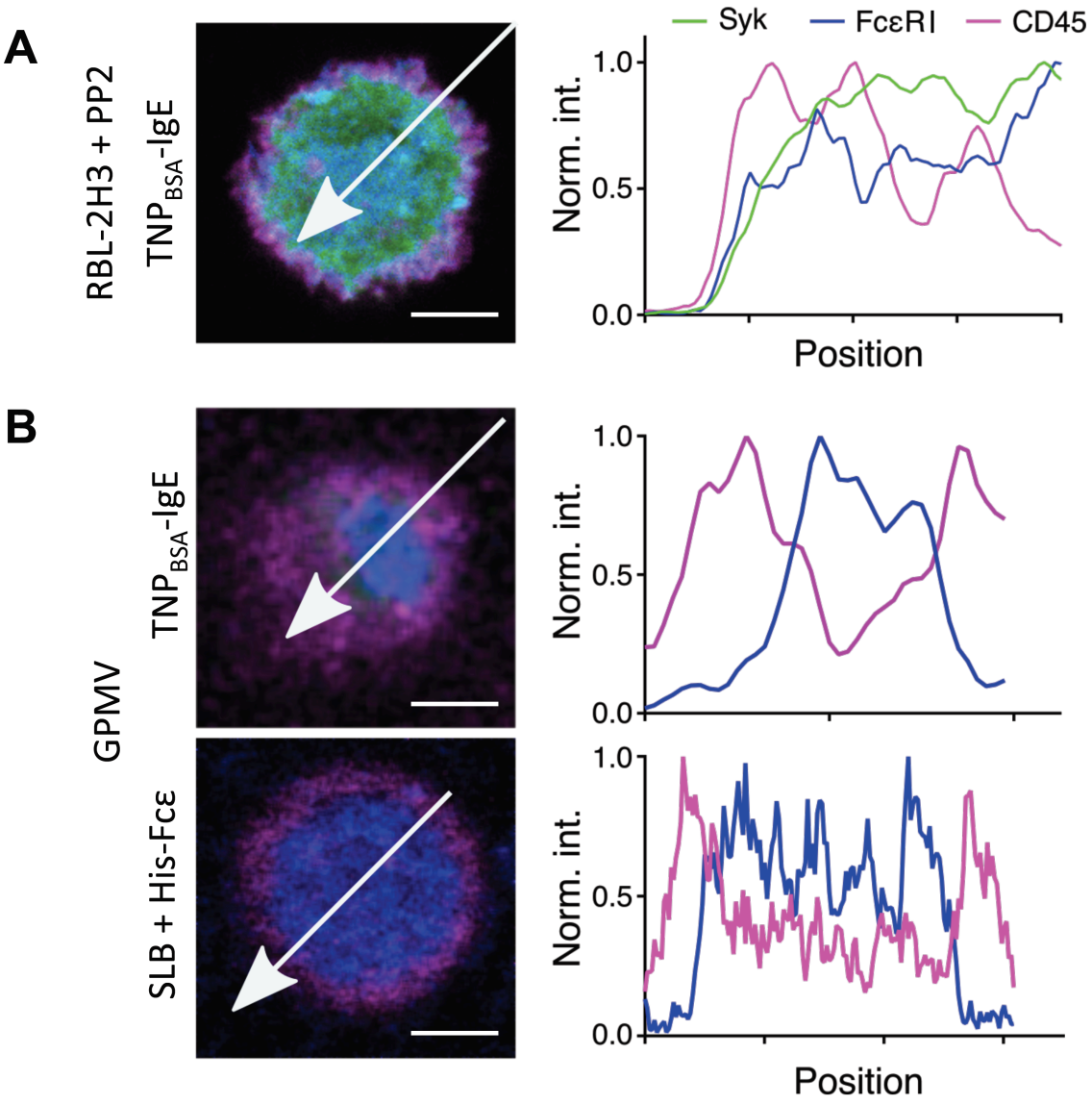

Fig. S5. CD45 exclusion is a passive process. (**A** and **B**) Left: Confocal microscopy analysis of Syk, FcεRI, and CD45 fluorescence at the basal surface of PP2-treated RBL-2H3 cells >5 min after contacting TNP_{BSA}-IgE-coated glass (A) and at the basal surface of RBL-2H3-derived GPMVs >5 min after contacting glass coated with TNP_{BSA}-IgE (B, top) or SLB loaded with His-Fcε (B, bottom). Scale bars, 5 μm. Right: Line profiles of the indicated fluorescence intensities of the cell sections corresponding to the arrows in the images. All images are representative of three independent experiments.

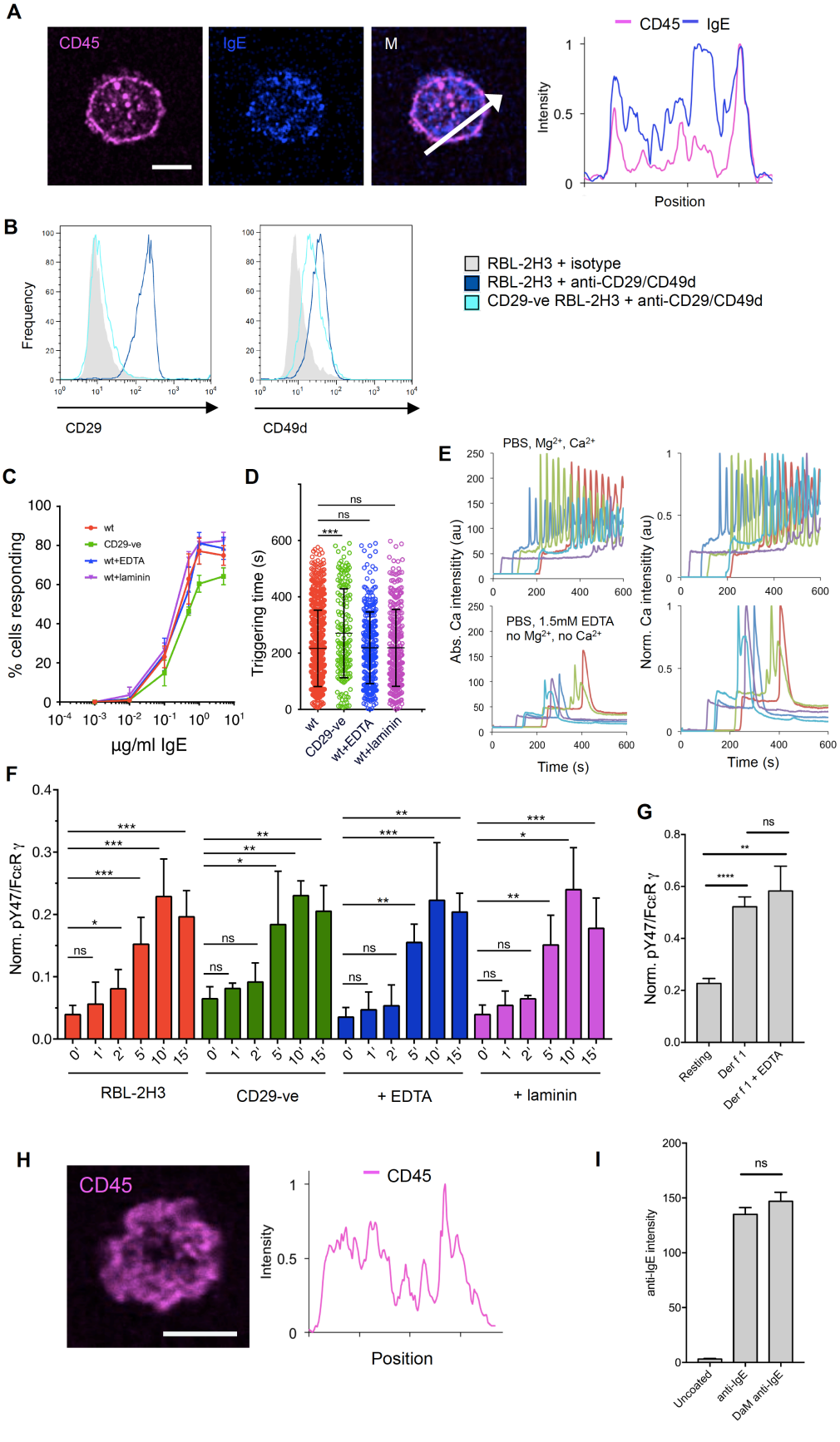
A
CD45
IgE
M
CD45
IgE
Intensity
Position
B
Frequency
CD29
CD49d
RBL-2H3 + isotype
RBL-2H3 + anti-CD29/CD49d
CD29-ve RBL-2H3 + anti-CD29/CD49d
C
% cells responding
µg/ml IgE
wt
CD29-ve
wt+EDTA
wt+laminin
D
Triggering time (s)
ns
***
wt
CD29-ve
wt+EDTA
wt+laminin
E
PBS, Mg2+, Ca2+
PBS, 1.5mM EDTA
no Mg2+, no Ca2+
Abs. Ca intensity (au)
Norm. Ca intensity (au)
Time (s)
F
Norm. pY47/FcεR γ
RBL-2H3
CD29-ve
+ EDTA
+ laminin
G
Norm. pY47/FcεR γ
Resting
Der f 1
Der f 1 + EDTA
H
CD45
Intensity
Position
I
anti-IgE intensity
Uncoated
anti-IgE
DaM anti-IgE

Fig. S6. Integrin activity is not required for CD45 exclusion or FcεRI-triggering in either RBL-2H3 cells or primary basophils. (**A**) Left: Confocal microscopy images of CD45 and IgE fluorescence at the basal surface of anti-Der f 1 hIgE–loaded primary human basophils >5 min after contacting Der f 1–coated glass in the absence of divalent cations. Scale bar, 5 μm. Right: Line profiles of fluorescence intensity corresponding to the sections indicated by the arrow. Data are representative of three independent experiments. (**B**) Flow cytometry analysis of the binding of anti-CD29 and anti-CD49d antibodies to WT and CD29-negative RBL-2H3 cells. Data are representative of three independent experiments (**C**) Percentage of RBL-2H3 cells exhibiting Ca^{2+} flux responses within 10 min of landing on glass coated with TNP_{BSA}-IgE (± rat laminin peptide) at the indicated concentrations of IgE. (**D**) Time between the landing of RBL-2H3 cells on the indicated surfaces and the peak of the first measured calcium flux respsonse at the highest IgE concentration (5 μg/ml). Each point represents a single cell and data are from five independent experiments. (**E**) Representative individual cell normalized Ca^{2+} intensity traces for RBL-2H3 cells landing on glass coated with TNP_{BSA}-IgE in the absence (top) and presence (bottom) of 1.5 mM EDTA. (**F**) RBL-2H3 cells were allowed to land on glass coated with TNP_{BSA}-IgE (± rat laminin peptide) for the indicated times ("+EDTA" indicates cells landing in the absence of divalent cations). Whole-cell lysates were then analyzed by Western blotting with anti–FcεRIγ-pY47 and anti-FcεRIγ and the relative intensities of the bands corresponding to FcεRIγ-pY47 and total FcεRIγ were determined as described earlier. (**G**) Primary human basophils loaded with anti-Der f 1 hIgE were allowed to land on Der f 1–coated glass for 10 min in the absence or presence of 1.5 mM EDTA. Whole-cell lysates were then analyzed by Western blotting with anti–FcεRIγ-pY47 and anti-FcεRIγ and the relative intensities of the bands corresponding to FcεRIγ-pY47 and total FcεRIγ were determined as described earlier. Data are means ± SD of three independent experiments. $*P < 0.05$, $**P < 0.01$, $***P < 0.001$, $****P < 0.0001$.(**H**) Left: CD45 fluorescence at the basal surface of primary human basophils >5 min after contacting glass coated with donkey anti-mouse IgG and mouse anti-hIgE. Scale bar, 5 μm. Right: Line profile of the fluorescence intensity across the section corresponding to the arrow. Image is representative of three independent experiments. (**I**) Fluorescence intensity of Alexa Fluor 647–conjugated mouse anti-hIgE deposited either directly or through donkey anti-mouse IgG on glass relative to the values from uncoated glass. Data are from three independent experiments; ns, not significant.

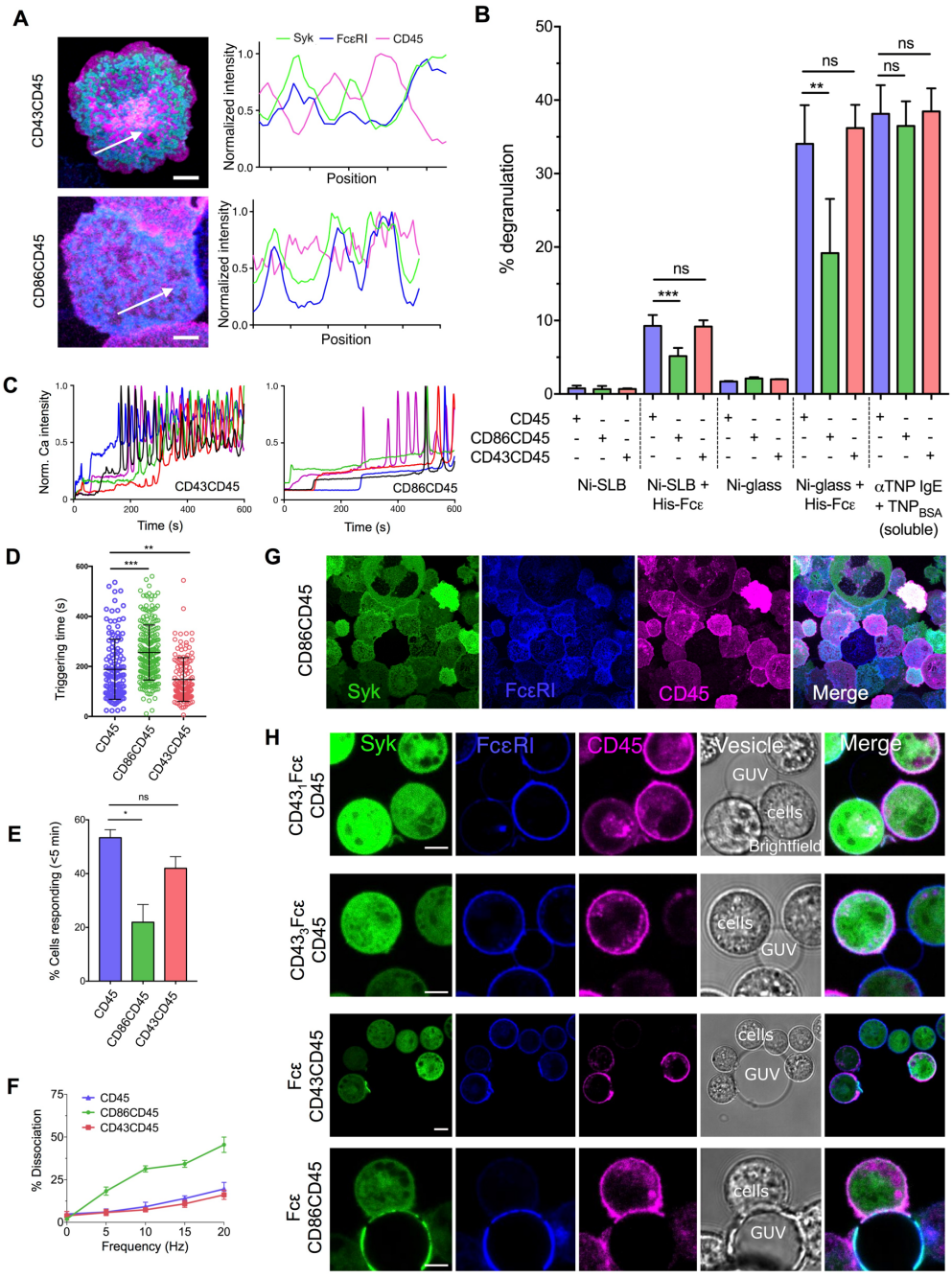

Fig. S7. Reducing the size of CD45 or increasing the size of ligand impairs both CD45 exclusion and FcεRI triggering. (**A**) Left: Confocal microscopy analysis of Syk, FcεRI, and CD43CD45 or CD86CD45 fluorescence at the basal surface of RBL-2H3 cells >5 min after contacting glass coated with TNP_{BSA}-IgE. Right: Line profiles of fluorescence intensity along the sections indicated by the arrows. (**B**) Degranulation responses of RBL-2H3 cells expressing CD45, CD86CD45, or CD43CD45 when contacting Fcε-presenting surfaces or when stimulated with soluble, crosslinking ligand. Data are means ± SD of three independent

experiments. (**C**) Representative individual cell normalized Ca^{2+} intensity traces for CD43CD45-expressing (left) or CD86CD45-expressing (right) RBL-2H3 cells contacting glass coated with TNP_{BSA}-IgE. (**D**) Times between the landing of WT, CD43CD45-expressing, and CD86CD45-expressing RBL-2H3 cells on glass coated with TNP_{BSA}-IgE and peak of the first measured calcium flux response. Each point represents a single cell and data are from four independent experiments. (**E**) Percentage of RBL-2H3 cells expressing CD45 chimeras that exhibited Ca^{2+} flux responses within 5 min of contacting glass coated with TNP_{BSA}-IgE. Data are means ± SD of four independent experiments. (**F**) Percentage of adherent RBL-2H3 cells expressing CD45 chimeras that were detached by mechanical agitation at different frequencies. Data are means ± SD of three independent experiments. (**G**) Wide fields of view of confocal microscopy images of Syk, FcεRI, and CD86CD45 fluorescence at the basal surface of RBL-2H3 cells >5 min after contacting glass coated with TNP_{BSA}-IgE. (**H**) Syk, FcεRI, and CD45, CD43CD45, or CD86CD45 fluorescence at the equatorial plane of RBL-2H3 cells interacting with GUVs loaded with Fcε, $CD43_1$Fcε, or $CD43_3$Fcε. For all images, scale bars are 5 μm; for all bar graphs, data are means ± SD. $*P < 0.05$, $**P < 0.01$, $***P < 0.001$, $****P < 0.0001$. All images are representative of at least three independent experiments.

Movie S1. CD45 is excluded from regions of FcεR1-ligand interactions on glass. Syk, FcεR1, and CD45 fluorescence at the basal surface of an RBL-2H3 cells contacting glass coated with TNP_{BSA}-IgE. Shown at 20× actual speed (2 s/frame).

Movie S2. CD45 exclusion is not affected by depletion of the β integrin CD29. Syk, FcεR1, and CD45 fluorescence at the basal surface of CD29-negative RBL-2H3 cells contacting glass coated with TNP_{BSA}-IgE. Shown at 20× actual speed (2 s/frame).

Movie S3. Decreasing the extracellular domain size of CD45 impairs its exclusion from regions of FcεR1-ligand interactions. Syk, FcεR1, and CD86CD45 fluorescence at the basal surface of an RBL-2H3 cell contacting glass coated with TNP_{BSA}-IgE. Shown at 20× actual speed (2 s/frame).